A Test Method for the Transfer Length of Prestressing Strand in Hollow Core Slabs

A THESIS SUBMITTED TO THE GRADUATE SCHOOL OF
THE UNIVERSITY OF MINNESOTA
BY

Jacob W. Robole

IN PARTIAL FULLFILLMENT OF THE REQUIREMENTS
FOR THE DEGREE OF
MASTERS OF SCIENCE

Dr. Arturo E. Schultz

June 2017

Acknowledgements

I would first like to acknowledge Dr. Arturo E. Schultz in the structural engineering group at the University of Minnesota. His guidance, support, and technical expertise was greatly appreciated throughout my time at the University of Minnesota. I would also like to extend a thank you to my committee members Drs. Lauren Linderman and Ryan Elliott.

Funding for this research project was provided by the Precast/Prestressed Concrete Institute through a Daniel P. Jenny Fellowship which is gratefully acknowledged. Without their generosity, the work that was done would not have been possible. Additional thanks would also like to be given to Dr. Richard Alan Miller (PCI Research and Development Council Chair) as well as all members of the steering committee for their guidance throughout this project.

I would also like to acknowledge Molin Concrete Products Company (Lino Lakes, MN) for their monetary donations as well as their in-kind efforts. With their help, materials for the project were able to be purchased. They were also responsible for the donation of a hollow core slab for testing in the Galambos Laboratory of the University of Minnesota, as well as allowing the authors to preform transfer length tests at their precast facility. A special thanks is also given to Paul Kourajian, Business Development and Research Engineer at Molin Concrete Products Company. His guidance throughout the project as well as his planning and communication made this project run smoothly and efficiently.

I would like to thank PCI Midwest (Mike Johnsrud, President, CEO, and Executive Director) for the travel funds granted. With their generosity the investigators were able to participate in PCI Conventions to report the findings of the investigation as well as partake in professional development at the PCI Convention.

Abstract

A method for measuring the transfer length of prestressing strand in HCS using a distributed strain sensor (DSS) was proposed. This DSS consists of a strip of material with strain gauges pre-attached to it. The DSS can then be attached to the HCS to measure strain when the strands are released. A finite element analysis was conducted to determine the feasibility of the proposed method. Experimental tests were then conducted to determine the proper adhesive for attaching the DSS to the HCS. Full-scale laboratory tests were subsequently conducted on a HCS that was loaded, and the strains measured on the HCS were compared to the strains recorded by the DSS. Lastly, two tests were conducted at a precast concrete plant to measure the transfer length in HCS.

Table of Contents

List of Tables

List of Figures

Relevant Notation

d_b = diameter of prestressing strand

D_{sl} = shear lag distance

E_c = modulus of elasticity of concrete

E_{ps} = modulus of elasticity of prestressing strand

e_{pt} = eccentricity of the prestressing strand

f_{bpt} = constant bond stress between concrete and prestressing strand, Eurocode

f'_{ci} = specified compressive strength of concrete at the initial time of prestress

F_{pt} = effective force in the prestressing strand

f_{se} = effective stress in prestressing steel after allowance for all prestress losses

f_{si} = stress in the prestressing strand before the saw cut

I_n = moment of inertia of the net section about the centroidal axil

L = length of the member

L_{pt} = transfer length of prestressing strand, Eurocode

L_t = transfer length of prestressing strand

M_1 = moment due to self-weight before the saw cut

M_2 = moment due to self-weight after the saw cut

M_{pt} = moment caused by eccentric prestressing force

P_k = stiffening parameter

P_p = peeling tensile stress parameter

SD = standard deviations

w_{sw} = load due to self-weight

x = distance along the length of the member

y_c = distance from the neutral axis to most extreme bottom fiber of the section

α_1 = strand release procedure factor, Eurocode

α_2 = strand area factor, Eurocode

δ = prestressing strand end slip

ε_o = strain gauge initial strain offset

ε_1 = concrete bottom surface strain from self-weight before the saw cut

ε_2 = concrete bottom surface strain from self-weight after the saw cut

ε_3 = concrete bottom surface strain from strand release

ε_A = strain measured by the DSS before the saw cut

ε_B = strain measured by the DSS after the saw cut

ε_{cA} = strain in the bottom of the member due to the eccentric prestressing force before the saw cut

ε_{cB} = strain in the bottom of the member due to the eccentric prestressing force after the saw cut

ε_{cm} = strain caused by the eccentric prestressing force of the member

σ_1 = stress due to self-weight before saw cut

σ_2 = stress due to self-weight after saw cut

σ_{pm0} = stress in the prestressing strand just after release, Eurocode

σ_{pt} = stress in the bottom of the member due to eccentric prestressing force

Φ = strand diameter, Eurocode

Chapter 1 Introduction

1.1 Hollow Core Floor Plank

Hollow core slabs (HCS) are precast, prestressed structural members that are fabricated at a plant. The slabs are cast on a prestressing bed at the plant that can be well over 300ft and then saw cut to the dimensions required for construction. HCS are cast with continuous voids along the length of the member. Figure 1-1 shows the cross section of several different types of HCS given in the PCI handbook for the design of HCS, Buettner and Becker (1998). The continuous voids are created to reduce the weight of the member and the amount of concrete that is used. The concrete removed from the voids contribute to flexural capacity of the member by a very small amount compared to the rest of the section. The voids in the HCS can also be used hide the mechanical and electrical lines that are required in buildings.

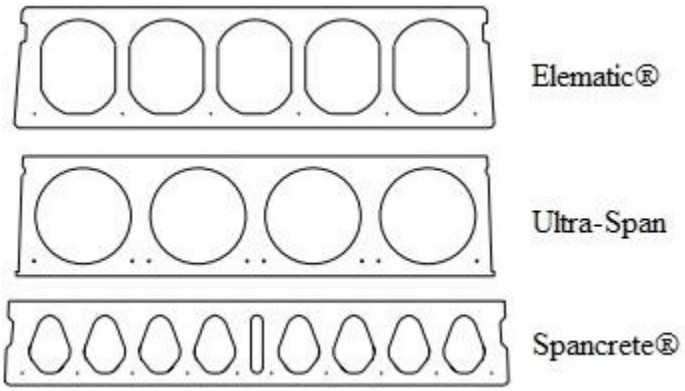

Figure 1-1: Typical HCS Cross-Sections, Buettner and Becker (1998)

HCS are fabricated in a similar method to other precast, prestressed structural members. Steel strand, typically in diameters of 0.5 or 0.6 in., is pulled across the bed and anchored into abutments on either end of the bed. The steel strand is then stressed in tension to typically 70% of the ultimate tensile strength of the strand. The concrete is cast on the bed around the strand and allowed to cure until it reaches its release compressive strength. This curing time is typically 18-24 hours. The release strength is needed in order to resist the

stresses from the prestressing strand when it is released, as well as the stresses from moving the member around the plant. Once the release compressive strength is reached, the strands are released and the slab is saw cut to the desired lengths for the building in which it will be used.

The major difference between HCS and other precast, prestressed members is the way that the concrete is cast. There are three different methods that HCS are cast. The two more common ways are with either an extruder or with a slip form. A third and less common method is using form work with pneumatic tubes to create the voids. The extrusion process uses a very dry concrete mix. The mix is fed into the top of the extrusion machine that moves along the length of the bed. The machine vibrates and uses augers to create the voids as it moves along the bed. The slip form method uses a machine that has tubes anchored to it that create the voids as the machine moves along the casting bed. The side formwork is typically stationary forms and the concrete used often has a slightly higher slump than the mix that would be used in the extrusion method. The less common method uses a wet concrete mix that is cast like other precast, prestressed members. Pneumatic tubes are used to create the voids in the concrete and need to be anchored to the formwork so that they do not float to the top of the wet concrete. In this process the casting beds are usually much shorter than the other methods so that the tubes are easier to work with.

Typical HCS have depths of 8, 10, and 12 in. Larger depth HCS (16in.) are becoming popular in the United States due to their ability to span longer distances and carry higher loads. Deeper HCS are common in Europe. In the United States the design of HCS is governed by the American Concrete Institute building code ACI 318-14. The Precast Concrete Institute also provides a design manual for the design of HCS.

1.2 Research Motivation

HCS are becoming increasingly popular in many building designs specifically in midrise buildings. A popular design is to have precast-wood mixed construction. The first floor, or first floor and basement, will be constructed out of precast members and will often be a parking garage or retail stores. The floors above it will be constructed out of wood and will

be residential units. These buildings can be as tall as 7 stories. As the building gets taller, the precast flooring that the woods structure is sitting on, typically HCS, needs to support a greater load.

HCS work very well to resist flexural forces. The ultimate flexural capacity can be predicted accurately using fundamental mechanics of materials. A designer can ensure ductile flexural failure. Shear failure on the other hand is less predictable. Most shear design equations are derived empirically and vary based on the member type and loading configuration. When the concrete does fail in shear, it does so in a very brittle failure mode. To increase the shear strength and the produce a ductile failure method, transverse reinforcement (i.e., ties and stirrups) is placed in the member.

However, due to the fabrication method of HCS, transverse reinforcement cannot be placed in the member because they would interfere with the extrusion or slip-forming machines that produce the HCS. Thus, in HCS, all of the shear resistance comes from the concrete or the prestressing strand. The shear forces in concrete without any transverse reinforcement are considered to be resisted by aggregate interlock across the crack face, shear transfer in the compression zone, and dowel action of the longitudinal reinforcement. In prestressed concrete design, the code does take into consideration the added aggregate interlocking caused by the prestressing. However, in the transfer length region of the member, the prestressing force varies, approximately linearly, until it reaches a value of zero at the end of the member.

In order to accurately determine where the prestressing force begins to decrease, the length of strand over which stress builds up from a value of zero to the effective prestress, i.e. the transfer length, needs to be known. Currently ACI 318-14 specifies a simplified estimate of the transfer length of $50d_b$ for all prestressed members. The simplification is based on Equation 1-1 which is also specified by ACI 318. If f_{se} in Equation 1-1 is assumed to be 150,000 psi then the equation simplifies to $50d_b$. This equation is based on previous research that has been conducted to determine the transfer length of different types of precast, prestressed concrete members. Some of these tests were conducted by installing

electrical resistance strain gauges on the prestressing strand. Other tests measured concrete surface strain with electrical resistance strain gauge or DEMEC gauges. In both cases, strain readings were taken before and after the strand was released. These tests were all conducted on precast members that were fabricated using the wet-cast method, that is, cast in stationary forms using a high slump concrete mix.

$$L_t = \frac{f_{se} d_b}{3{,}000} \qquad (1-1)$$

To the best of the Authors' knowledge, little research has been conducted to measure the transfer length in HCS and verify that the ACI 318-14 approximation of transfer length given in Equation 1-1 or the simplification of $50d_b$ is appropriate. Palmer and Schultz (2010) conducted transfer length tests on two HCS in their investigation of the shear capacity of deep (16 in.) HCS. Walraven and Mercx (1983) also conducted two transfer length tests as part of their investigation of the flexural and shear capacity of HCS. Using strain gauges on the prestressing strand for determining the transfer length is not suitable for HCS because the lead wires for the strain gauges would interfere with the extrusion or slip-form machine. For this reason Walraven and Mercx (1983), and later Palmer and Schultz (2010), measured concrete surface strains in the transfer length tests that were conducted.

It is thought that the transfer length in HCS may be different than in other precast members because of the manner in which they are cast, and because they are cast using a much drier concrete mix. This could affect the consolidation around the prestressing strand making the bond between the prestressing stand and the concrete weaker. Therefore, the transfer length in HCS may be longer than in wet-cast concrete products. An underprediction in the transfer length means that a designer is considering the full effect of the prestressing force at a shorter distance from the end of the member than what it may really be and, as a consequence, overprediction of the flexural and shear capacities would follow near the ends of the member.

1.3 Research Objectives

An analytical and experimental research program was undertaken with the goal of developing a quick, easy, and efficient method for determining the transfer length in HCS as well as other precast, prestressed members for which the strain cannot be measured directly on the prestressing strand. In this document, a method was proposed and an analytical study was conducted using finite element analysis in order to verify the proposed procedure and to determine the relevant parameters, such as material properties and measurement dimensions. Small-scale tests were performed as well as full-scale tests in laboratory in order to validate the method. Finally, two transfer length tests were conducted at a precast concrete plant to verify the ease with which it can be deployed in the field to obtain accurate readings.

Chapter 2 Behavior of Transfer Length

2.1 What Is Transfer Length?

All precast, pretensioned members have a region at their ends known as the 'transfer length' or 'transmission length'. This is the length, measured from the end of the beam that is required to transfer the full tensile force in the strands into compressive force in the concrete. When a precast, pretensioned member is fabricated, the prestressing strand is tensioned and then the concrete is cast around the strand. When the strand is released, it wants to shorten and return to its relaxed state. However, when the concrete hardens, a bond is formed between concrete and strand. As the released strand tries to relax, the force from the strand is transferred to the concrete through interface shear stresses known as bond stresses between the strand and the surrounding concrete. The prestressing force does not transfer in its entirety to the concrete immediately at the end of the member, but grows in an approximately linear manner until it reaches its full magnitude. Figure 2-1 from Caro et al. (2013) shows the idealized stress in a prestressing strand along member length after the strand is released.

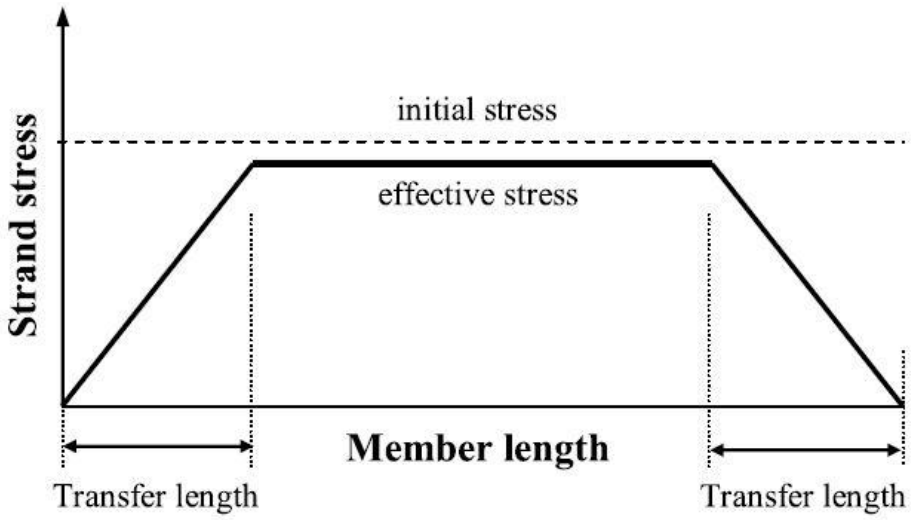

Figure 2-1: Stress in the prestressing strand along the member length

2.2 Parameters That May Affect Transfer Length

There are several parameters that are thought to potentially affect the transfer length in a precast, pretensioned member. All of these parameters affect the bond that occurs between the concrete and the prestressing strand. In HCS, one parameter that may affect the bonding of the concrete to the prestressing strand is the depth of the member. The prestressing strand is typically placed in the bottom of the member, and with the very dry concrete mix that is used in HCS it may be more difficult to get good consolidation of the concrete around the prestressing strand.

Another parameter that is thought to affect the transfer length is the method used for casting the concrete member. The fabrication methods for HCS are proprietary. Different types of HCS casting machines may consolidate the concrete more effectively than others, thus creating different levels of bond strength between the concrete and the prestressing strand. The way that plants release the strand can affect the transfer length as well. It is common practice to flame-cut, using an oxygen-acetylene torch, the individual strands in order to release them. Some plants, however, have moveable abutments for their HCS production. The moveable abutments can be separated to introduce tension into the strand, and moved towards each other to release the strand. Strand release using these moveable abutments is a more controlled process for the prestressing force and may cause a shorter transfer length because the bond between the prestressing strand and the concrete will not be disturbed as much.

Chapter 3 Literature Review

3.1 Research on Transfer Length in HCS

This section discusses previous theoretical and experimental research that has been conducted on HCS. The limited amount of research on transfer length in HCS, as well as research in other precast, prestressed members and on prestressing strand bond will also be discussed. Due to the limited amount of research that has been done specifically on the transfer length in HCS, some of the papers discussed do not contain information pertaining to transfer length. For conciseness, this information will not be discussed.

3.2 Russell and Burns (1997)

In this experimental study, the authors conduct an investigation of the transfer length on wet-cast pretensioned members in order to compare the effects that the prestressing strand diameter has on the transfer length of the member. In this study, the authors specifically look at 0.5-in. strand and 0.6-in. strand. At the time of this study 0.6-in. is just beginning to gain popularity in the precast industry.

The authors fabricated eighteen single-strand pretensioned members. Eight of the specimens were fabricated with 0.5-in. strand and ten with 0.6-in. strand. The members had a rectangular cross section 12.7-cm tall and 10.2-cm wide. Each specimen was 3.66-m long. Figure 3-1 shows these dimensions. The single prestressing strand was placed in the center of the cross sections. The specimens were cast using a wet concrete mix. After 48 hours, the strands in the specimens were cut with a torch.

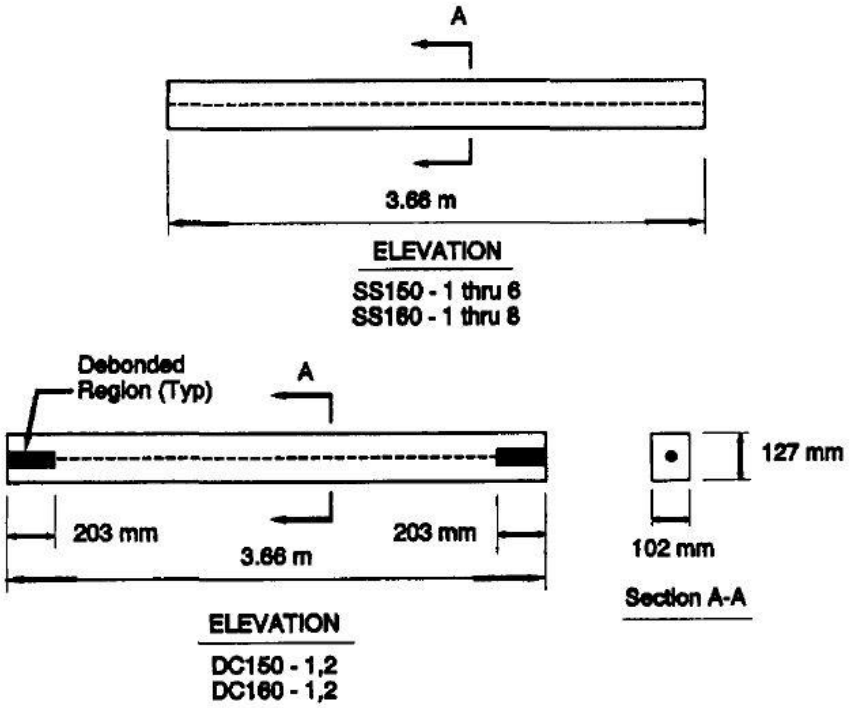

Figure 3-1: Russel Burns (1997) Specimen Dimensions

To measure the transfer length at the time of release, the authors used detachable mechanical strain gauges (DEMEC gauges) to measure the strain in the surface of concrete of the specimen closest to the prestressing strands. The authors used DEMEC gauges on opposite faces of the specimen, at an elevation equal to that of the strands, in order to eliminate any strain that could be caused by eccentricity of the strand. The DEMEC gauges were used to measure the strain at both the cut end of the specimen and the dead end of the specimen. Strain readings were taken before and after the strand was released. When the strand is released, the concrete will shrink because it is being put into compression by the prestressing strands. This shrinkage of the concrete will vary in the transfer length region where the value of the precompression force is varying.

In order to determine what would be defined as the transfer length the authors decided to use the following definition called the 95% AMS (Average Maximum Strain) Method. The transfer length is defined as the length along the tendon in which the measured strand strain profile changes from a value of zero at the cut end to the first instance of a value of 95%

of the peak strain plateau. The authors outline the following steps for determining the transfer length.

1. Plot the concrete surface strain profile.
2. Determine the AMS (Average Maximum Strain) for the specimen by computing the numerical average of all the strains contained within the strain plateau of the fully effective prestress force.
3. Multiply the AMS by 0.95 and construct a line corresponding to this value.
4. Transfer length is determined by the intersection of the 95% line with the strain profile.

A value of 95% of the average maximum strain is used in order to eliminate any errors caused by random strain trends that can occur in the region where the full transfer has occurred. Figure 3-2 shows a strain profile for one specimen from a test conducted by Russell and Burns with the 95% AMS line graphed as well.

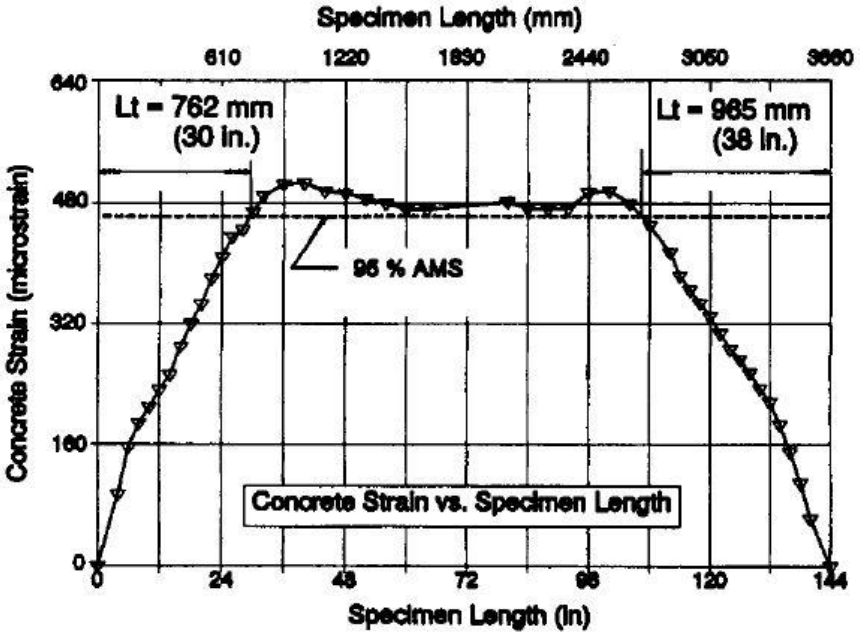

Figure 3-2: Strain Profile from Russell and Burns (1997)

In the tests that were conducted, Russell and Burns measured transfer lengths that were consistently greater than the $50d_b$ estimate that is given by ACI and AASHTO for both the 0.5-in. and 0.6-in. diameter strand. The average transfer length that was measured for the 0.5-in. strand was $67.2d_b$ and the average transfer length that was measured for 0.6-in. strand was $66.2d_b$. These results show that the relationship between prestressing strand diameter and transfer length is linear, and it may not be well estimated by the code assumptions. The authors propose the following two equations to calculate transfer length based on their results.

$$L_t = 0.0725 f_{se} d_b \quad (SI) \qquad (3-1)$$

$$L_t = \frac{f_{se} d_b}{2} \quad (US\ Units) \qquad (3-2)$$

These equations include the magnitude of the prestressing force as well as the diameter of the prestressing strand. These equations yield an estimate for transfer length that is closer to the $67d_b$ that was observed in the tests along with a 20% factor of safety.

3.3 Walraven and Mercx (1983)

Walraven and Mercx (1983) reported the first experimental study that measured the transfer length of prestressing strand in HCS directly. As part of the experimental study that was conducted to investigate the flexural and shear capacity of HCS, the authors conducted tests on two HCS in order to measure the transfer length of the prestressing strand. Each test was conducted on a 20-foot long, 10-inch deep HCS with six ½" diameter strands in them. Reference points were installed on the bottom concrete surface along the six prestressing strands on each side of the centerline for 40 inches. The slab was then sawn at the centerline and the strain due to the saw cut was measured and plotted. The point at which the strain change vanished was determined to be the transfer length. Figure 3-3 shows the strain profile that was measured.

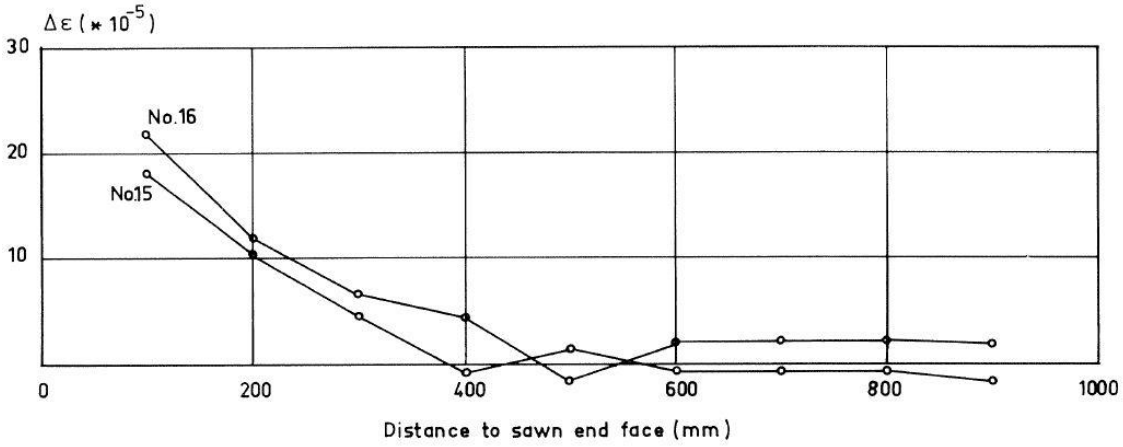

Figure 3-3: Concrete Surface Strain Profile Recorded by Walraven & Mercx (1983)

From the strand profile the transfer length was determined to be 400mm (15.75-in.) and 500mm (19.69-in.) for Tests One (No. 15) and Two (No. 16) respectively. This translates to $32d_b$ and $40d_b$, both of which are less than $50d_b$ prescribed by ACI 318.

3.4 Palmer and Schultz (2010)

In 2010, Palmer and Schultz conducted two exploratory transfer length tests in conjunction with their investigation into the web shear strength of deep HCS. The two tests were conducted on 16-in. deep HCS from two different manufacturers. The authors conducted the transfer length study because they hypothesized that with a dry/low slump concrete mix and a deep HCS, the concrete around the prestressing strand will not be as well consolidated as it might be in other precast members. This would reduce the strength of the bond between the prestressing strand and the concrete and lead to a longer transfer length.

The tests were conducted using a modification of the test procedure pioneered by Walraven and Mercx (1983). The test was conducted by placing a 20ft HCS on three supports, one in the center and two at the ends, and saw cutting the slab at the center (10ft from the end). Figure 3-4 shows and elevation view of their test set up. Two lines of linear electrical resistance strain gauges were placed along webs of the HCS on both sides of the line to be cut. The strain gauges were attached directly to the concrete. The strain gauges were placed at intervals of six inches in the first test and eight inches in the second test. In the second

test vibrating wire strain gauges were also used with the electrical resistance strain gauges. Strain measurements were taken before the saw cut, when the HCS was resting on the three supports, as well as several times after the saw cut released the prestressing strand.

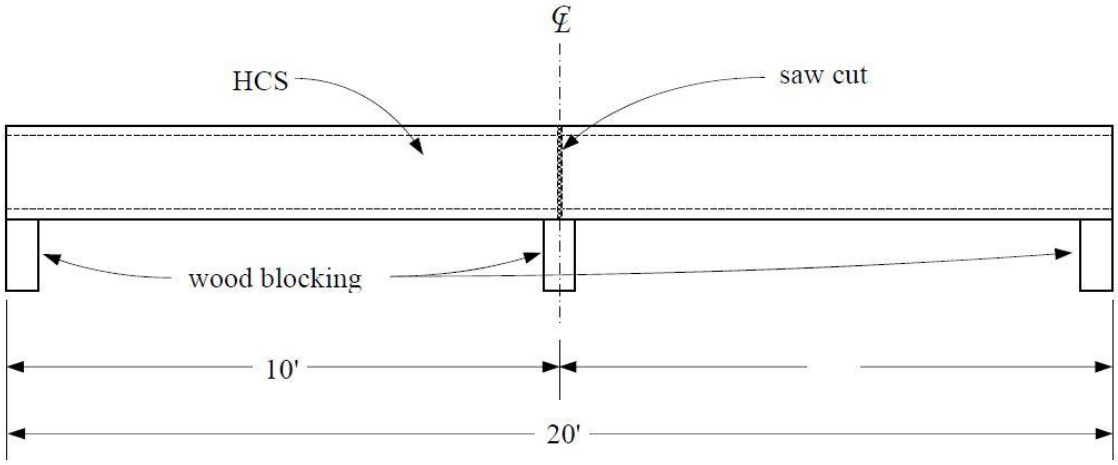

Figure 3-4: Palmer and Schultz (2010) Transfer Length Test Layout

Using this test set up, the authors measured the change in surface strain of the concrete nearest the prestressing strands. The change in strain of the concrete is inverse to the change in strain of the prestressing strand. When the strand is released it wants to shrink to its original state before it was stressed. When the precompression force is decreased in the transfer length region due to the strand release, the concrete wants to expand to its original uncompressed state.

In order to determine the transfer length from the tests, the authors evaluate the change in strain of the concrete before and after the saw cut. The authors corrected this change in strain reading because the support conditions change before and after the saw cut. The author's do not give a good definition of how the strain readings were corrected. It is implied that before the saw cut there is one member with a center support causing negative moment in the center and after the saw cut there are two simply supported members. This may not be a correct assumption to make because it assumes that all three supports are at the same height. This would be an unrealistic situation. Figure 3-5 shows the corrected change in strain measurements for the first test that was conducted. The first point at a

distance equal to zero from the saw cut was obtained from interpolation of the other points. This point was needed in order to define the transfer length. This point could not be measured however because the strain gauges have a finite length, and the saw-cut end of the slab rested on the center support which also had a finite dimension.

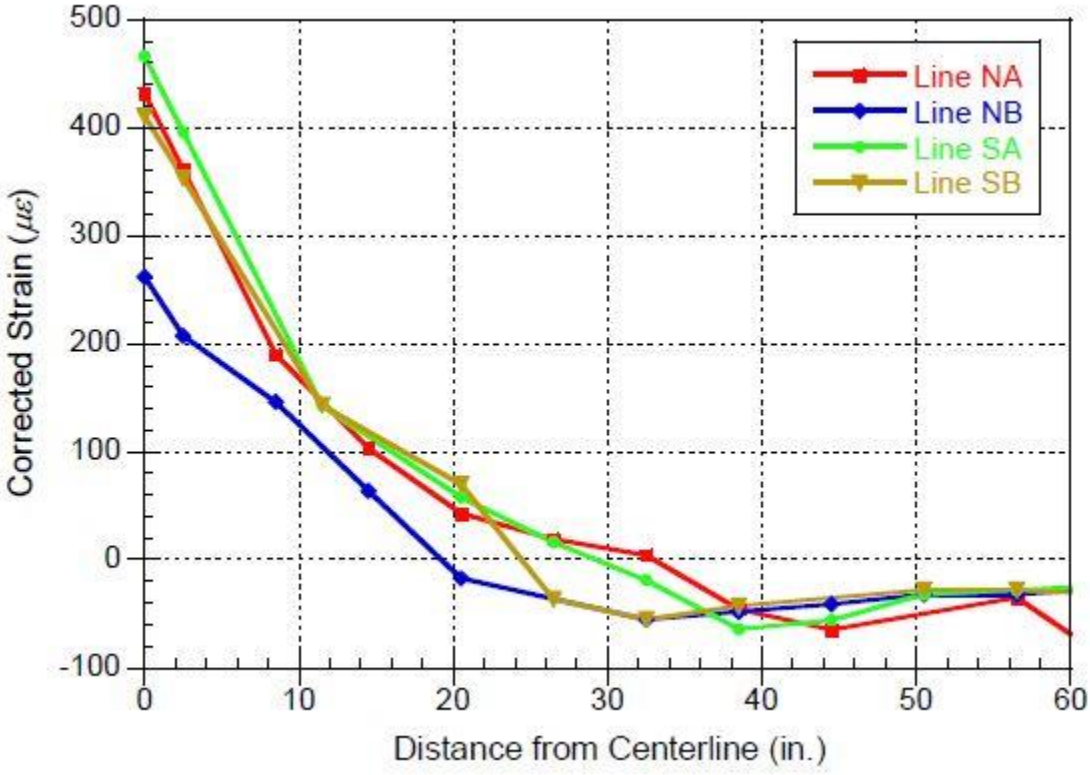

Figure 3-5: Corrected Strain Changes from Palmer and Schultz (2010)

In order to define the transfer length, Palmer and Schultz (2010) used modified versions of the method that Russell and Burns (1997) proposed. The two methods used are given below.

> *Method I* - The length along the HCS bottom face in which the measured concrete strain change profile varies from a maximum value at the cut end to the first instance of a value that represents a reduction of 95% of the peak strain change recorded.

Method II – 95% of the length in which the concrete surface strain change drops from a maximum value at the cut end to the first instance of the smallest strain change recorded.

The results that the authors obtained from using these two methods are given in Table 3-1. These procedures yielded transfer lengths larger than $50d_b$, which is the commonly-used estimate of transfer length recommended by ACI 318, for the HCS from one of the producers (Test 1).

Table 3-1: Palmer and Schultz (2010) Transfer Lengths

Test Number	Average L_t [in.] – Method I	Average L_t [in.] – Method II	Average L_t/d_b – Method I	Average L_t/d_b – Method II
Test 1	31.61	35.15	63.23	70.30
Test 2	25.81	28.50	46.93	51.82

3.5 Brooks, Gerstle and Logan (1988)

In this experimental investigation, the authors look at the effect that the initial strand slip has on the strength of HCS. When HCS are produced, a very long continuous element is cast and the desired lengths are saw-cut from the long casting. When the HSC is saw cut, there is some initial strand slip at the face of the saw cut where the strand shrinks back into the concrete. This strand slip is very small, typically 1/32-3/32in, but it is large enough be measured. The purpose of this study was to relate the magnitude of this ends slip to the strength of the HCS.

In order to relate the initial strand slip to the strength of the HCS the authors use what they call Strand Slip Theory (Appendix G). In this approach, a constant uniform bond stress is assumed along the transfer length, and equilibrium requires a linear distribution of strand axial stress. The strand stress translates to a linear distribution of axial strain, and when it is integrated along the strand it yields the end-slip. With the Strand Slip Theory, the initial end slip can be related to the transfer length using Equation 3-3. In this equation, δ is the

measured initial end slip, E_{ps} is the modulus of elasticity of the prestressing strand, and f_{si} is the stress in the prestressing strand before the saw-cut. From here the maximum prestressing force that can be developed at a given distance from the end of the slab can be calculated, and the shear and moment capacities can be obtained from that value of prestressing force. This can be used to define a moment capacity profile along the length of the HCS.

$$L_t = \frac{2\delta E_{ps}}{f_{si}} \qquad (3-3)$$

In the experimental portion of the study, 8-in. deep HCS were tested until failure. The HCS were loaded with a single point load at a varying distance from the support. Before and during the tests, the strand slips were measured. All but one of the HCS that were tested had an end slip that was greater than the allowable end slip. The allowable end slip was calculated using Equation 3-3 and the design code equations for transfer length.

In all of the tests that were conducted with an initial end slip greater than the calculated allowable end slip, the design code estimated higher moment capacities than the failure moment. This is expected because slabs that were selected for testing had excessive end slip, implying that their transfer length is longer than the estimated length according to ACI 318. The allowable end slip is defined as the initial end slip at the saw cut that results in a transfer length equal to Equation 3-4. Equation 3-4 is provided by ACI 318 as an estimate of the transfer length. In this equation, f_{se} is the stress in the prestressing strand after all losses and d_b is the diameter of the prestressing strand. Using this formula for the transfer length, the capacity or maximum load for the member were calculated using the V_{ci} and V_{cw} equations for shear provided by ACI 318.

$$L_t = \frac{f_{se} d_b}{3000} \qquad (3-4)$$

The End Slip Theory was a conservative prediction for the failure load in all but two of the tests. Figure 3-6 shows a graph of the ratio of the failure moment to the predicted

failure moment at the location where the load was applied. In this graph it can be seen that the End Slip Theory prediction is a more conservative prediction for the failure load of the HCS than the code assumptions for slabs with excessive end slip. This slight over prediction of moment capacity in most of the tested slabs was taken by the authors that the end-slip theory also overpredicts transfer length slightly.

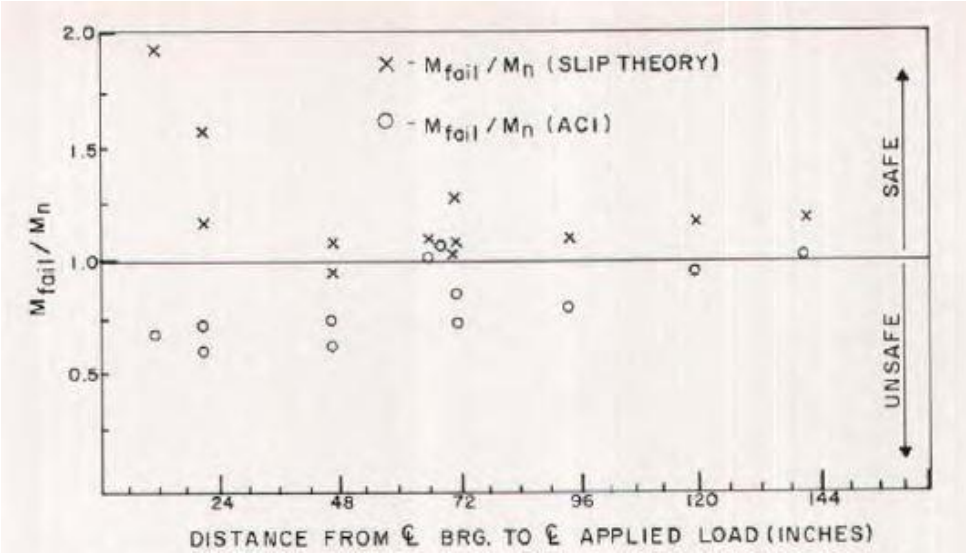

Figure 3-6: Ratio of observed failure moment to predicted failure moment

3.6 Marti-Vargas and Hale (2013)

In this paper, the authors compile the results of several tests that have been conducted in the past to measure transfer length. The authors then compare these results to the Eurocode (2004), ACI 318 (2011), and AASHTO (2012) code previsions for transfer length. The transfer length is a function of how well the bond stress between the prestressing strand and the concrete can transfer the prestressing force. This bond stress is created by three components. They are adhesion, friction, and mechanical action.

The Eurocode gives Equation 3-5 as an estimation of transfer length. In this equation α_1 accounts for the release procedure, α_2 is the strand area factor, ϕ is the strand diameter, σ_{pm0} is the strand stress just after release, and f_{bpt} is the constant bond stress between the concrete

and the strand. This bond stress is calculated based on the strength of the concrete at the time of release as well as properties of the type of prestressing strand used.

$$l_{pt} = \alpha_1 \alpha_2 \phi \frac{\sigma_{pm0}}{f_{bpt}} \qquad (3-5)$$

The equation used by the Eurocode to approximate the transfer length takes into consideration concrete strength, properties of the prestressing strand, and the release procedure. Based on previous research these are parameters that have been known to have some impact on the transfer length. The equation that is used in ACI 318 is given in Equation 3-6. In this equation, f_{se} is the prestressing force after all losses and d_b is the diameter of the prestressing strand.

$$L_t = \frac{f_{se} d_b}{3000} \qquad (3-6)$$

Unlike the Eurocode approximation for transfer length, the ACI 318 equation for transfer length only considers the diameter of the prestressing strand. It also uses the effective prestressing force (prestress force after all losses) while the Eurocode uses the initial prestressing force. This is also what is seen in AASHTO, the North American bridge design code.

The authors then compiled transfer length results from previous experiments and compared them to the code predictions. All of the tests that were compiled were conducted between 1970 and 2007. In these transfer length studies, the transfer lengths were determined by either measuring the surface strain of the concrete, a strand push-pullout test, or measuring the strand force at various cross sections. It appears that none of the transfer length measurements that were compiled by Marti-Vargas and Hale (2013) were conducted on specimens that were cast with a dry concrete mix.

The authors then compared the code predictions for transfer length with what was seen in the published studies. The ACI 318 predicted values for transfer length that varied only

from 23.6-in. to 31.5-in. because it is based only on prestressing force and strand diameter. The Eurocode predictions varied from 25.6-in. to 51.2-in.. The greater range for the Eurocode follows because it also considers properties of the concrete. Figure 3-7 and Figure 3-8 shows the ratio of the calculated transfer length to the transfer length that was recorded in the testing. Figure 3-7 is for ACI 318 and Figure 3-8 is for the Eurocode.

It can be seen from these figures that, on average, both code assumptions overpredict the transfer length in most cases, especially when the measured transfer length is less than 400mm (15¾ in.) On average the Eurocode predicts a transfer length that is 1.73 times greater than what was observed while the ACI 318 code predicts a transfer length that is 1.27 times greater than what was observed. ACI 318, however, underpredicts the transfer length in about 40% of the tests.

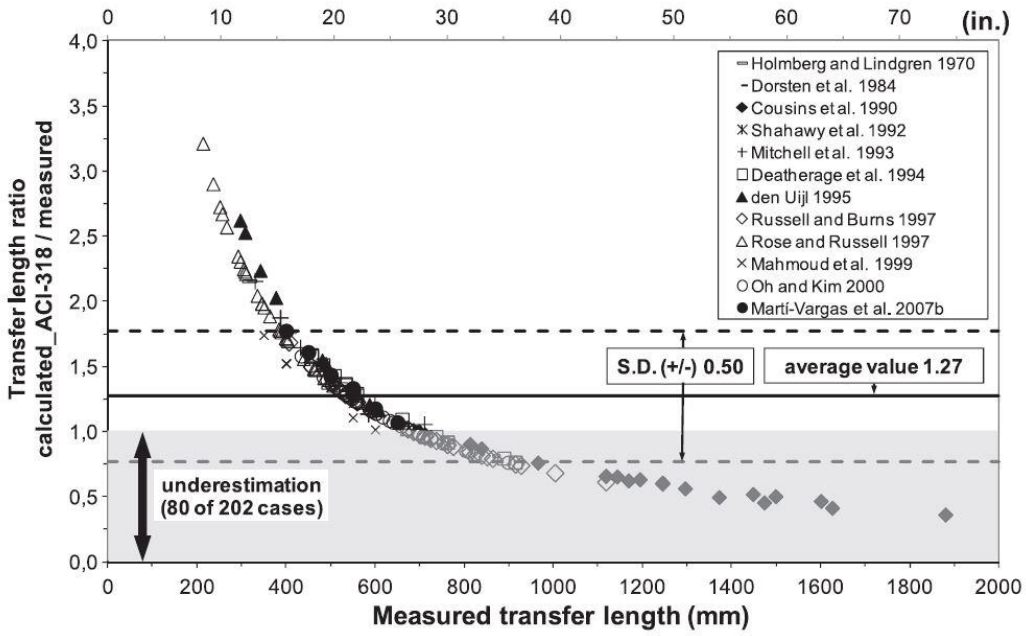

Figure 3-7: Ratio of ACI 318 prediction of transfer length to measured transfer length

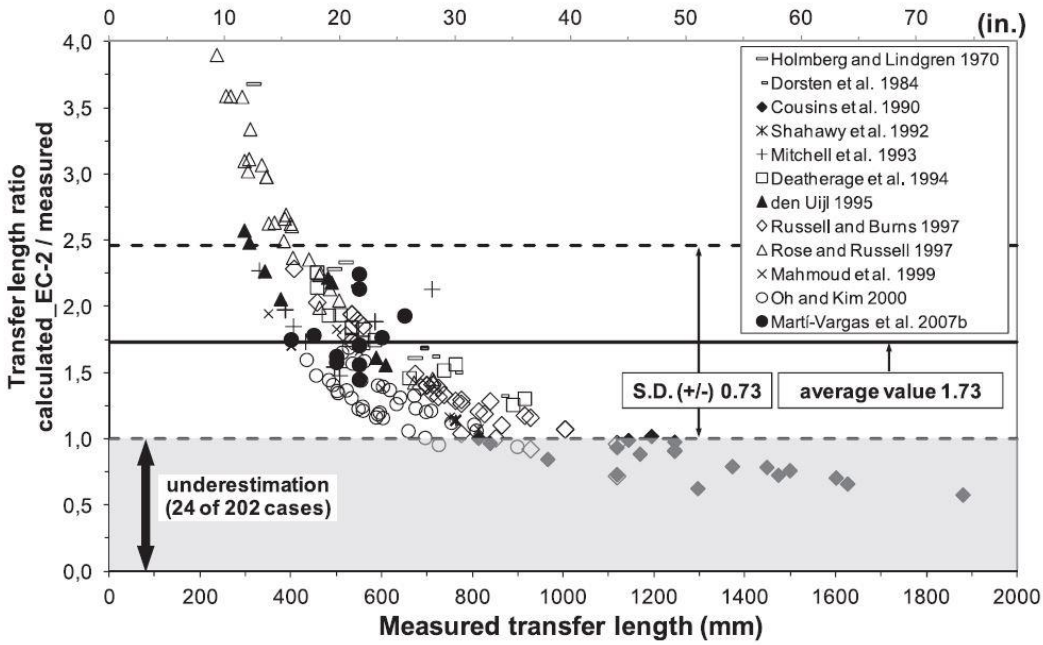

Figure 3-8: Ratio of Eurocode prediction of transfer length to measured transfer length

3.7 Marti-Vargas (2006)

In this experimental study, the authors investigate the transfer length and development length of seven wire prestressing strand embedded in concrete. In order to determine the transfer length and development length of the strand, the authors propose a testing procedure that they call ECADA. This test procedure is a combination of pull-out test and a strand push-in tests. The test setup allows a single specimen to be tested using the strand push-in test and then having a strand pull-out test conducted just my moving a hydraulic actuator. By conducting the two different tests on the same specimen, the authors are able to produce transverse expansion of the prestressing strand (Hoyer Effect) for their pull out tests. This transverse expansion occurs when the strand is released. Due to the Poisson effect of the prestressing strand, the strand gets wider after release. This creates a wedging effect that can cause the strand to have a greater pull out strength. The Hoyer effect is present in HCS transfer length tests where the HCS is saw cut such as what Walraven and Mercx (1983) and Palmer and Schultz (2010) conducted.

Strand pull-out and push-in tests are two tests that have been used in previous research for determining the transfer length and development length for prestressing strand. The pull out test is conducted by embedding a length of prestressing strand into concrete and then pulling on the strand and recording the force at which the strand pulls out. Various embedment lengths can be used to find at which embedment length will cause the strand to reach its maximum capacity.

The push-in test works by stressing a strand between two plates with a third plate fixed in the middle. A concrete specimen is cast around the prestressing strand with one end of the specimen bearing on the center plate. The strand is then released above the specimen and the strand gets pushed into the concrete specimen because the center plate does not allow it to move towards the bottom plate. Figure 3-9 shows a setup for a strand push-in test.

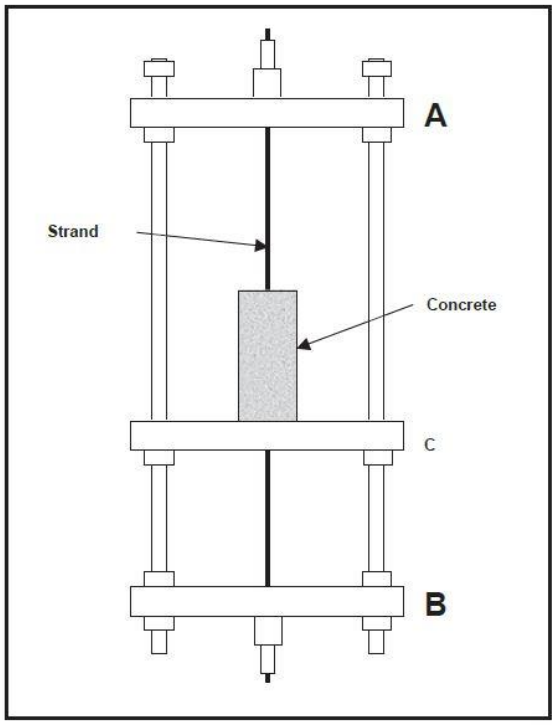

Figure 3-9: Strand Push-In Test Setup

In order to combine both of these tests, the authors proposed the setup that is shown in Figure 3-10. In this test setup the strand is stressed between plates D and B. A concrete

specimen is then cast so that it is bearing on plate C. Once the concrete is at the desired strength for testing, the strand is released at plate D. This causes the strand to be pushed into the concrete specimen. The hydraulic actuator is then positioned at plate B and a strand pullout test is conducted. This test setup allows for transverse expansion of the strand caused by the strand push-in test to occur before the strand pull-out test is conducted. This is a better representation of what occurs in a precast member when it is released.

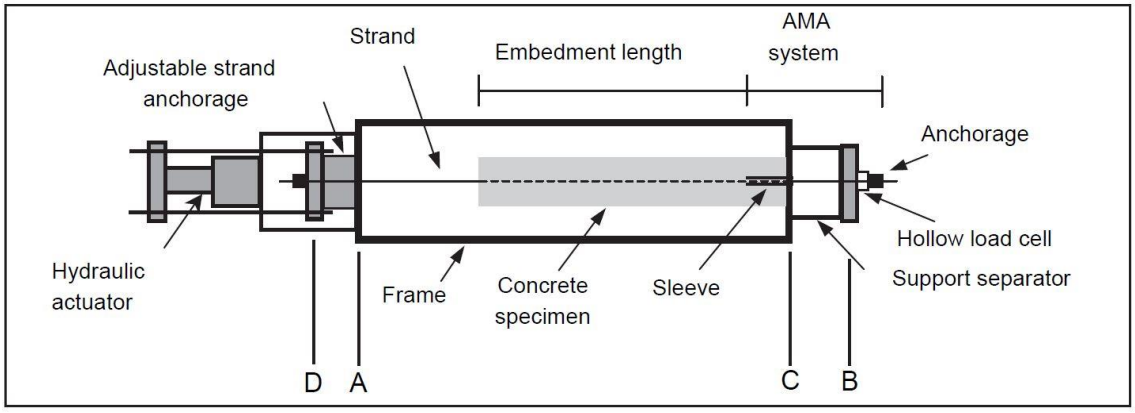

Figure 3-10: ECADA Test Setup

In this experimental program, the authors tested specimens with different embedment lengths, concrete mixtures, and concrete strengths. Based on the results of the test, the authors saw a linear relationship between the initial concrete strength and the transfer length. As the initial concrete strength increases the transfer length decreases. The authors proposed the following equation, given in U.S. Customary units, for calculating transfer length from initial concrete strength.

$$L_t = 29.85 - 0.0016 f'_{ci} \qquad (3-7)$$

This equation was developed for strand with a diameter of 0.5-in. Based on the results that were seen from these tests, the authors found that the ACI estimate of transfer length to be $50d_b$ to be a conservative assumption.

Chapter 4 Proposed Method for Evaluating Transfer Length

4.1 Distributed Strain Sensor

The method proposed for measuring the transfer length in HCS utilizes a device called a Distributed Strain Sensor (DSS). The DSS consists of a thin rectangular strip of material that has electrical resistance foil strain gauges attached to it along one face. The strip is attached using an adhesive to the bottom face of a HCS beneath a prestressing strand. The DSS is used in in a similar method to what Palmer and Schultz (2010) employed for their transfer length tests. However, with the DSS, the electrical resistance foil gauges are attached to the DSS instead of directly to the bottom concrete surface of the HCS. Figure 4-1 shows the proposed DSS attached to a HCS. The gauges are pre-wired with electrical leads, and the leads are connected to a portable data logger for rapid acquisition of the strain data.

Figure 4-1: DSS Attached to HCS during Field Tests

4.2 Proposed Transfer Length Test

4.2.1 Proposed Test Setup

The proposed test set up is similar to the transfer length tests conducted by Palmer and Schultz (2010). The process begins when the strands are released in the precasting bed and

the HCS sections are cut to size. As quickly as possible, a section of HCS, roughly 20ft in length, is lifted from the bed and placed on supports at each end of the slab so that work can be performed underneath the HCS. While the HCS is resting on the supports, the DSS are installed using a rapid setting adhesive. The DSS is installed beginning near the centerline of the HCS, that is where the HCS will be saw cut during the transfer length test, and extending toward the supports. The DSS are also placed directly beneath a prestressing strand. For repetition, the DSS are installed so as to mirror each other across the centerline of the HCS. The HCS is then lifted back onto the precasting bed and placed on three supports, one at each end and one in the middle. The middle support is located directly underneath the location where the slab is to be saw cut. Figure 4-2 shows the DSS attached to the HCS resting on the supports ready to be sawn.

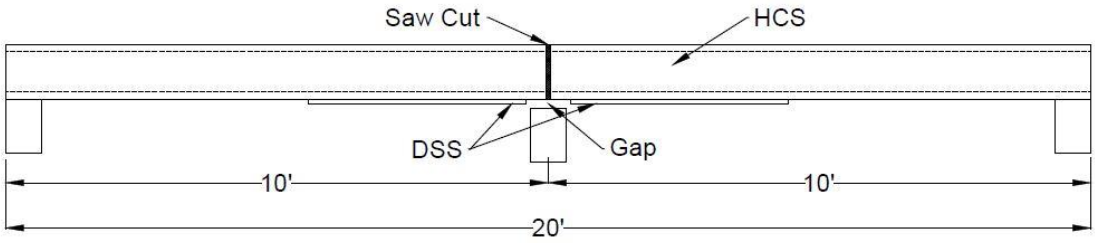

Figure 4-2: Proposed Transfer Length Test Elevation

The HCS is then saw cut along the centerline. There should be a small gap between the center support and the HCS. The gap need not be large; just enough so that there is no bearing of the HCS on the center support. This is needed in order to prevent negative bending in the HCS before it is saw cut, discussed in Appendix E.1. Strain readings are taken before the HCS is saw cut, as well as several times after cutting. The change in strain before and after the cutting is used to determine the transfer length. When the HCS is cut, the initial precompression strain in the concrete is released at the cut line. The distance from the gauges to the cut section in the HCS is inversely proportional to the magnitude of precompression strain that is released upon cutting. These strain changes are restrained by the bond between the prestressing strand and the concrete, and this restraint decreases the closer the gauges are to the far ends of the HCS. At the end of the transfer length, that is away from the cut section, there should be no change in strain reading.

4.2.2 Proposed Methods for Determining Transfer Length

The methods for determining the transfer length from the measured concrete surface strain change is the same as what Palmer and Schultz (2010) used. These two methods are modified versions of what Russell and Burns (1997) used. The definition that Russell and Burns (1997) used for transfer length required the strain in the prestressing strands to be known, whereas the DSS measures the strain in the concrete around the prestressing strand. Therefore, the Russell and Burns methods had to be modified. Russell and Burns defined the transfer length as the length along the tendon in which the measured strand strain profile changes from a value of zero at the cut end to the first instance of a value of 95% of the peak strain recorded. A value of 95% is used in order to eliminate any error that can occur from the strain readings. Strain readings taken using linear electrical resistance foil strain gauges can be noisy and can often show random strain trends. Eliminating the last 5% of the peak strain should eliminate these random trends.

The first method, which is referred to as Method I, defines the transfer length as the length along the HCS bottom face in which the measured concrete strain change decreased by 95% of the peak strain change from the maximum value at the cut end. For the second method, Method II, the transfer length will be defined as 95% of the length over which the concrete surface strain change drops from a maximum value at the cut end to the first instance of the smallest strain change recorded. Both Method I and Method II are used to determine the transfer length when the DSS is used in the field.

4.3 Advantages of the Distributed Strain Sensor

There are several important advantages that the DSS provides over other methods for measuring the transfer length in HCS. The first of which is how quickly and easily the DSS can be installed and be made ready to test. Determining the transfer length in a HCS can be a lengthy process. Strain readings in the strand or adjacent concrete surface should be taken at the time when the plant cuts the HCS to length for installation. This is usually 18-24hrs after the HCS are cast. This will give the most accurate representation of what will

happen with a typically HCS when it is cast and stripped. Taking readings at different times could result in a higher concrete strength and a less accurate transfer length reading.

The DSS allows for a much quicker installation. A layer of fast-setting adhesive can be applied to the DSS, and the DSS can be attached immediately to the HCS. The DSS can be installed and be ready for testing in a matter of minutes. If the electrical resistance foil strain gauges are attached directly to the HCS, it takes several hours to prepare the surface of the HCS and attach each gauge individually. Additionally, the process of wiring the strain gauges lead wires to the data acquisition system is also time-consuming. The quick installation of the DSS, as well as the opportunity to have the DSS lead wires connected to the data acquisition system prior to installing the DSS, enables the transfer length test to be conducted in a time duration much closer to when the slabs would be saw cut in the normal production process.

Another advantage of the DSS is the ability to reuse the strain gauges for multiple tests. After one test is conducted, the DSS can be removed from the HCS. The adhesive and concrete chips can be removed from the metal surface, and the DSS can be reused again in another test. This is a large cost savings if many transfer length tests are to be conducted because electrical resistance foil strain gauges cost approximately $15 per gauge at the time of writing this document. Foil gauges that are bonded to a concrete surface cannot be reused. Thus, in a transfer length test where the gauges are bonded directly to the HCS, all of the gauges used in that test cannot be reused for another test.

The DSS also allows for the gauges to be preinstalled before each test. The installation of electrical resistance foil strain gauges is a detail-oriented process that must be performed with care. The surface on which the gauge is to be bonded needs to be prepared and cleaned meticulously. An unclean surface may result in incorrect strain readings, or no readings at all. Thus, gauges can be installed on the DSS in a clean environment before deploying to a precast plant for testing. If the gauges are installed directly on the HCS, installation must be performed at the precast plant where dust can affect the integrity of the strain gauge installation. At the precasting plant the gauges would also have to be installed upside down

because they need to be bonded to the bottom of the HCS. This makes it more difficult to get adequate bond between the gauge and the bonding surface because the bonding adhesive will naturally want to drip off the bottom of the HCS. While the DSS is also installed upside down on the bottom face of the HCS, the continuous rigid strip provides backup that prevents loss of adhesive from dripping.

4.4 Concerns with Distributed Strain Sensor

While there are many advantages to the DSS, there are several concerns that need to be addressed for effective use in transfer length tests. The first of these is that there may be some localized reinforcing effect caused by the DSS after it is bonded to the HCS. If the DSS were made from a material such as steel, which has a considerably larger modulus of elasticity than concrete, it may act like external reinforcing. If the concrete is locally reinforced by the DSS, the strain readings will be smaller than for the slab without the DSS, this testing artifice will result in shorter transfer lengths.

Another concern with the DSS is the manner in which the strain will vary along the length of the DSS. Ideally the strain in the DSS should match the strain in the concrete exactly. Since the DSS and the adhesive are made from different materials that may not be the case. The DSS may disturb the strain field along the length of the DSS, including shear lag at the ends of the DSS as the strain builds up starting at the end of the DSS.

The preceding concerns are addressed in the analytical and experimental testing phases of the DSS methods development program that is described in this document.

Chapter 5 Finite Element Analysis of DSS

5.1 Model Set Up

In order to verify the feasibility of using the DSS in transfer length tests on HCS, an analytical study was conducted before proceeding with laboratory testing. A linear, elastic three-dimensional (3D) finite element model was constructed using the software ABAQUS. The models were defined with sufficient features to investigate the applicability of the DSS for measuring surface strains in HCS. Therefore, the principal goal of these analyses was to simulate accurately the stress and strain interaction between the DSS and the bottom surface of the HCS under conditions that are present upon release of the strand. For this reason, the concrete and steel were assumed to be linear elastic, and the prestressing strands were not modeled.

This structure that was modeled and analyzed using finite element methods was also used in large-scale laboratory tests. The structure consists of a simply supported HCS with two line loads across the width. The line loads are equidistant from the supports so as to create a constant moment region in between the two lines. A constant moment region means that there is also a constant strain in that region, and the DSS were attached to the HCS in the constant moment region. The strain in the DSS was compared to the strain on the bottom face of the HCS. Figure 5-1 shows the system that was modeled.

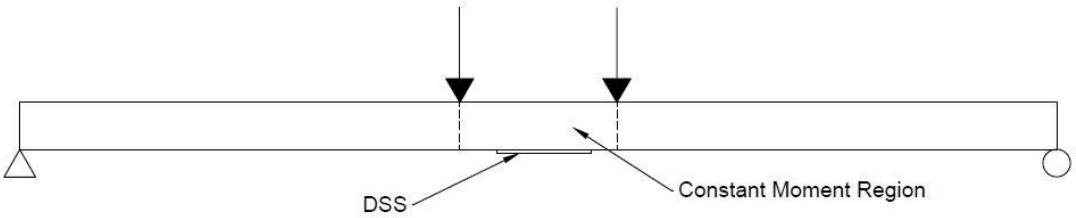

Figure 5-1: System for finite element analysis

In the finite element model of the HCS structure in Figure 5-1, the prestressing strands were not simulated, given that accurately representing the prestressing strands can greatly increase the computational time and their effect on the stress-strain interaction of the DSS

and concrete surface is negligible. This analysis was conducted to investigate the local behavior of the DSS interaction with the concrete surface of the HCS and to see how the strain in the DSS compares to the strain in the HCS. Exact strains are not necessarily required because a qualitative profile of the surface strains along the bottom of the HCS will suffice to determine the transfer length. Figure 5-2 shows the cross section of the HCS which feature the cross section of the product donated by Molin Concrete Products Company for the laboratory tests. The finite element model was created with this cross section using eight-node brick elements that were approximately four inches on each side for the HCS, and 0.25 inches on each side for the DSS.

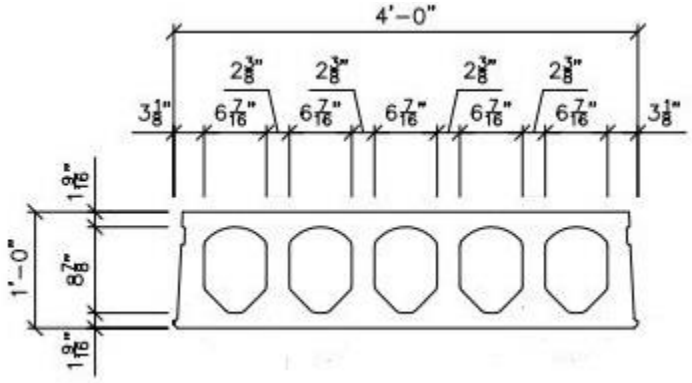

Figure 5-2: HCS Cross Section

In modelling the prototype structural system, perfect bond was initially assumed between the HCS and the DSS in Phase I. This scenario is an unlikely idealization, but was used initially to investigate the viability of the DSS System. In other words, if the DSS produced unwanted disturbances in the measured strain fields when perfectly bonded, then it would likely be inadequate for more realistic cases of adhesive bond. Perfect bond was modeled using a tie constraint in ABAQUS and tying the nodes connecting the DSS elements to the HCS elements. In the analyses for Phase II, the adhesive was simulated allowing relative deformation between the DSS and HCS surface.

The DSS was 'installed' on the bottom surface of the HCS model in the constant moment region. Figure 5-3 shows the top and bottom of the HCS in the 3D model set up. The DSS

can be seen along the bottom of the HCS, and the lines on the top surface of the HCS are the locations where the area loads were applied.

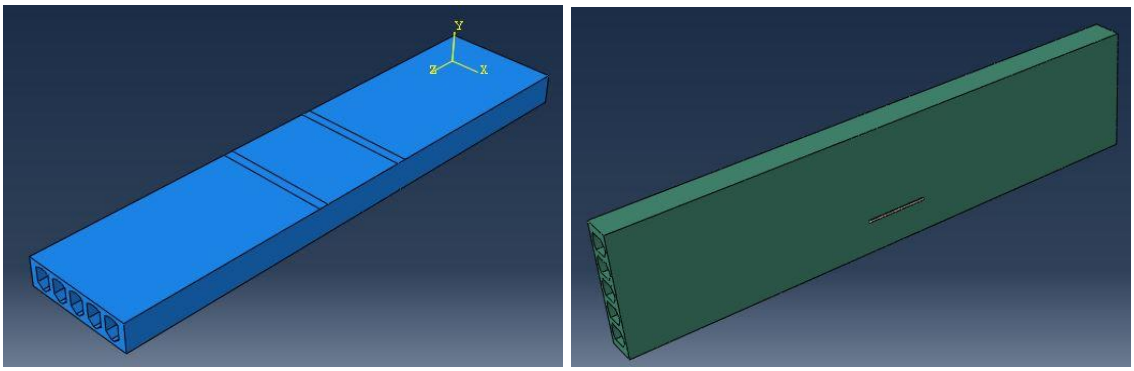

a) Top of HCS b) Bottom of HCS

Figure 5-3: 3D FEA Setup

Boundary conditions for the supports were defined by preventing the nodes at the bottom of the HCS at each end from moving vertically. At one end, the nodes at the bottom were not allowed to move horizontally along the axis of the HCS to simulate a pin, whereas at the other end, unrestrained horizontal movement was allowed to represent a roller condition.

5.2 Variables Investigated and Performance Criteria Evaluated in Phase I

5.2.1 Variables Investigated

The finite element analysis in Phase I was conducted in order to determine the feasibility of using the DSS in transfer length tests as well as to determine some variables affecting the performance of the DSS. These variables include the DSS material, as well as the width, thickness, and length of the DSS. These variables were investigated in order to limit the number of laboratory tests that followed the analytical effort of the project.

In total, three different materials were investigated. They were A36 steel, Alloy 6061 aluminum, and Plexiglas® Acrylic Polymer. These materials were chosen because they are

readily available for fabricating the DSS, they are quite economical, they are easily cut and machined, and they offer a range of elastic moduli for investigating their applicability for the DSS material. Steel is the ideal choice for making the DSS because it is very durable and could be used for repeated tests. However, it is the stiffest and may locally reinforce the HCS, thus affecting the strain readings. Aluminum offers a high durability as well, but it has a lower elastic modulus so the localized reinforcing effect would be less pronounced than for steel. Plexiglass is the least durable but has an elastic modulus most similar to that of concrete. See Appendix A.1 for a list of the material properties that were used in the analysis.

The dimensions of the DSS were also investigated. A thicker and wider strip of material would make the DSS more durable but it would also increase the total cross sectional area of the DSS. A larger cross sectional area would possess greater stiffness and would have the potential effect of increased local reinforcing of the HCS. A total of two widths for the DSS were analyzed, one inch and two inches. Three thicknesses were also analyzed: ¼ inch, $^{3}/_{16}$ inch, and $^{1}/_{8}$ inch. The length of the DSS was investigated in the finite analysis even though it is a dimension for which there is less freedom in its selection. In order to be used in a transfer length test, the DSS longitudinal dimension needs be larger than the transfer length. This could be as long as five feet. Nevertheless, this variable was still investigated.

Several layouts with multiple DSS strips were investigated, in addition to one DSS strip attached to the HCS in the constant moment region. The first layout, show in Figure 5-4, is two DSS strips attached side-by-side. This layout was investigated to see the effect of having two DSS strips attached to a HCS for a transfer length test. This layout would allow for multiple transfer length readings to be taken from a single saw cut. The second layout, shown in Figure 5-5, is two shorter DSS strips laid end-to-end and attached to the HCS. Attaching two shorter DSS strips would be easier than attaching one long DSS. This gap in the DSS might cause discontinuities in the measured strain profile along the length of the DSS.

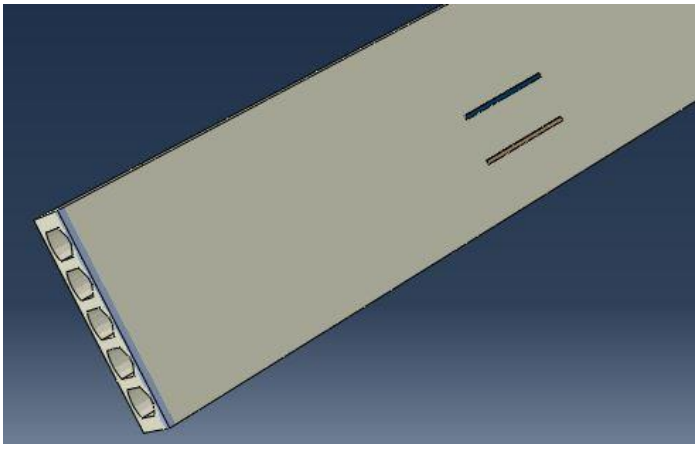

Figure 5-4: Side by side DSS layout

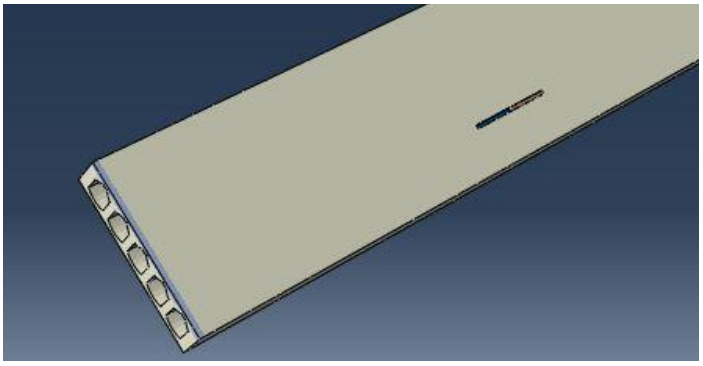

Figure 5-5: End to end DSS Layout

5.2.2 Performance Criteria

In order to determine if the proposed DSS is a viable option for use in measuring the transfer length of prestressing strand in HCS, several performance parameters were monitored in the finite element analysis. These parameters were chosen to evaluate various aspects of the performance of the DSS.

The first criterion that was monitored in the Phase I finite element analysis was the longitudinal strain profile on bottom face of the HCS across its width at the location where the DSS was attached. The intent here was to determine the extent to which the bonded DSS act like external reinforcement. To monitor this criterion, the stiffening parameter P_k was defined as the normalized change in longitudinal strain across the bottom face of the

HCS at the location where the DSS was attached. P_k can be computed using Equation 5-1. In this equation, $\varepsilon_{l,max}$ and $\varepsilon_{l,min}$ are the maximum and minimum longitudinal strains in the strain profile across the width of the HCS.

$$P_k = \frac{(\varepsilon_{l,max} - \varepsilon_{l,min})}{\varepsilon_{l,max}} * 100\% \qquad (5-1)$$

The second criterion that was evaluated was the longitudinal strain profile along the length of the DSS. The goal here would be to investigate if the DSS replicate the patterns of moment imposed on the HCS. The parameter D_{sl} was created to evaluate this criterion. D_{sl} is defined as the distance from the end of the DSS to a point where the longitudinal strain profile along the length of the DSS changes by less than 4%.

The last criterion that was evaluated in the finite element analysis was the tensile force (stress) between the DSS and the HCS at the ends of the DSS. Because of different stiffness properties and flexural shapes for the HCS and DSS, Peeling stresses (i.e tensile stresses normal to the bonded surfaces) can be generated at the ends of the DSS. If sufficiently large, the peeling stresses could break the adhesive bond between HCS and the DSS. To evaluate this criterion, the parameter P_p was defined as the tensile peeling force recorded normalized by the square root of the compressive concrete strength stress f'_c. If P_p was less than a value of 4 it was determined that no peeling would occur. This evaluation of P_p assumes that if peeling occurs it will occur in the concrete just below the adhesive layer.

5.3 Phase I Finite Element Results

In the finite element analysis that was conducted in Phase I, it was seen that changing the parameters of the DSS had little effect on the behavior of the model. While there were some slight changes in different strain values that were evaluated, they were small enough that they would fall within the noise of a strain gauge reading.

5.3.1 Transvers Distribution of Longitudinal Strain

Figure 5-6 shows the longitudinal strain across the width of the bottom of the HCS in the constant moment region. This path crosses where the DSS was attached to the HCS. For the graph that is shown in Figure 5-6, a 24-in. DSS made from steel was attached. The width of the DSS was one inch and the thickness was one-eighth of an inch.

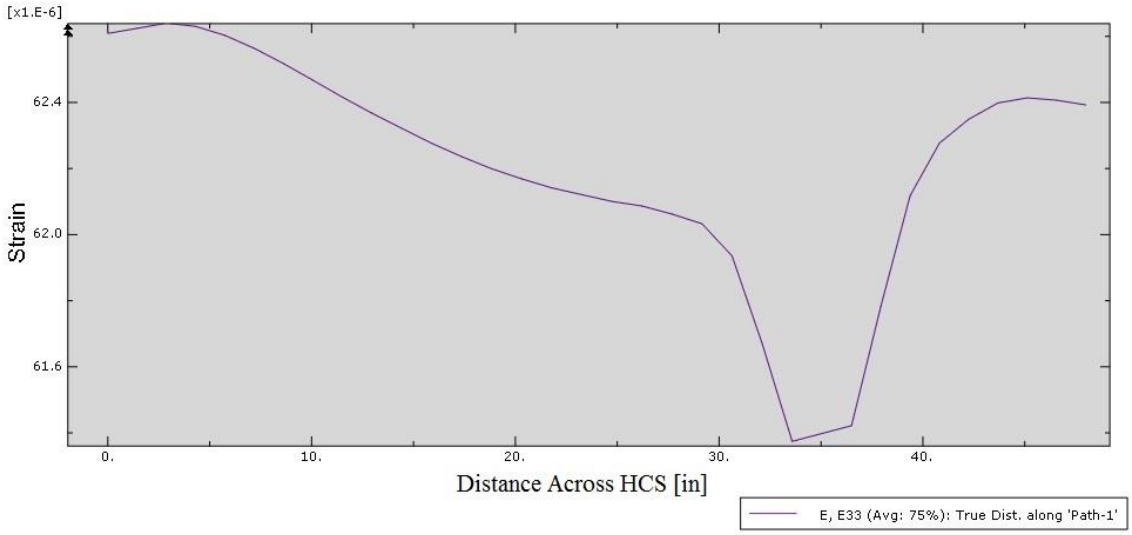

Figure 5-6: Strain across width of HCS

It can be seen in Figure 5-6 that there is a part of the graph where longitudinal strain decreases across the width of the HCS. This is the location of the DSS, and the decrease in the longitudinal strain is expected because the DSS, being made of a stiffer material, locally reinforces the HCS. The magnitude of this reduction in longitudinal strain is less than two microstrains ($\varepsilon < 2\text{x}10^{-6}$). The corresponding P_k value is 1.9% for the analysis reported in Figure 5-6. For other cases, Table 5-1 summarizes the reductions in strain in each case that was analyzed, as well as the corresponding P_k. It is also noteworthy that the reduction in longitudinal strain due to the stiffening effect of the DSS is within the noise that is typically seen when using electrical resistance foil strain gauges. It can be seen in Table 5-1 that changing the material, width, and thickness of the DSS affected the normalized change in longitudinal strain, P_k, by amounts less than 4%. Increasing modulus of elasticity of the

DSS material and increasing the cross sectional area of the DSS (increasing width and thickness) all increase parameter P_k.

Table 5-1: Normalized Change in Longitudinal Strain across HCS Width – Single DSS Layout

DSS Properties used in Analysis	P_k [%]
Steel, 12"x 1/8"x 1"	2.4
Steel, 24"x 1/8"x 1"	1.9
Steel, 40"x 1/8"x 1"	0.96
Steel, 24"x 1/8"x 2"	3.5
Steel, 24"x 3/16"x 1"	3.2
Steel, 24"x 1/4"x 1"	4.4
Aluminum, 24"x 1/8"x 1"	0.96
Plexiglass, 24"x 1/8"x 1"	0.64

5.3.2 Longitudinal Distribution of Longitudinal Strain in the DSS

The strain along the DSS was also measured. Figure 5-7 shows the longitudinal strain along the length of a 40 inch steel DSS with a width of one inch and a thickness of one-eighth inch. It can be seen that the strain along the length of the DSS is nearly constant except at the ends. At each end there is a shear lag where it takes some distance for the shear strains transferred from the HCS to the DSS to build up the longitudinal strain in the DSS. In this case that length is about two and a half inches. Shear lag was seen in all DSS that were modeled using the finite element method. The length of the shear lag increased slightly when the thickness of the DSS was increased. The shear lag distance D_{sl} for each DSS modeled can be seen in Table 5-2. The length of the shear lag were all approximately 2-3 inches for each DSS except for the case where the material of the DSS was Plexiglass. In this case the length of the shear lag was much lower.

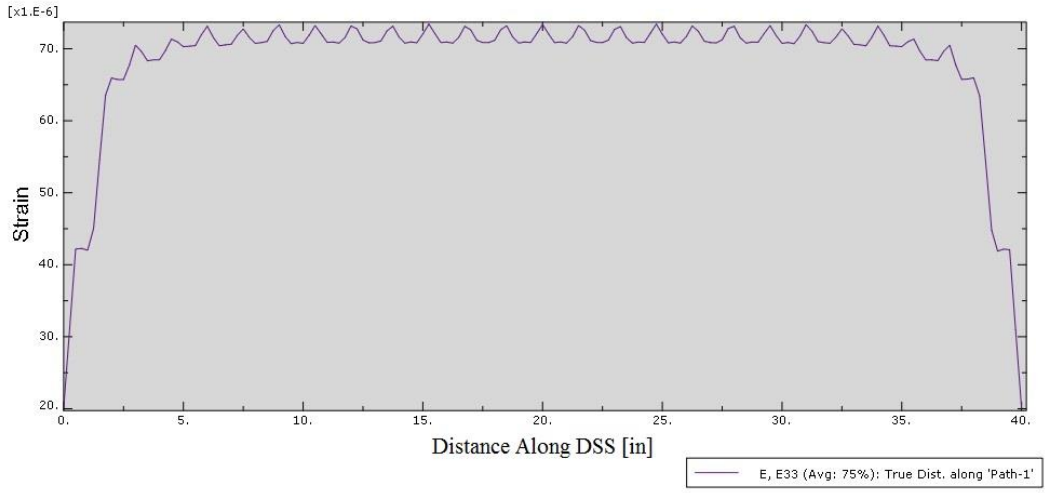

Figure 5-7: Strain along the Length of the DSS

Table 5-2: Shear Lag Distances – Single DSS Layout

DSS Properties used in Analysis	D_{sl} One [in]	D_{sl} Two [in]
Steel, 12”x 1/8”x 1”	3.0	2.3
Steel, 24”x 1/8”x 1”	2.5	2.3
Steel, 40”x 1/8”x 1”	2.5	2.5
Steel, 24”x 1/8”x 2”	2.5	2.3
Steel, 24”x 3/16”x 1”	2.7	2.5
Steel, 24”x 1/4”x 1”	3.3	3.2
Aluminum, 24”x 1/8”x 1”	2.5	2.1
Plexiglass, 24”x 1/8”x 1”	0.8	0.9

5.3.3 Multiple DSS Layouts

The layout of the DSS strips was investigated as well. Two different layouts were modeled. The first layout had two 24-inch DSS next two each other across the width of the HCS, and the second layout had two 12-inch DSS strips laid end-to-end longitudinally along the HCS.

This first layout was investigated to determine if two DSS could be used at the same time to measure transfer lengths below adjacent strands on the same side of one saw cut. If this

can be done, then multiple transfer length measurements could be taken in a single transfer length test. The major concern with this procedure is that having two DSS can produce even greater stiffening effect than a single DSS thus affecting the strain readings on the bottom of the HCS. Figure 5-8 shows the longitudinal strain of the bottom of the HCS across its width where the two DSS are attached in the constant moment region. Two locations where the longitudinal strain in the bottom of the HCS decreases were observed. These two locations coincide with the location of the two DSS. It can be seen that like with the single DSS strip that the magnitude of these two decreases are very small, about two microstrains ($\varepsilon \sim 2\text{x}10^{-6}$). The strain magnitude at the DSS locations did not decrease below the values computed for a single DSS. In Figure 5-6, for a single DSS of the same properties, the maximum strain was about 62 microstrains, and when two DSS were attached the maximum strain was still about 62 microstrains. Table 5-3 shows the computed value for the parameter P_k for this layout. The P_k value is slightly larger (~0.5%) than the case for a single DSS with the same properties.

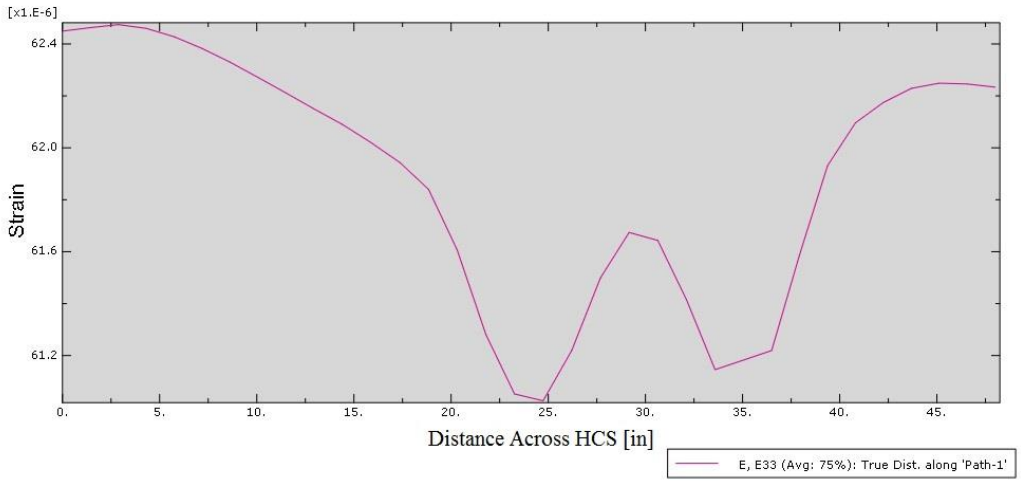

Figure 5-8: Strain across HCS for Two DSS

Table 5-3: Normalized Change in Longitudinal Strain across HCS Width – Multiple DSS Layout

DSS Properties used in Analysis	P_k [%]
Two Steel 24"x 1/8"x 1" Side-by-Side	2.4
Two Steel 12"x 1/8"x 1" End-to-End	1.9

For the layout with two DSS laid end-to-end longitudinally, the largest concern was with the continuity of longitudinal strain where one DSS ends and the other one begins. In particular, since each DSS will have a shear lag distance (D_{sl}), the addition of these two lengths would create a large disturbance in the strain profile. Figure 5-9 shows the longitudinal strain profile along the length of the two DSS. It can be seen that the strain reading is approximately constant along the two DSS away from the shear lag regions. However, in the shear lag regions the sudden end of the DSS creates a disturbance. Interestingly, in the shear lag regions where the DSS are closest to each other, the strain actually increases over the shear lag region. The conclusion here is that if two DSS are used, accurate strain measurements cannot be made for a total length of two shear lag distances ($2D_{sl}$) where the DSS are installed end-to-end. The shear lag distance D_{sl} can be seen in Table 5-4.

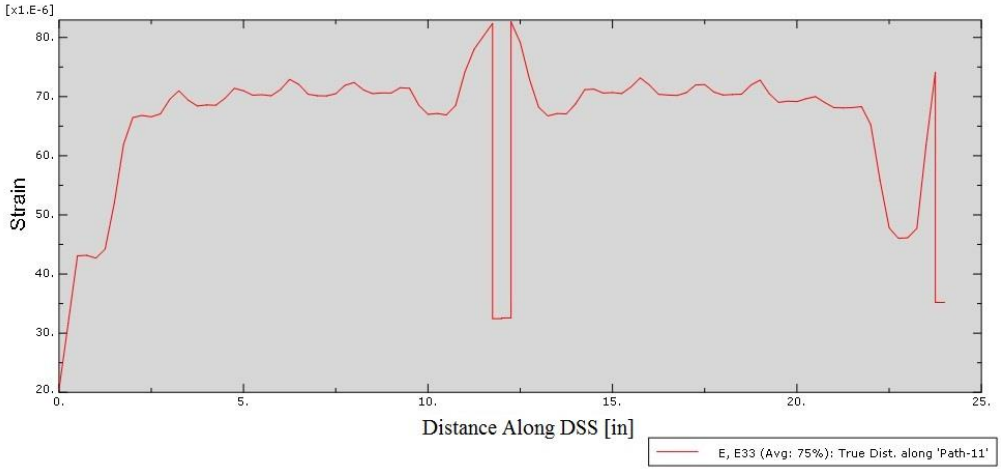

Figure 5-9: Longitudinal Strain along Two DSS Laid End-to-End

Table 5-4: Shear Lag Distances – Multiple DSS Layout

DSS Properties used in Analysis	D_{sl} One [in]	D_{sl} Two [in]	D_{sl} Three [in]	D_{sl} Four [in]
Two Steel 24"x 1/8"x 1" Side-by-Side	2.5	2.3	2.5	2.3
Two Steel 12"x 1/8"x 1" End-to-End	2.4	1.4	1.4	2.3

5.3.4 Tensile Peeling Stresses

The tensile peeling stresses at the ends of the DSS were also monitored. This was done to ensure that the DSS would not debond from the HCS due to the applied moment during testing. Table 5-5 shows the tensile peeling stress as well as the tensile peeling parameter P_p for each layout. The tensile stress was measured at each end of the DSS and the maximum value was recorded. No real pattern can be seen between the variables of the DSS and the tensile peeling stress. However, all of the values of P_p are much lower than the upper limit of 4. The maximum value of P_p that was computed was 0.80.

Table 5-5: Tensile Peeling Stresses and Tensile Peeling Parameter P_p

DSS Properties used in Analysis	Tensile Stress [psi]	P_p
Steel, 12"x 1/8"x 1"	54.61	0.58
Steel, 24"x 1/8"x 1"	56.23	0.59
Steel, 40"x 1/8"x 1"	25.78	0.27
Steel, 24"x 1/8"x 2"	67.04	0.71
Steel, 24"x 3/16"x 1"	29.84	0.31
Steel, 24"x 1/4"x 1"	83.65	0.87
Aluminum, 24"x 1/8"x 1"	17.26	0.18
Plexiglass, 24"x 1/8"x 1"	75.44	0.80
Two Steel 24"x 1/8"x 1" Side-by-Side	56.11	0.59
Two Steel 12"x 1/8"x 1" End-to-End	57.7	0.61

5.3.5 Observations from Phase I Finite Element Analysis

After conducting all of the finite element analyses in Phase I, it was determined that the DSS strip could be made out of steel. Moreover, the steel strip dimensions should be one inch wide and one-eighth of an inch thick. Steel was chosen as the appropriate material because it was seen that the type of material did not affect the computed readings in the DSS, and steel is a durable material that is readily available. Also, strain gauges that are temperature compensated for steel are more common and readily available than those for other materials. The width of one inch was selected because it was wide enough to give plenty of surface for adhesive to attach the DSS but not too wide that a lot of adhesive would be used each time it was attached. Lastly, a thickness of one-eighth of an inch was chosen as a middle ground for a thickness that would be durable so that the DSS could be used for many tests, and a thickness that would be flexible enough to conform to the camber of the HCS.

5.4 Phase II Finite Element Analysis

A second phase of finite element analyses was conducted after the adhesive tests that are described in Chapter 6. In these models, the adhesive that was used to fasten the DSS to the HCS was modeled. The adhesive was represented by a thin strip in the finite element model with a predetermined modulus of elasticity and thickness that would be similar to that of the adhesive that was used in the physical tests. The thin strip also had the same width and length as the DSS. The adhesive element was fixed to the DSS using tie constraints, while the other side was attached to the HCS using tie constraints as well. This set-up assumed a perfect bond between the adhesive and the two materials it was attaching. However, being a deformable material, the adhesive enables relative motion between the HCS and the DSS. The adhesive was assumed to be linear elastic and that the loading would not fail the bond between the adhesive and the bonded materials. The material properties that were used for the adhesive can be found in Appendix A.1.

The Phase II finite element models were analyzed, in a similar manner to that used for the Phase I finite element models. The only difference in the computed responses of the HCS structures was that the shear lag distance, D_{sl}, at the ends of the DSS increased even further

than that computed for Phase I models. The D_{sl} was observed to vary with the modulus of elasticity of the adhesive, as well as the thickness of the adhesive film. As the modulus decreased and the thickness increased the shear lag distance, D_{sl}, would increase. Using the selected parameters for the adhesive that was chosen (cyanoacrylate) D_{sl} increased from two inches to three inches. This shear lag was found to increase when the modulus of elasticity of the adhesive was decreased and the thickness of the adhesive increased. The results of these analyses are summarized in Table 5-6 and Table 5-7. An adhesive thickness of 0.05 inches was used for these results.

Table 5-6: Normalized Change in Longitudinal Strain across HCS Width with Adhesive Modeled

DSS Properties used in Analysis	P_k [%]
Steel 12”x 1/8”x 1”	2.9
Steel 40”x 1/8”x 1”	0.9

Table 5-7: Shear Lag Distances with Adhesive Modeled

DSS Properties used in Analysis	D_{sl} One [in]	D_{sl} Two [in]
Steel 12”x 1/8”x 1”	4.2	3.9
Steel 40”x 1/8”x 1”	4.9	5.0

Combining the observations of Phases I and II, the final design of the DSS that would be used in the full-scale laboratory tests was a DSS that was fabricated from steel and had a width of one inch and a thickness of one-eighth of an inch. The idea of using multiple DSS for one transfer length test was considered plausible and will be explored further in the full-scale laboratory tests. The idea of using multiple DSS laid end-to-end was abandoned due to the added shear lag length where two DSS ends came together. The expected shear lag that was to be observed in future testing was approximately 4-5 inches with a minimum of 2.5 inches.

Chapter 6 Adhesive Tests

6.1 Test Setup

A series of three preliminary small-scale test were conducted to determine the optimal adhesive for attaching the DSS to the HCS in the full-scale laboratory test. In this test several small steel strips were attached to a rectangular concrete specimen with different types of adhesives. Electrical resistance strain gauges were attached to the steel strips as well as to the concrete, and the concrete specimen was loaded axially. The strains the concrete and the steel strips was recorded. The goal of these tests was to see which adhesives best transferred the strain from the concrete to the steel, as well as get an indication for the workability of each adhesive. The latter included both sufficient viscosity, to prevent flow of the wet adhesive, and sufficient set time to enable proper installation of the steel strips.

Figure 6-1 shows the set up that was used in the first two adhesive tests (AT1 and AT2). The concrete specimen was 6 inches square and 24 inches long. It was loaded concentrically along the 24-inch axis. In the first test (AT1), the steel strips that were used were three inches, one inch wide, and one-eighth of an inch thick. A strain gauge was installed at the center of each steel strip. Instrumented steel strips were attached on opposite sides of the concrete specimen, with each type of adhesive included for that test. This would allow an average strain to be calculated between the two sides to correct for any bending that may occur due to accidental eccentricity of the axial loading. On the same sides that the instrumented steel strips were attached to, an electrical resistance strain gauge was also attached directly to the concrete surface. During each test, the load applied to the specimen was recorded in addition to the strains in all of the gauges.

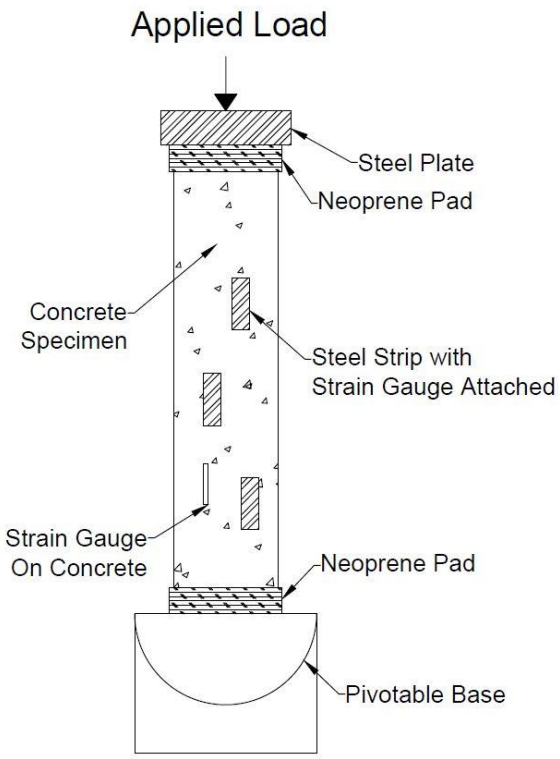

Figure 6-1: Preliminary Adhesive Test Setup

Several criteria were used to select the adhesives that would be tested. The most important criterion was that the glue have sufficiently fast set and cure times. The set time is defined as the time it takes the adhesive to harden sufficiently so that the steel strip is no longer moveable, while the cure time is the amount of time needed for the adhesive to reach its full strength. The set time of the adhesive needed to be short because the DSS would be attached to the underside of the HCS. The shorter the set time of the adhesive, the less time the DSS would have to be held in place under the HCS. The cure time also needed to be short so that the transfer length test could be conducted soon after the DSS was attached. The transfer length tests have to be conducted shortly after the HCS are sawn at the plant.

Other criteria that were used to select the adhesives were the purchase price and the availability of the adhesive. One of the goals of the project was to develop an inexpensive method for determining the transfer length. The adhesive also needed to be easily available so that it would be easy to conduct the transfer length tests and easy for others to replicate the tests at any precast concrete plant. Tables 6-1 and 6-2 show the adhesives that were

used in the adhesive tests. The adhesive types and bonding chemicals are presented in Table 6-1 and the manufacturers of the adhesives, as well as the test number the adhesive was used in, are given in Table 6-2. In the search for adhesives to test, other adhesives were found that appeared to fit the set and cure time requirements. However, these other adhesives were not tested because they were either too expensive or too difficult to obtain.

Table 6-1: Adhesive Bonding Chemicals

Adhesive No.	Brand Name	Type	Bonding Chemical
1	JB Weld Clear Syringe	2-Part Epoxy	Diglycidyl bisphenol
2	Gorilla Glue Super Glue	Cyanoacrylate	Cyanoacrylate
3	Gorilla Glue Epoxy	2-Part Epoxy	Bisphenol A-epichlorohydrin polymer, (3-(2,3-Epoxypropoxy)propyl)trimethoxysilane
4	VHB Tape	Tape	Proprietary Acrylic Adhesive
5	Liquid Nails	1-Part Epoxy	Proprietary polymer blend, trimethoxyvinylsilane
6	Hilti HiT RE 500	2-Part Epoxy	Proprietary polymer blend
7	Loctite Superglue Gel	Cyanoacrylate	Cyanoacrylate
8	EZ Bond I-161500	Cyanoacrylate	Cyanoacrylate

Table 6-2: Adhesive Manufacturers and Tests

Adhesive No.	Brand Name	Manufacturer	Test
1	JB Weld Clear Syringe	JB Weld	AT1
2	Gorilla Glue Super Glue	Gorilla Glue	AT1
3	Gorilla Glue Epoxy	Gorilla Glue	AT2
4	VHB Tape	3M	AT1
5	Liquid Nails	PPG Industries	AT1
6	Hilti HiT RE 500	Hilti	AT2
7	Loctite Superglue Gel	Henkel AG & Co.	AT2 & AT3
8	EZ Bond I-161500	K & R International	AT3

In the adhesive tests, the concrete prism was loaded with a stepped linear protocol. The prism was loaded from zero kips to 60 kips at a linear rate of 0.05 kips/sec. At every five-kip interval the load was paused and several strain readings were taken. Once a maximum load of 60 kips was reached and several strain readings were taken, the prism was unloaded at the same rate and readings were taken every five kips again. A maximum load of 60 kips was chosen because it would cause strains in the concrete specimen of similar magnitude to what was expected in the full-scale laboratory test.

6.2 Adhesive Tests Conducted

6.2.1 Test AT1

In the first adhesive test, four adhesives purchased at a local hardware store were used. These adhesives can be seen in Tables 6-1 and 6-2 above, and they consisted of 2-part epoxy, 1-part epoxy, cyanoacrylate, and double-sided tape. Figure 6-2 shows a graph of the results from this test. The graph shows that strain increases with the axial load applied to the concrete specimen. The curve labeled “concrete” corresponds to the strain reading from the strain gauges placed directly on the concrete specimen.

The graph in Figure 6-2 illustrates clearly that only Adhesive No. 2 (the superglue) and No. 1 (the JB weld epoxy) transferred any of the strain from the concrete specimen to the steel strip. The other two adhesive showed no change in strain with increasing in axial load.

It can also be seen that the magnitude of the strain in the steel strip attached with Adhesive No. 2 (superglue) and the steel strip attached with Adhesive No. 1 (JB weld epoxy) do not have the same magnitude as the strain that was measured in the concrete. This difference is to be expected because of the shear lag that was seen in the finite element models. In the set up used in test AT1, the steel strip strain gauges were 1.5 inches from the edge of the strip. Whereas in the finite element analysis, the shear lag distance (D_{sl}) was about 2.5 inches from the edge of the strip assuming a perfect bond between the DSS and HCS. Therefore these strips were reading strains within their shear lag distance and not full strain that was observed in the concrete.

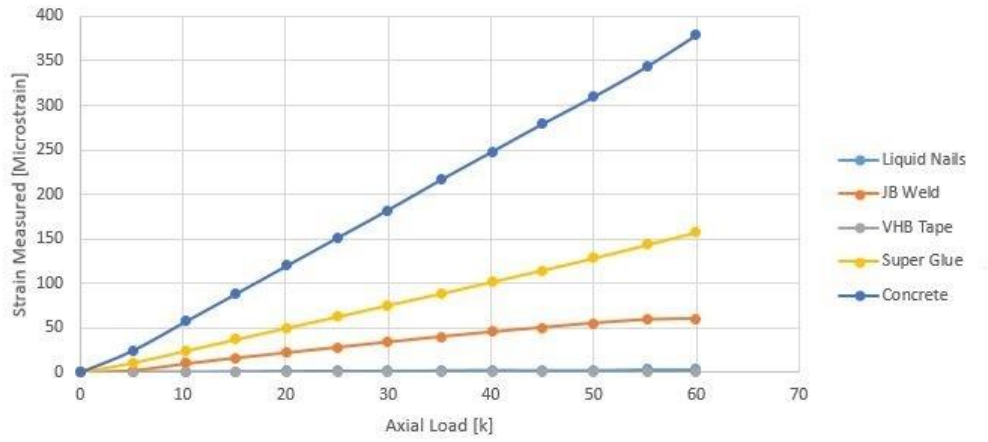

Figure 6-2: Adhesive Test AT1

6.2.2 Test AT2

The second adhesive test (AT2) was conducted in a very similar fashion as the first adhesive test (AT1), except that different adhesives were used. Figure 6-3 shows the results from test AT2. Similar to results seen from AT1, Adhesive No. 3 (gorilla glue epoxy) did not show any change in strain with increasing in axial load. Adhesive No. 6 (Hilti epoxy) appeared to follow the concrete strain well until a load of about 35 kips after which it dropped off. The reason for the sudden decrease in strain is unknown, but it is surmised that the bond between the adhesive and the steel began to fail.

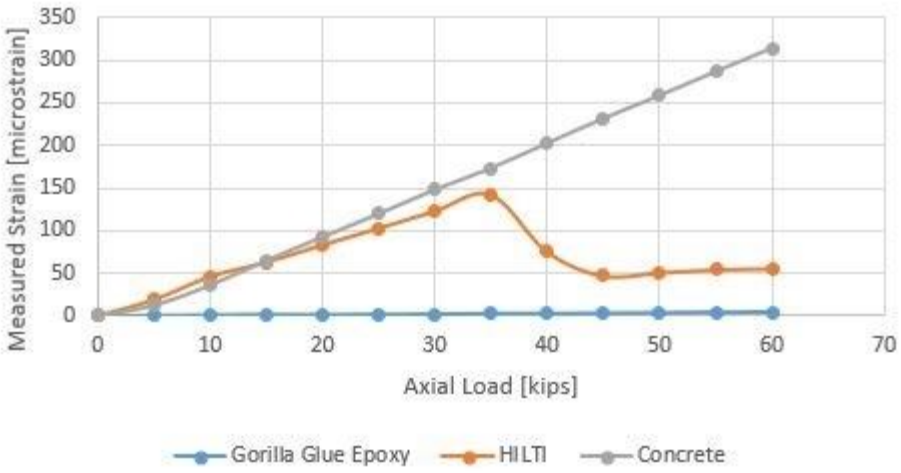

Figure 6-3: Adhesive Test AT2

6.2.3 Test AT3

After conducting the first two adhesive tests, it was determined that Adhesive No. 2, a cyanoacrylate adhesive, would be the optimal choice use in the full-scale test to attach the DSS to the HCS. The only difficulty with cyanoacrylate adhesives is their fast set times. Therefore, in the third adhesive test (AT3), two slow setting cyanoacrylate adhesives were used (Adhesive No. 7 and 8). In test AT3, 12-inch long steel strips were used instead of the three-inch long strips that were used in the previous two tests (AT1 and AT2). Strain gauges were placed three inches from each end of the steel strip, as well as at the center of the strip. Strips were attached on opposite sides of the concrete specimen like in the previous tests. LVDT gauges were also attached on all four sides of the concrete specimen to measure the strain in the concrete in addition to the strain gauges attached directly to the concrete surface.

The results for the third adhesive test can be seen in Figure 6-4. In the plot shown in this figure, the value that is shown for the strain for the adhesives is from the strain gauge that was attached at the center of the strip. This gauge should be outside of the shear lag lengths, D_{sl}, from either end of the strips. The strain value labeled "Force Strain" is the strain calculated from the force measured in the load frame and used a modulus of elasticity, E_c,

estimated from the ACI 318 formulas. Both adhesives (No. 7 & 8) were able to transfer the strain from the concrete specimen to the steel strip with very little loss of strain. The strains measured in the strip attached with Adhesive No. 8 (EZ-Bond adhesive) had values between the strain recorded with the LVDT gauges and the strain recorded with the electrical resistance strain gauges attached directly to the concrete. The strain from Adhesive No. 7 (Loctite) was slightly below the other strain readings.

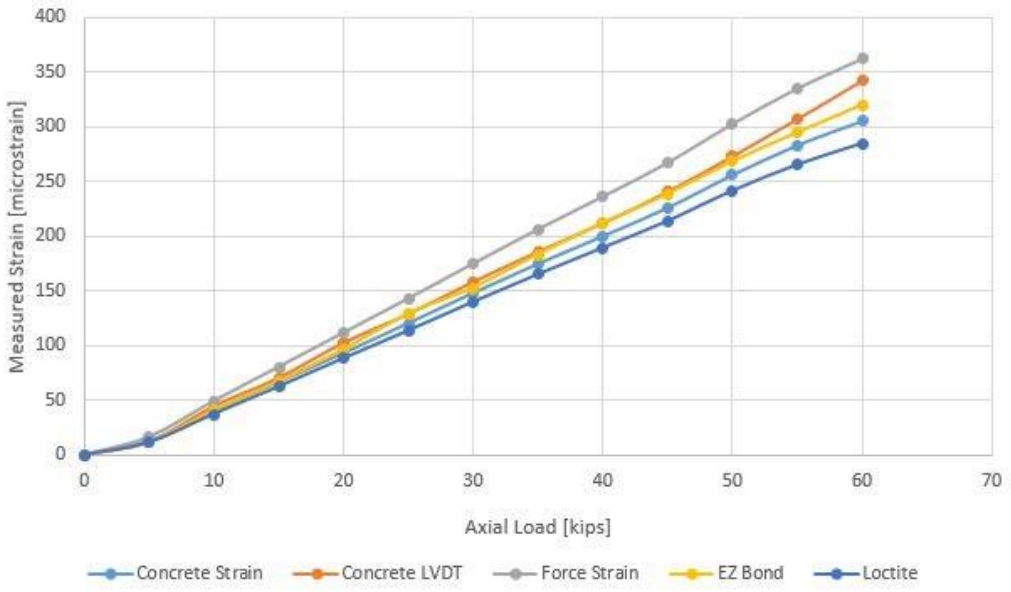

Figure 6-4: Adhesive Test AT3

The strains that were measured in the gauges 3 inches from the end of the strip were slightly less than the strains recorded by the center gauge, though not by a large amount. These gauges were believed to be in the shear lag. The small difference in the strain readings between the center gauge and the edge gauges implies that the edge gauges are near end of the shear lag. This would indicate a slightly shorter shear lag than what was observed in Phase II of the finite element model where the shear lag was approximately 4-5 inches.

6.3 Conclusion

Based on the results from adhesive tests AT1, AT2, and AT3, it was decided that Adhesive No. 8 (EZ-Bond cyanoacrylate glue) would be the optimal choice to be used in the full-scale laboratory tests. This adhesive was chosen because it had a sufficiently slow setting time, compared to other cyanoacrylates, so that the DSS strips could still be attached without rushing the process. However, the set time was fast enough so that the DSS strips could still be attached in a matter of minutes and the transfer length tests conducted quickly. In adhesive test AT3, the Adhesive No. 8 (EZ-Bond cyanoacrylate) appeared to transfer the strain to the DSS better than the other slow setting super glue that was used (Adhesive No. 7).

Other factors that were used to select Adhesive No. 8 (EZ-Bond cyanoacrylate) were that a large volume of the adhesive could be purchased for a small amount of money. This product could be purchased for about $2.20/oz. while the other cyanoacrylate that was tested had a purchase price of approximately $18.40/oz. While searching for suitable adhesives, other slow setting cyanoacrylates were identified but they were either more expensive or difficult to obtain.

Chapter 7 Full Scale Laboratory Test Program

7.1 Laboratory Test Setup

A full-scale test was conducted in the University of Minnesota's Theodore V. Galambos Structural Engineering Laboratory to verify the DSS ability to measure concrete surface strains accurately so as to enable their use for determining the transfer length of prestressing strand in HCS. The full-scale tests were conducted to determine how easily the DSS could be bonded to the bottom of the HCS, as well as to see how the strains measured using the DSS compared with strains measured using electrical resistance strain gauges installed directly on the bottom face of the HCS. Additional factors such as the length of the DSS, the simultaneous use of multiple DSS, and the influence of moment gradients were investigated.

The setup for the laboratory tests is similar to the setup that was modeled in the finite element analysis. The laboratory setup can be seen in Figure 7-1 and features a 20-foot section of HCS that was provided by Molin Concrete Products Company and was brought into the Galambos Laboratory. The HCS was supported on each end by a stiffened steel beam that spanned between two steel column supports that were, in turn, bolted to the laboratory floor. The support columns were placed 16'-8" apart. A ¾-in. thick piece of neoprene padding was placed between the HCS and the support beams to ensure uniform bearing stress over the HCS supports and to minimize any twisting moment from loading on uneven surfaces such as the bottom of the HCS.

At longitudinal distances of 6'-8" from each support, load frames were erected over the HCS (Figure 7-1). The two load frames consisted of a beam spanning between two columns over the HCS. A hydraulic actuator, not shown in Figure 7-1 for clarity, was attached to each beam and used to load the HCS during the tests. The bottom end of each hydraulic actuator (MTS double-ended 35-kip servo-controlled hydraulic actuator) was attached to a wide-flange steel beam that spread the hydraulic actuator load into a uniform line load across the width of the HCS. Between the wide flange beam and the HCS, gypsum cement was placed so as to provide uniform bearing between the loading beams and the HCS.

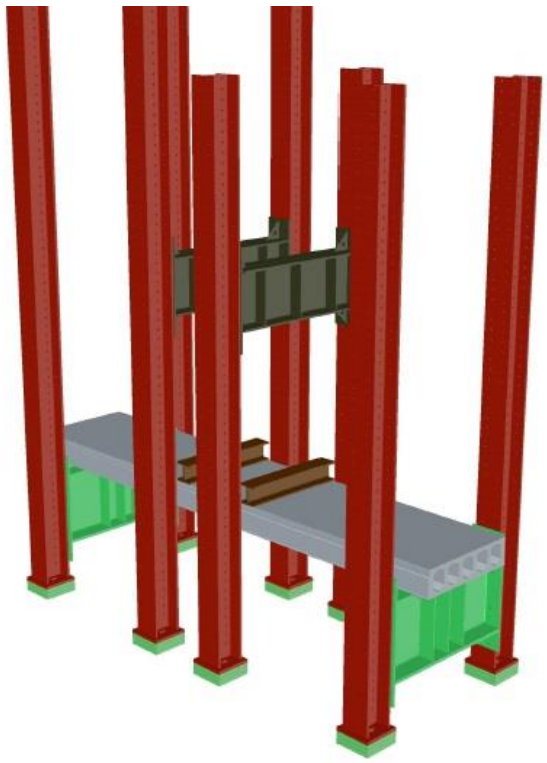

Figure 7-1: Full Scale Laboratory Testing Setup

Two loading lines that are equidistant from each support creates a uniform moment region in the center of the HCS if the two loads are equal magnitude. The 3'-4" constant moment region that was generated in the HCS is the location where the strains were measured during the full-scale laboratory tests.

7.2 Instrumentation and Data Collection

In the constant moment region, electrical resistance strain gauges were attached directly to the bottom face of the HCS and a parallel DSS was installed as well (Figure 7-2). Strain readings that were nominally the same were expected from the gauges on the HCS and the DSS to enable comparison for verification of the proposed sensor. In order to get the most accurate comparison between the two sets of gauges, the gauges on the HCS and the DSS were installed symmetrically about the longitudinal center-line of the HCS (Figure 7-2). In Figure 7-2, the two lines of sensors on the right of the HCS in Figure 7-2 are the strain gauges that were attached directly to the bottom face of the HCS. The two lines on the left

side are the gauges on the two DSS which were 24in. (center left) and 36in. (far left) and one of 24 inches (left center) from the centerline. Using this set up, the left center DSS was compared to the line of gauges attached to the immediate right of the centerline of the HCS, and the DSS on the far left was compared to the line of gauges attached to the far right of the centerline of the HCS. All lines of sensors were attached to the HCS directly below a prestressing strand. The spacing of all gauges in a line was two inches. Figure 7-3 shows a plan view of the gauge layout. In Figure 7-3, the dashed lines represent the prestressing strand in the HCS. The HCS that was donated for the full-scale laboratory tests had two prestressing strands in each interior web. The electrical resistance gauges and DSS were fastened directly below one of these prestressing strands.

Figure 7-2: Strain Gauge Layout

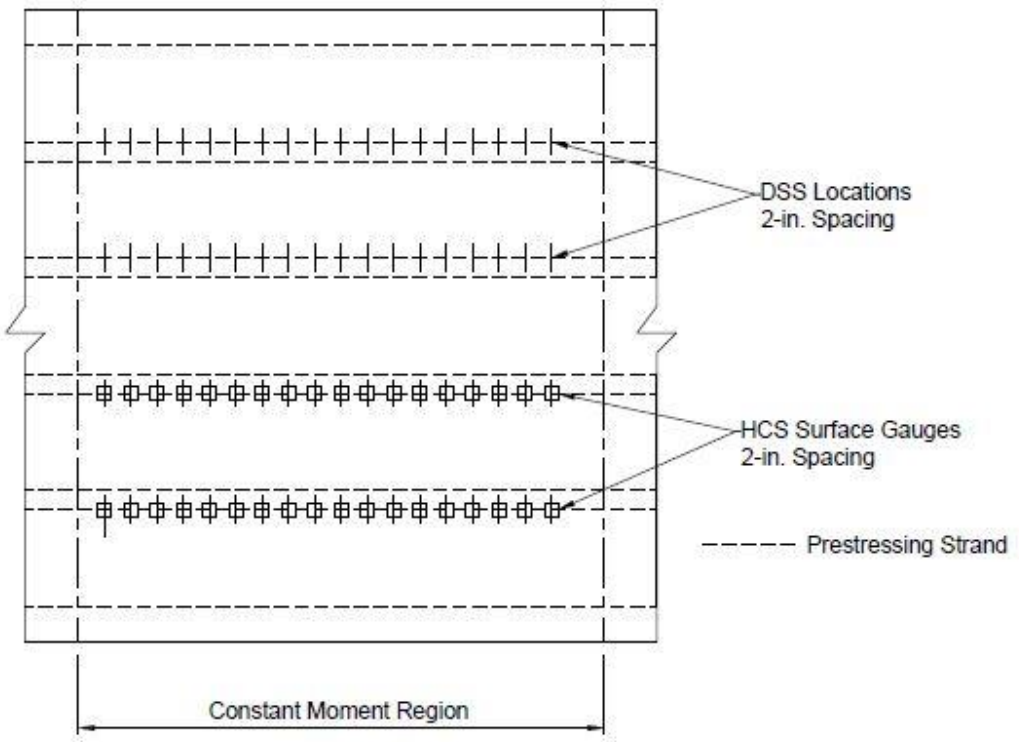

Figure 7-3: Plan View of Strain Gauge Layout

A portable data acquisition system was used to record the DSS strain data in preparation for the field tests in the precast plant. A Campbell Scientific CR1000 portable data collection system with three AM16/32B multiplexers was used. Campbell Scientific 4WFB350 completion resistors were used with each gauge to enable quarter-bridge configurations when taking the strain readings. This setup compensated for any temperature change effects and resistance induced by the relay contacts of the datalogger in the strain readings. For more information on data acquisition, see Appendix C.2.

Due to the limited availability of Campbell Scientific 4WFB350 completion resistors, only the strain gauges installed on the DSS were read using the Campbell Scientific CR1000 portable data acquisition unit. The strain gauges that were attached directly to the bottom surface of the HCS were recorded using the dedicated data acquisition system in the Galambos Laboratory which is a National Instruments SCXI data acquisition system with 96 channels.

7.3 Laboratory Test Schedule

In the full-scale laboratory tests, different DSS layouts as well as different loading patterns were used to investigate the applicability of the DSS for measuring the transfer length in HCS. DSS of different lengths were used to illustrate the effect of sensor length on the accuracy and reliability of recorded strains. A longer DSS could pose a larger stiffening effect on the HCS and generate a lower strain reading than a shorter one. For the tests that were conducted, two DSS were fabricated with lengths of 36 inches and 24 inches. These are shorter than what would be needed in transfer length tests, but they were made so that they would fit comfortably within the 40-inch constant moment region of the HCS test setup. The complete schedule of full-scale laboratory tests is given in Table 7-1.

Table 7-1: Full-Scale Laboratory Test Configurations

Test Number	DSS Configuration	Moment Loading
FT1	Single 36-in. DSS	Constant
FT2	Single 36-in. DSS	Linear
FT3	36-in. and 24-in. DSS Side-by-Side	Constant

Layouts of one DSS versus two DSS used at a time were investigated. The ability to uses two DSS devices at a time would be a great advantage. Such capability would enable multiple strain profiles from which to compute transfer lengths during a single test. For example, two parallel DSS on each side of the saw cut would yield a total for four transfer length readings from a single test.

Two different loading patterns were investigated in the full-scale load tests of the HCS. The first loading pattern had equal loads in both of the hydraulic actuators in the test setup (Figure 7-1). This loading produced a constant moment region, therefore a theoretical constant strain region (Figure 7-4a), where the DSS were attached. Such testing enabled accurate comparison of the strain readings along the parallel DSS, as well as comparison between the DSS gauges and the gauges applied directly to the HCS. However, when the DSS are used for transfer length testing in the field, the strain profiles will not correspond

to a constant moment region. The strains will vary along the transfer length of the HCS. Thus, a second loading pattern that produces a variable moment region, therefore a variable strain region, was also investigated. In the second loading pattern, only one of the two hydraulic actuators was loaded (Figure 7-1). The load in the other actuator was held at a constant load equal to zero. Figure 7-4b shows the loading and strain diagrams for the second loading pattern.

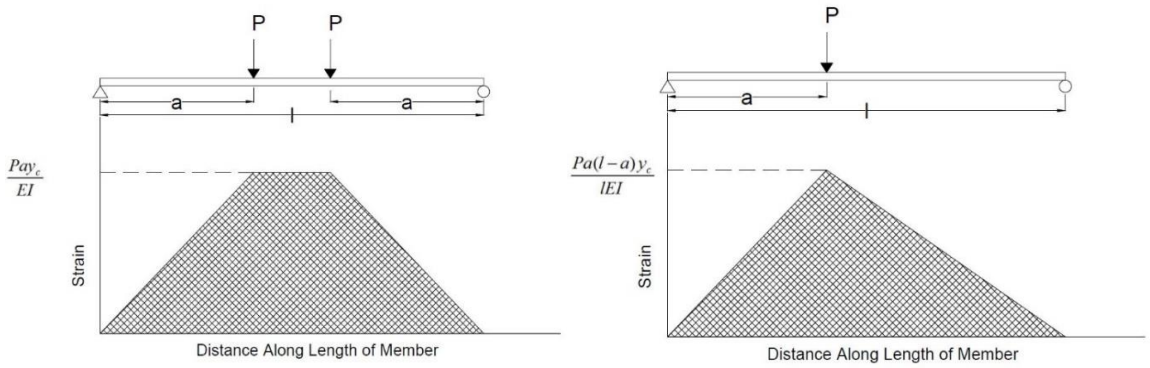

a) Constant Moment b) Variable Moment

Figure 7-4: Loading and Strain Diagrams for Two Load Patterns

Two different layouts of the DSS devices were used in the tests. The first layout had a single 36-in. DSS attached to the HCS. The second layout had a 36-in. and a 24-in. DSS attached to the HCS, parallel to each other, at the same time Figure (7-2). The DSS layout with a single 36-in. DSS was loaded using both of the loading patterns described above. The DSS layout with two DSS side-by-side was loaded using the loading pattern in Figure 7-4a. Table 7-1 gives the DSS layout and loading pattern for each test.

7.4 Test Results

The first test (FT1) that was conducted was with a 36 inch DSS attached to the HCS. The HCS was loaded at a constant rate of 0.05k/sec until a load of 10 kips was reached in each actuator (Figure 7-4a). The load was then held for 15 minutes while multiple strain readings were taken. Strains were recorded every 30 seconds. The load was then increased at the same rate until a maximum load of 20 kips was reached in each actuator. This load was then held for 15 minutes while strain readings were taken. At each load that was held, a

total of 30 strain readings were recorded for each gauge. The magnitude of the maximum load was selected to correspond to 66% of the load that would cause the prestressed HCS section to crack. The specimen was then unloaded at the same rate that it was loaded. When reporting the strain data, all readings that were recorded for a given loading stage (either 10kips or 20kips) were averaged to eliminate the effect of temporal fluctuations from electrical noise in the strain circuits.

Figure 7-5 shows the comparison between the strain readings in the DSS and in the HCS for both loads of 10 kips and 20 kips for test FT1. It can be seen in Figure 7-5 that the strain readings in the DSS closely match the concrete surface strain readings in the HCS, and there is a one-to-one relationship between the readings. In fact, the readings in the DSS are actually smoother and show less variation along the gauged length than do the readings in the HCS. Theoretically, the strain gauges should all be of the same magnitude because they are measured in a region of constant strain. This smoothing out effect is believed to be due to the fact that the steel of the DSS is a homogeneous material whereas the concrete is not. It is more difficult to use electrical resistance foil strain gauges on nonhomogeneous material such as concrete because they measure localized strain. In concrete the strain gauge could be on top of a 'hard' spot, i.e. a piece of aggregate, or on top of a 'soft' spot, i.e. a pocket of cementitious material or a void. Due to the different material properties in these cases the strain reading will exhibit variations similar to those observed in Figure 7-5 for the gauges installed directly on the concrete surface. However, the 'filtering' effect provided by the DSS is beneficial for measuring transfer lengths since the trend in strain is more important than highly localized deviations due to concrete inhomogeneity.

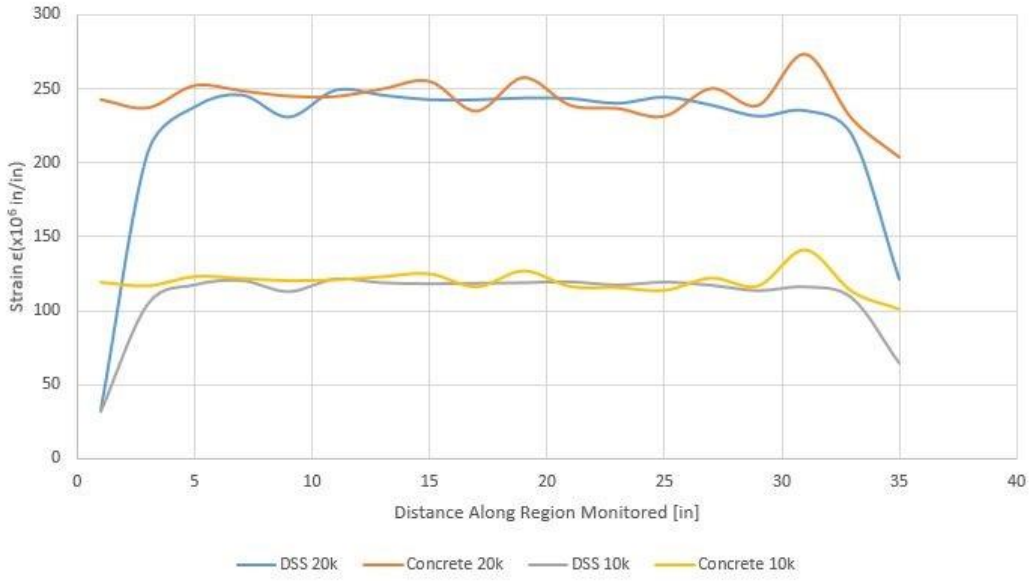

Figure 7-5: 36in DSS Constant Moment

The shear lags that were seen in the finite element analysis at the end of the DSS can also be observed in Figure 7-5 for test FT1. In this test, the shear lag distance, D_{sl}, was about three to four inches, which is a value slightly less than the 4-5 in. lag length obtained in the Phase II finite element analysis described in Section 5.4. Additionally, the observed D_{sl} value in test FT1 was the same length for both the 10-kip and the 20-kip load levels.

The same loading procedure was used again but this time for a test (FT2) in which load was only applied to the HCS with one actuator. The other actuator was held at a constant load of zero. This produced a variable strain region that would be more similar to what would be seen in a transfer length test (Figure 7-4b). Figure 7-6 shows the strain reading in the DSS and concrete of the HCS for a load of 20 kips in one actuator. Again, it can be seen that the strain recorded by the DSS closely mimics the trend in the strain profile for the HCS. The 'filtering' effect of the DSS can be seen again, as well as the 3-4 inch long shear lag distances.

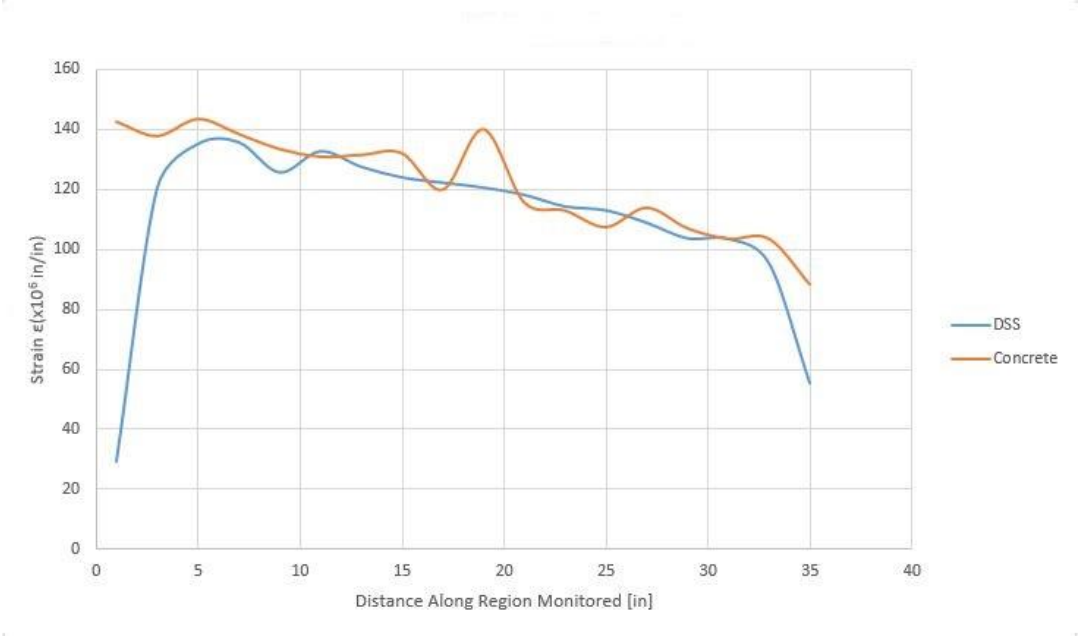

Figure 7-6: 36in DSS Variable Moment

In test FT3, a second DSS of 24-in. length was attached to the HCS alongside the 36-in. DSS using the layout shown in Figure 7-2. This setup was used to investigate the potential stiffening effect caused by having two DSS attached simultaneously. Figure 7-7 shows the strain readings in both the DSS and the HCS at load levels of 10 kips and 20 kips for both the 36-in. DSS and the 24-in. DSS. Figure 7-7a is the strain comparison for the 36-in. DSS and Figure 7-7b is for the 24-in. DSS. The computed results are almost identical for the constant strain region, notwithstanding the difference in DSS lengths. Thus, there appears to be no stiffening effect associated with side-by-side DSS installed on a HCS.

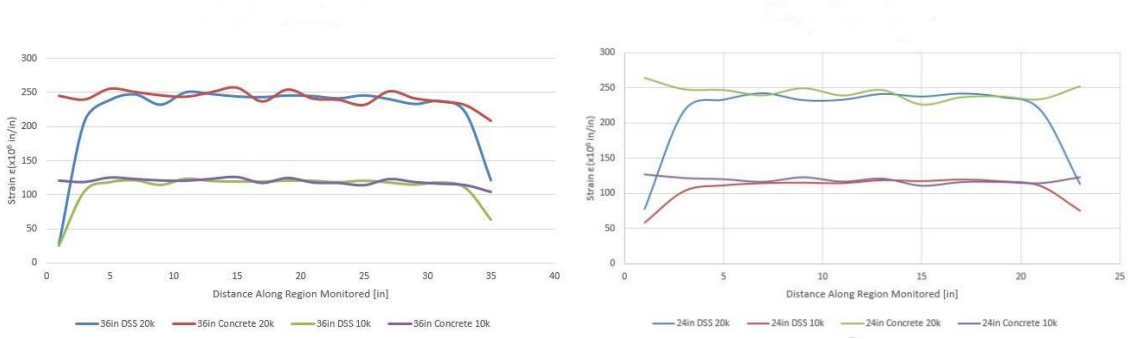

a) 36-in. DSS b) 24-in. DSS

Figure 7-7: Side-by-Side 36-in. and 24-in. DSS Layout

In order to make sure that there was not a global stiffening effect caused by having two DSS attached, the surface strains in the HCS were compared between the test having only one DSS (FT1) and the test having two DSS attached (Test FT3). Figure 7-8 shows this comparison, with Figure 7-8a showing the entire length of the region of concrete surface strains that was monitored. Figure 7-8b shows a portion of the graph in Figure 7-8a, from 4 to 24 in. along the constant moment region. These strain readings were the concrete surface strains that were compared to the strains recorded in the DSS in tests FT1 and FT3. The surface strain readings in the concrete faces of the HCS are about the same whether one or two DSS are attached. Some discrepancy can be seen in Figure 7-8b, but it is very small. There is one point towards the end of the monitored region, between 30 and 32 in. in Figure 7-7a, that has some deviation from the single DSS specimen. This variation is believed to be due to an error in the gauge reading and not the influence of the added DSS.

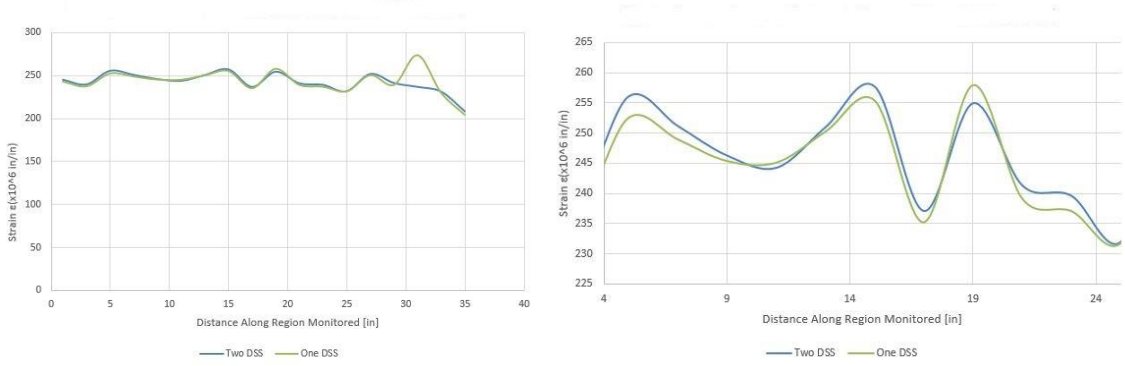

a) Full Monitored Length b) Portion of Monitored Length

Figure 7-8: Concrete Surface Strain Comparison

The full-scale laboratory tests demonstrated that the DSS can provide accurate concrete surface strain readings and, in fact, even better readings due to the 'filtering' effect that was observed. The DSS did not stiffen the HCS when it was fastened to the concrete surface causing any localized reduction in strain measurements. It was also demonstrated that multiple DSS could be attached to the HCS without altering any concrete surface strains allowing for multiple DSS to be used in transfer length tests.

Chapter 8 Field Verification

8.1 Test Setup

8.1.1 Test Procedure

Two transfer length tests (LT1 and LT2) were conducted at a precasting plant with the procedure employing the DSS devices using a similar test method to that reported by Palmer and Schultz (2010). The two tests were initially planned on back-to-back days, with the slabs cast on the day before testing. The slab specimens for the transfer length tests were cast on the previous day, and the specimens were released and stripped on the day of testing.

For the transfer length tests, four DSS were constructed with a 5ft length. For each slab specimen, two DSS were attached to the bottom face of the slab on each side of the centerline which was to be sawn. Each DSS had a total of 27 electrical resistance foil strain gauges. The strain gauges were installed with a spacing of two inches, and with the first gauge attached four inches from each end of the DSS. The four-inch distance was intended to skip the region of the shear lag distance, D_{sl}, which was seen in the laboratory tests and finite element analysis. Strain measurements in this region do not represent accurate strain readings and thus, could not be used to determine transfer length.

On the day of testing, the HCS specimens were stripped and removed from the casting bed. They were placed on two temporary supports next to the casting bed. This created room underneath the HCS to attach the DSS on the bottom face of the HCS. Figure 8-1 shows a picture of the HCS on the temporary supports with the four DSS in place. Each DSS was fastened directly beneath the center of one of the webs in the HCS because this position ensured the closest placement to a prestressing strand. The end of the DSS closest to the HCS centerline was placed 2.5 inches from this line or (i.e. where the HCS was to be sawn). The 2.5-inch distance provided room for the center support when the HCS was cut. Figure 8-2 shows to which webs the DSS were attached. The layout shown is for two DSS on one side of the HCS. Two other DSS strips were attached on the other side of the HCS centerline. Thus, DSS Three mirrored DSS One and DSS Four mirrored DSS Two.

Figure 8-1: HCS on Temporary Supports

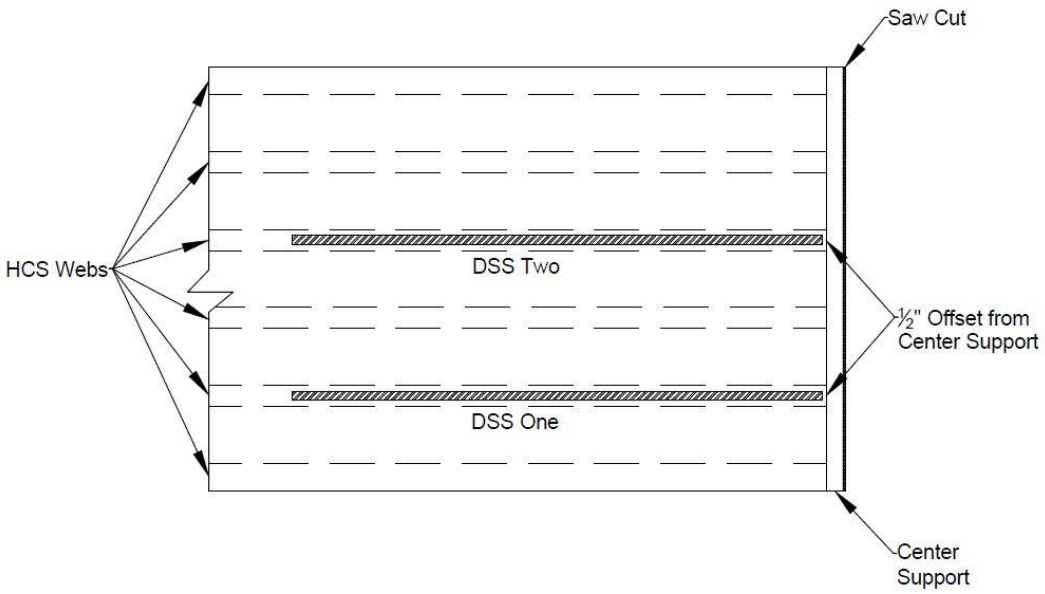

Figure 8-2: DSS Layout Diagram

Once the DSS were attached to the HCS, the HCS was lifted with the crane and placed back on the casting bed on three supports to leave a gap between the bottom of the HCS and the top of the casting bed. Two of the supports were placed at the ends of the HCS, and the third support was located along the centerline of the HCS where it was to be sawn. The supports were so placed to leave a gap between the HCS and the center support so as to ensure no negative moment was generated in the HCS. In other words, the HCS was fully supported by the end supports only.

Once the instrumented HCS was placed on the casting bed, the data acquisition system was powered on and strain readings were taken for five minutes. The slab was then sawn and allowed to rest on the three supports for 30 minutes while the data acquisition continued to take strain readings. The strain change readings that were recorded before and after cutting were used to determine the transfer length. Figure 8-3 shows the HCS on the bed while it is being sawn.

Figure 8-3: HCS being Saw Cut

Due to technical difficulties with the data acquisition system, the first slab was not tested on the day it was stripped initially from the casting bed. Instead, both slab specimens were tested on the second day. At the time of saw cutting, the first slab was approximately 40 hours old and the second slab was approximately 19 hours old. Concrete strengths at the time of cutting are given in Appendix F.2.

8.1.2 HCS Specimens

The HCS that were tested in the transfer length phase of the investigation were produced at a local precast plant, Molin Concrete Products Company in Lino Lakes, MN. Molin Concrete Products Company uses the Elematic precasting system for their production of HCS, and the HCS in this study were produced using Elematic's Heavy 12-inch cross section. This cross section can be seen in Figure 8-4. The difference between the two HCS test specimens was the strand pattern that was used. The first HCS, designated 1248-92, had six 0.5-in. prestressing strands, one in each web. The second HCS, designated 1248-204, had eight 0.6-in. prestressing strand (two in each interior web) and two 0.5-in. prestressing strand (one in each exterior web). The 1248-204 strand pattern is the one that is shown in Figure 8-4. Table 8-1 shows the plants strand pattern designations and the strands that were used, as well as the total area of the strand. All strands were stressed to 70% of the ultimate tensile stress.

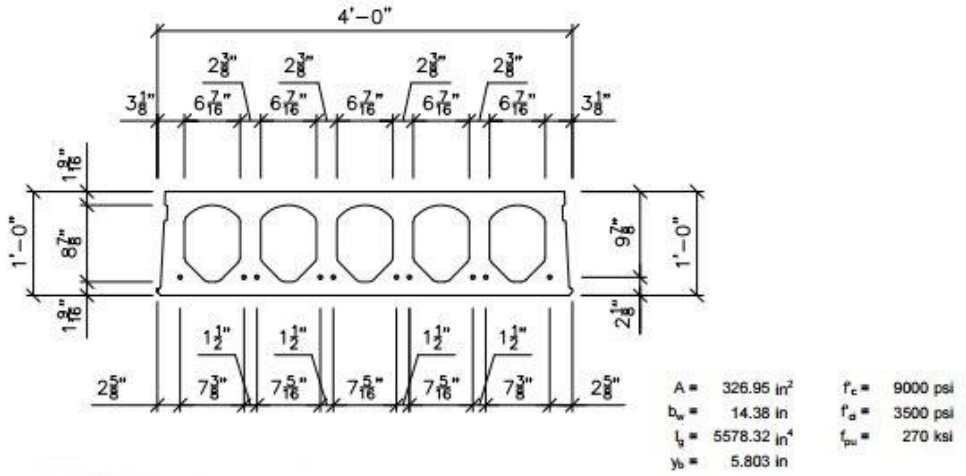

Figure 8-4: Cross Section of HCS Used in Field Tests

Table 8-1: Strand Patterns

Strand Designation	Strand No. and Size	Strand Area [sq. in.]	f_{si} [ksi]	Estimated f_{se} at release* [ksi]
1248-204	Eight 0.6-in. & two 0.5-in.	2.042	189	172
1248-92	Six 0.5-in.	0.918	189	164

* Losses were estimated using Zia (1979)

8.2 Determining Transfer Length

8.2.1 Data Processing

The change in strain of the HCS concrete surface produced by the saw cut was used to determine the transfer length. When the strand in the HCS is released as a consequence of the saw cut, the concrete in the transfer length region becomes uncompressed proportional to the force released in the strand. This decompression can be measured as a change in strain spanning from before to after the saw cut. However, the release of the strand is not the only mechanism that causes a change in concrete surface strain. The gravity effect due to the changing support conditions, as well as the changing eccentric prestressing force from the saw cut also cause changes in strain.

Figure 8-5 shows the changing support conditions of the HCS before (1) and after (2) the saw cut, as well as the strain diagram due to self-weight for these two conditions. Before the HCS is sawn, it is simply supported between the two outside supports because a small gap was left between the center support and the HCS. After the saw cut, there are two shorter sections of one-half the length that are simply supported. This causes a change in strain that is largest near the center of the slab specimen before cutting, where the strain due to self-weight goes from a maximum before the saw cut, to a value of zero after the saw cut.

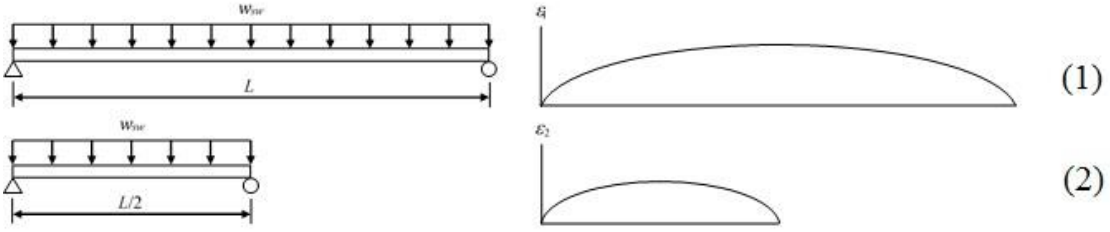

Figure 8-5: Support Conditions and Strain Diagrams Before and After the Saw Cut

Another mechanism that causes a change in the strain before and after the saw cut is the change in the eccentric prestressing force. When the HCS is cast, the prestressing strand are placed in the bottom of the HCS cross section. When the strand is released, this eccentric force causes a compressive strain in the bottom of the HCS and is what gives the member its camber. This compressive force decreases after saw cutting in the transfer length region. The compressive force varies linearly from a value of zero at the cut end to a maximum value at the end of the transfer length. Figure 8-6 shows a graph of the prestressing force magnitude before (1) and after (2) the saw cut.

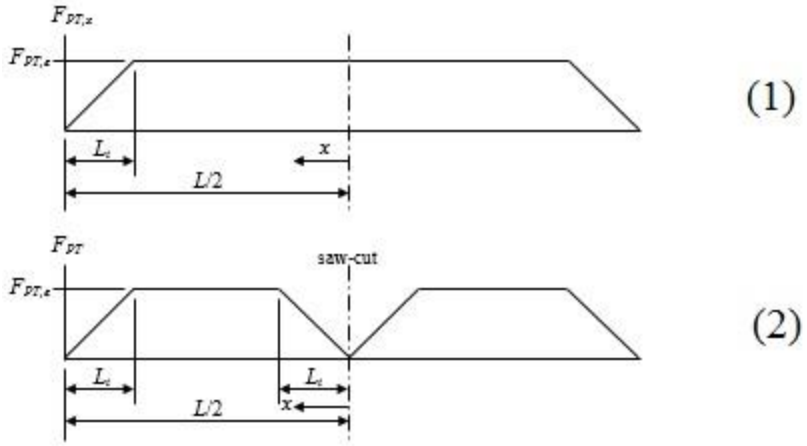

Figure 8-6: Changing Eccentric Prestressing Force Before and After the Saw Cut

Accounting for the change in strain caused by these forces, the change in strain due to the strand release can be calculated. See Appendix F.2 for a thorough explanation of the corrections for these mechanisms that were incorporated in the data processing method.

8.2.2 Defining Transfer Length

To determine the transfer length from the change in strain data, several definitions were used to determine the transfer length from strain change data. Palmer and Schultz (2010) proposed two methods for determining the transfer length that were modified from procedures proposed by Russell and Burns (1997). These two methods are defined below.

> *Method I* - The length along the HCS bottom face in which the measured concrete strain change profile varies from a maximum value at the cut end to the first instance of a value that represents a reduction of 95% of the peak strain change recorded.
>
> *Method II* – 95% of the length in which the concrete surface strain change drops from a maximum value at the cut end to the first instance of the smallest strain change recorded.

The two methods above were used to define the transfer length in the tests that were conducted. In addition to these two methods, a third method is proposed here, Method III.

Method III is similar to the 95% AMS Method used by Russell and Burns (1997). Due to the test procedure, the change in strain is maximum at the cut end and not in the center of the specimen as was seen in the tests Russell and Burns (1997) conducted. Figure 8-7 shows the strain profile for the Russell and Burns (1997) tests on the left and an example the strain profile for the HCS tests that were conducted is on the right. The proposed procedure for Method III is as follows.

1. Plot the corrected change in strain profile.
2. Determine the average minimum change strain (AMCS) for the specimen by computing the numerical average of all the strains contained within the inverted strain plateau.
3. Subtract the AMCS from the maximum change in strain at the cut end of the HCS and multiply this difference by 0.95.
4. Add the product from step 3 to the maximum change in strain at the cut end to get the 95% AMCS line.
5. Plot the 95% AMCS line on the strain profile graph.
6. The corresponding length from the cut end where the 95% AMCS line intersects the strain profile is determined to be the transfer length.

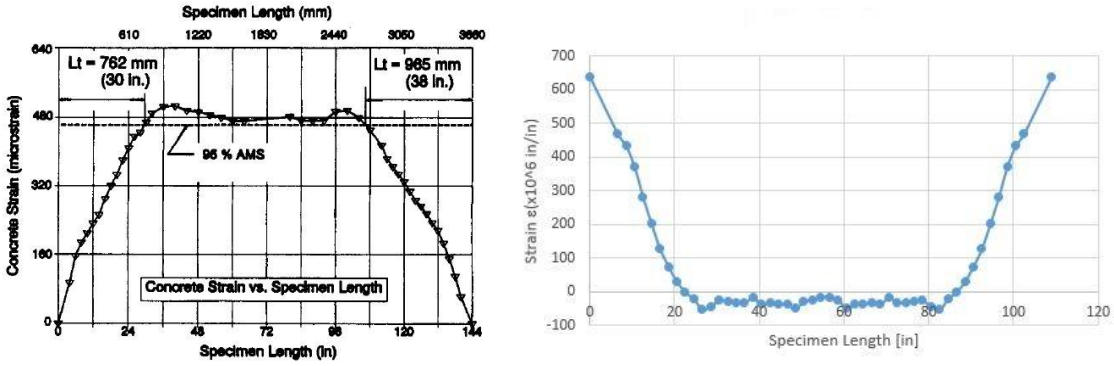

a) Strain Profile Russell and Burns (1997) b) Strain Profile from Field Tests

Figure 8-7: Strain Profile for Transfer Length Tests

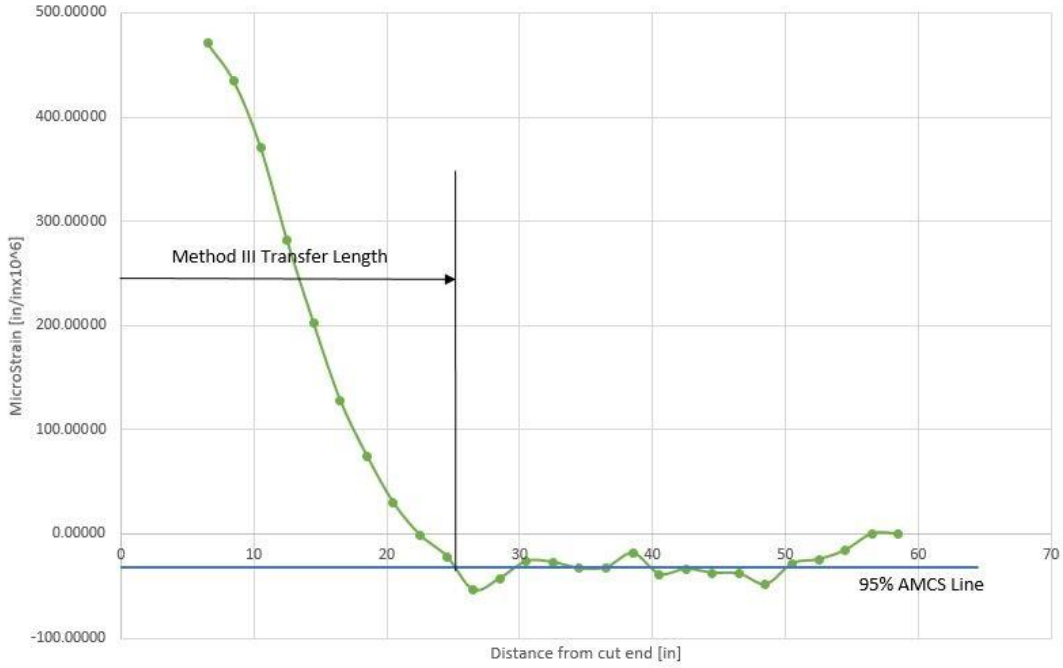

Figure 8-8: Strain Profile and Method III Transfer Length

Figure 8-8 above shows a corrected strain profile for one of the tests conducted with the 95% AMCS line plotted. The subsequent transfer length is indicated as well. All of the methods mentioned for determining the transfer length require the change in total strain change value at the cut end to be known. However, at the center support, due to the finite length of an electrical resistance foil strain gauge, as well as the shear lag at the ends of the DSS, this reading cannot be measured during the test: The strain gauges had to be installed past the region where the cut slabs would bear against the center support, and there is a 3- to 4in. shear lag, D_{sl}, past the edge of the DSS strips before the strain gauge data is no longer affected by the shear lag. In order to obtain this value, a linear regression of the values outside of the inverted strain plateau was used.

8.3 Test Results

8.3.1 Test LT1

Table 8-2 shows the transfer lengths, L_t, computed for the four DSS in Test LT1 using the three methods described above. The table also has the computed average and standard

deviation for each method, and it also presents the values for the average plus either one or two standard deviations. The three methods for determining the transfer length all produced similar results. When considering transfer lengths for prestressing strand, it is common to normalize the transfer length by the nominal diameter of the strand. Table 8-3 shows the normalized transfer lengths, L_t/d_b, for the average, average plus one standard deviation, and average plus two standard deviations for each of the three methods. ACI 318 can be used to obtain a simplified conservative estimate of the normalized transfer length, L_t/d_b, of 50 if an effective prestress magnitude, f_{se}, of 150,000 psi is assumed in the ACI 318-14 formula $(f_{se}/3{,}000)d_b$. This value is slightly larger than the normalized transfer lengths that were seen for the average plus two standard deviations.

Table 8-2: Test LT1 Transfer Length Results

DSS Number	Method I Transfer Length, L_t [in.]	Method II Transfer Length, L_t [in.]	Method III Transfer Length, L_t [in.]
DSS 1	19.91	21.38	20.83
DSS 2	13.62	13.78	14.59
DSS 3	18.42	19.48	18.93
DSS 4	16.81	17.58	17.06
Average	17.19	18.06	17.85
Standard Deviation	2.33	2.81	2.31
Avg + SD	19.52	20.87	20.16
Avg +2SD	21.58	23.68	22.47

Table 8-3: Test LT1 Normalized Transfer Length Results

	Method I, L_t/d_b	Method II, L_t/d_b	Method III, L_t/d_b
Average	34.38	36.12	35.7
Avg + SD	39.04	41.74	40.32
Avg + 2SD	43.16	47.36	44.94

8.3.2 Test LT2

The transfer lengths, L_t, computed for Test LT2 are given in Table 8-4 in a similar manner as they were presented for Test LT1 above. The transfer lengths computed for Test LT2 are longer than what was seen in Test LT1. This is most likely due to the fact that larger prestressing strand (0.6-in. diameter) was used in the HCS specimen in Test LT2 than was used in Test LT1 (0.5-in diameter). Additionally, the concrete at the test time for Specimen

LT2 was younger (19 hours) than for Specimen LT1 (40 hours). The additional curing time for test LT1 could have enhanced cement paste hydration and increased bond capacity, thereby reducing the transfer length. Strand diameter is another parameter that is believed to affect transfer length because the larger ratio of strand cross-sectional area to surface area for larger strand require a longer length to dissipate the effective prestress.

Table 8-4: Test LT2 Transfer Length Results

DSS Number	Method I Transfer Length, L_t [in.]	Method II Transfer Length, L_t [in.]	Method III Transfer Length, L_t [in.]
DSS 1	22.10	23.28	21.86
DSS 2	18.74	19.48	18.97
DSS 3	25.79	27.08	24.99
DSS 4	23.36	25.18	22.67
Average	22.50	23.78	22.12
Standard Deviation	2.54	2.81	2.15
Avg + SD	25.04	26.59	24.27
Avg +2SD	27.58	29.40	26.42

The transfer length values from Test LT2 were also normalized using the prestressing strand nominal diameter. These normalized values for L_t/d_b can be seen in Table 8-5. The normalized transfer length values are slightly larger than the values that were obtained from Test LT1 for all three methods (Table 8-3). As noted for Test LT1, the normalized transfer lengths are lower than the ACI 318-14 implied value of 50, even though the average plus two standard deviations are just below the ACI 318 estimate of 50.

Table 8-5: Test LT2 Normalized Transfer Length Results

	Method I, L_t/d_b	Method II, L_t/d_b	Method III, L_t/d_b
Average	37.5	39.63	36.87
Avg + SD	41.73	44.32	40.45
Avg + 2SD	45.97	49.00	44.03

8.4 Discussion of the Transfer Length Test Procedure using DSS Devices

During the transfer length tests, several problems or difficulties were encountered that could be improved upon in future tests that use this testing procedure. The first and major

problem was with the data acquisition wiring and the set up time before the tests. In order to get as low strength of concrete as possible, tests were conducted early in the morning when the precast plant starts stripping the beds. On the first day it took several hours of wiring and troubleshooting before the data acquisition system was working. This time could have been saved by going to the precasting plant the day before and setting up so that everything would be ready first thing in the morning the next day.

Another problem that was encountered was the length of the lead wires on the electrical resistance strain gauges. The strain gauges that were used had a three-meter (9.84-ft) lead wires preinstalled by the manufacturer. It is recommended that the lead wires not be shorter than this, and whenever possible longer lead wires are recommended. There were times when it was difficult to move the HCS to the bed with the crane while the DSS devices were wired to the data acquisition system. The HCS had to be moved slowly and the data acquisition system had to be moved along with it. When the HCS was saw cut, the data acquisition had to be set directly in front of the HCS where it was to be sawn. This location was in the path of water and slag from the concrete saw, and the data acquisition system had to be covered by a plastic tarp which was not ideal for the operator. Some electrical resistance strain gauge manufacturers make strain gauges with five-meter lead wires (16.4-ft) that are preinstalled, and such option should work better. If not, lead wires could also be spliced onto the preinstalled lead wires to lengthen them.

Chapter 9 Conclusion

9.1 Summary

The work that was described in this report was conducted to determine an expedient, easy, and effective way for determining the transfer length of prestressing strand in HCS. The proposed DSS method allowed for quick and easy use of electrical resistance foil strain gauges to determine the concrete strain change along the bottom of the HCS. The DSS (distributed strain sensor) is a thin strip of steel with electrical resistance strain gauges attached to it which can be quickly attached to a HCS to recorded strain readings. The DSS test method allows for fast and easy determination of the transfer length in HCS. It is also inexpensive because the DSS can be reused from one test to another without having to purchase and install new strain gauges. The work included linear finite element analysis, small-scale adhesive tests, large-scale slab tests, and field-deployed transfer lengths tests.

9.2 Results and Observations

To verify using the DSS method to measure the transfer length of prestressing strand in HCS, a finite element model of a HCS slab section was constructed including the DSS devices. With this finite element analytical effort, several variables of the DSS were investigated including the material properties (modulus of elasticity), the geometric properties (thickness, width, and length), and the layout. Information gleaned from the finite element analysis was used to design the full-scale tests that were conducted in the laboratory. From the finite element analysis it was determined that the DSS devices should be constructed from steel strips that are one-eighth of an inch thick and one inch wide. The length of the DSS did not affect the strain readings and should be chosen to be longer than the transfer length that is expected to be measured. Additionally, a shear lag distance, D_{sl}, was observed at each end of the DSS.

A small-scale adhesive test was conducted to determine the most appropriate adhesive for attaching the DSS to the bottom of the HCS for the transfer length tests. Tests were conducted by attaching small steel strips, which were instrumented with electrical resistance strain gauges, to a prismatic concrete specimen, 24-in. tall, 6-in. wide, and 6-in.

deep, with various adhesives and loading it in uniaxial compression. The strains in the steel strips and the concrete were measured and compared to evaluate the ability of the adhesive to transmit the concrete strains to the steel strips. It was deemed necessary for the adhesives that were used in these tests to be inexpensive adhesives that could be purchased easily online or from a local hardware store. Based on these tests it was determined that a slow-setting cyanoacrylate based adhesive would be used, specifically EZ Bond I-161500 cyanoacrylate. This adhesive allowed for a quick cure time and short shear lag length at an inexpensive cost.

Full-scale laboratory tests were conducted using a 20-foot long section of HCS. Strain gauges were attached directly to the concrete on the bottom face of the HCS. DSS were also attached to the bottom of the HCS. Upon loading the HCS, the strains in the DSS and the HCS were measured and compared. Through appropriate loading schemes, constant and variable strain regions were investigated, as well as the use of multiple DSS devices. The strains measured in the DSS closely resembled the strains that were measured in the HCS in all tests performed with the added benefit that the DSS provided a more uniform distribution of stresses.

Lastly, the DSS devices were used in two transfer length tests at precast plant. The DSS were attached to a segment of HCS that was subsequently sawn. Through judicious selection of the test setup and the saw cutting process, transfer length regions were created in the strand on both sides of the saw cut. The DSS were used to measure the changes in strain of the bottom concrete surface near the prestressing strands. These changes in strain were used to determine the transfer length of the strand. By taking into account the changing support and prestress conditions during the cutting process, the changes in strain due to the strand release were identified. The transfer lengths that were obtained from these tests were close to ACI 318 provisions for transfer length. The average plus two standard deviations of the normalized transfer length L_t/d_b was very close to the simplified conservative estimate of 50 that is recommended by ACI 318-14.

In summary, the DSS method proved to be quick and easy to use, as well as inexpensive to implement once the DSS devices were fabricated. The DSS test procedure is a very attractive alternative for conducting future tests to determine the transfer length of strand in HCS.

9.3 Recommendations for Future Work

While the proposed transfer length testing procedure seemed to work well, only two tests on HCS were conducted in the field (i.e. a precast plant). More transfer length tests on HCS should be conducted using the proposed DSS method to identify other improvements and to gain experience before this procedure can become an accepted method for determining the transfer length of strand in HCS.

Investigation into different parameters that affect the transfer length of strand in HCS should be done. These variables could include, but would not be limited to, manufacturing method (i.e. wet-cast, slip-formed, or extruded), concrete mix (including fiber-reinforced mixes), slab depth, slab cross-section, and prestressing configuration.

REFERENCES

1. ACI Committee 318, *Building Code Requirements for Structural Concrete (ACI 318-11) and Commentary (ACI 318R-11),* American Concrete Institute, Farmington Hills, MI, 2011.
2. ACI Committee 318, *Building Code Requirements for Structural Concrete (ACI 318-14) and Commentary (ACI 318R-14),* American Concrete Institute, Farmington Hills, MI, 2014.
3. Ashby, Michael F. Jones, David R. H.. (2012). *Engineering Materials 1 - An Introduction to Properties, Applications, and Design* (4th Edition). Elsevier.
4. Barnes, R.W., Grove, J.W., and Burns, N.H. (2003). "Experimental Assessment of Factors Affecting Transfer Length." *ACI Struct. Jour.*, 100(6): 740-748.
5. Brooks, M. D., Gerstle, K. H., & Logan, D. R. (1988). Effect of initial strand slip on the strength of hollow-core slabs. *PCI Journal, 33*(1), 90-111
6. Buettner, D.R., and Becker, R.J., *Manual for the Design of Hollow Core Slabs*, Precast/Prestressed Concrete Institute, 2nd Edition, Chicago, IL, 1998.
7. Caro, L. A., Martí-Vargas, J. R., & Serna, P. (2013). Time-dependent evolution of strand transfer length in pretensioned prestressed concrete members. *Mechanics of Time-Dependent Materials, 17*(4), 501-527.
8. Deng, Y., Morcous, G., and Ma, Z.J. (2016). "Strand bond stress–slip relationship for prestressed concrete members at prestress release." *Mat. & Struct.*, 49: 889–903.
9. Evonik Industries AG, (2013). Technical Information Plexiglas®. (January), 1-7. Retrieved from http://www.plexiglas.de/sites/lists/PM/DocumentsAP/211-1-PLEXIGLAS-GS-XT-en.pdf
10. Guyon Y. (1958). *Béton précontrainte. Étude théorique et expérimentale*. Paris: Ed. Eyrolles.
11. Helbawi, H., Zhang, L., & Zarudi, I. (2001). Difference in subsurface damage in indented specimens with and without bonding layer. *International Journal of Mechanical Sciences, 43*(4), 1107-1121.

12. Martí-Vargas, J. R., Arbelá, C. A., Serna-Ros, P., Fernández-Prada, M. A., & Miguel-Sosa, P. F. (2006). Transfer and development lengths of concentrically prestressed concrete. *PCI Journal, 51*(5), 74-85.
13. Martí-Vargas, J.R., Arbeláez, C.A., Serna-Ros, P. and Castro-Bugallo, C. (2007). "Reliability of Transfer Length Estimation from Strand End Slip." *ACI Struct. Jour.*, 104(4): 487-494.
14. Martí-Vargas, J. R., and Hale, W. M. (2013). Predicting strand transfer length in pretensioned concrete: Eurocode versus North American practice. *Journal of Bridge Engineering,* (December), 1270-1280.
15. Martí-Vargas, J.R., Hale, W.M., García-Taengua, E. and Serna, P. (2014). "Slip distribution model along the anchorage length of prestressing strands." *Eng. Struct.*, 59: 674–685.
16. Palmer, K. D., and Schultz, A. E. (2010). Web shear strength of precast, pretensioned concrete hollow core slab units.
17. Park, H. and Cho, J.-Y. (2014). "Bond-Slip-Strain Relationship in Transfer Zone of Pretensioned Concrete Elements." *ACI Struct. Jour.*, 111(3): 503-514.
18. Russell, B., & Burns, N. H. (1997). Measurement of transfer lengths on pretensioned concrete elements. *ASCE Journal of Structural Engineering, 123*(5), 541-549.
19. Walraven, J. C, Mercx, W. P. M. (1983). The bearing capacity of prestressed hollow core slabs. *HERON,* 28(3), 1-46
20. Zia, P. and Mostafa, T. (1977). "Development Length of Prestressing Strands." *PCI Jour.*, 22(5): 54-65.
21. Zia, P., Preston, H. K., Scott, N. L., Workman, E. B. (1979). "Estimating Prestress Losses." *Concrete International,* June, 32-38.

Appendix A Finite Element Analysis

This section provides information pertaining to the finite element analysis that was conducted to investigate the DSS when bonded to the HCS. Material properties that were used are given in A.1, and A.2 summarizes results that were obtained from the analysis.

A.1 Material Properties

Table A-1 shows the material properties that were used in the finite element analysis. The properties used for the steel and aluminum are well-known values that have been determined by numerous experimental investigations and widely available in the technical literature (Ashby, 2012). The modulus of the concrete was computed using the approximation from ACI 318-14 of 57,000 times the square root of the compressivestrength of the concrete (ACI Committee 318, 2014). The design strength of the concrete in the HCS provided by the local precast plant of 9000 psi was used.

The material properties for plexiglass were obtained from the Evonik Corporation website for their product Plexiglas® (Evonick Industries AG, 2013). The Evonik Corporation holds the patent for plexiglass and is a supplier and distributer of the material as well.

An estimate for the elastic modulus and Poisson's ratio for cyanoacrylate was obtained Helbawi et al. (2001) who conducted tests to determine the material properties for a cyanoacrylate adhesive. It is not the same adhesive as that used in this investigation, but for the preliminary model in this investigation, it was assumed to be a reasonable estimate.

Table A-1: Material Properties of Model

DSS Material	Location in Model	Elastic Modulus [ksi]	Poisson's Ratio
Concrete (f'_c = 9ksi)	HCS	5407.5	0.2
Steel	DSS	29,000	0.3
Aluminum	DSS	10,000	0.32
Plexiglass	DSS	479	0.37
Cyanoacrylate	Glue Layer	175	0.25

A.2 Analysis Results

Results that were obtained from the finite element analysis that was conducted are provided in this section. The first group of figures are for the Phase I analysis where the adhesive layer was not modeled. The second group of figures are for the Phase II analysis where the adhesive layer was modeled.

Phase I - No Adhesive Modeled

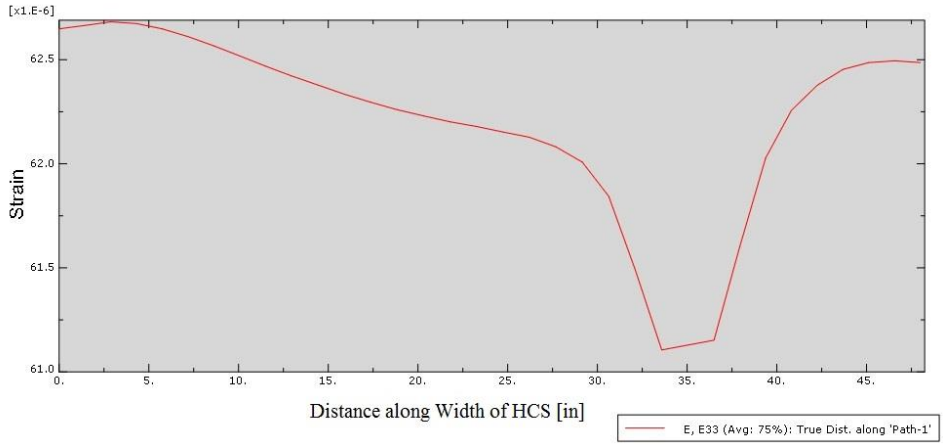

Figure A-1: Strain along Width of HCS, 12"x1/8"x1" Steel DSS

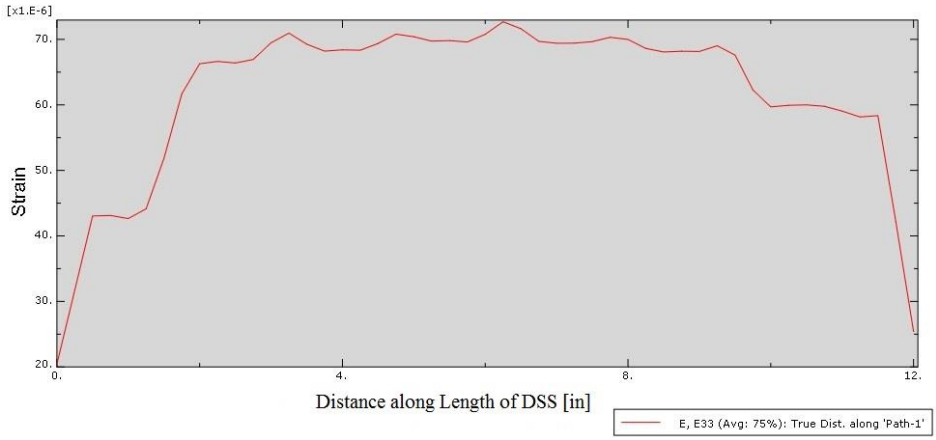

Figure A-2: Strain along Length of DSS, 12"x1/8"x1" Steel DSS

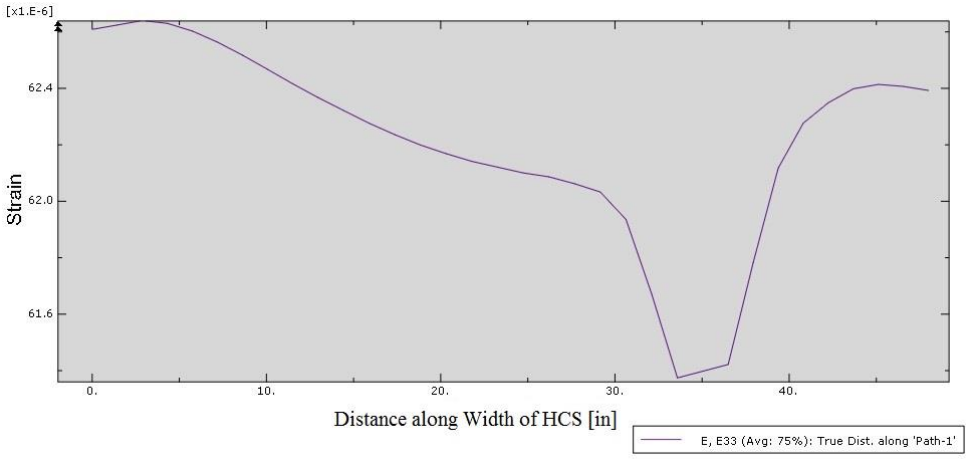

Figure A-3: Strain along Width of HCS, 24"x1/8"x1" Steel DSS

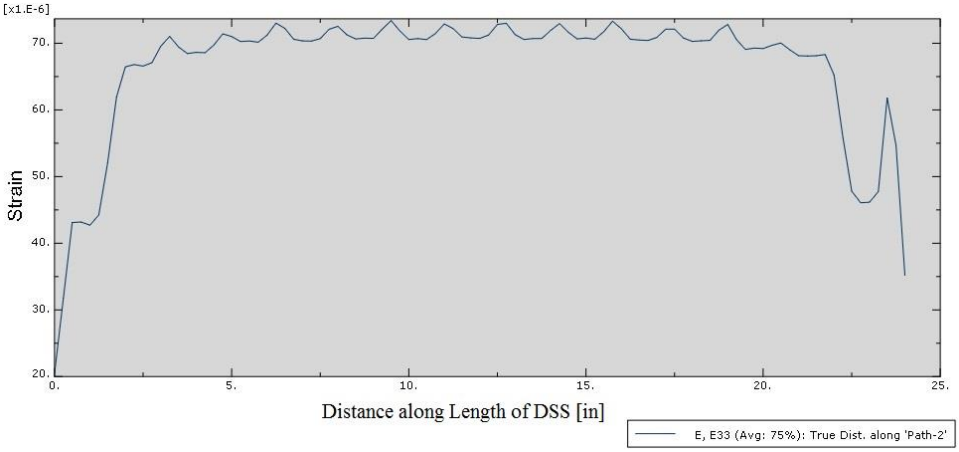

Figure A-4: Strain along Length of DSS, 24"x1/8"x1" Steel DSS

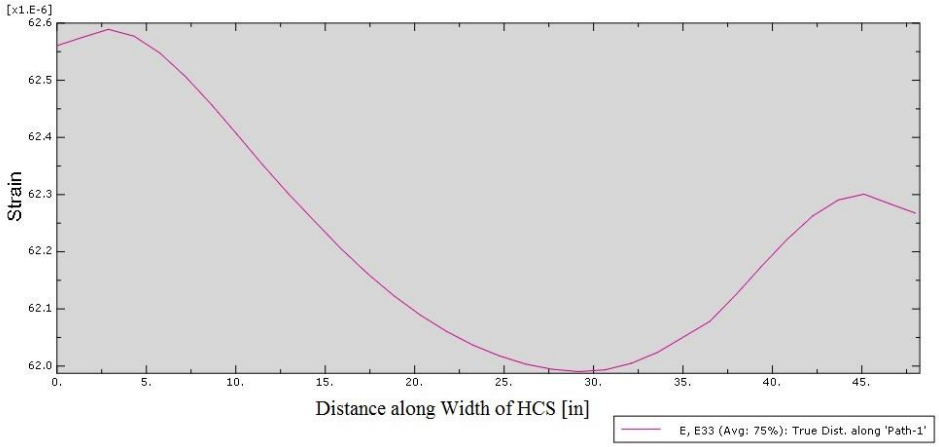

Figure A-5: Strain along Width of HCS, 40"x1/8"x1" Steel DSS

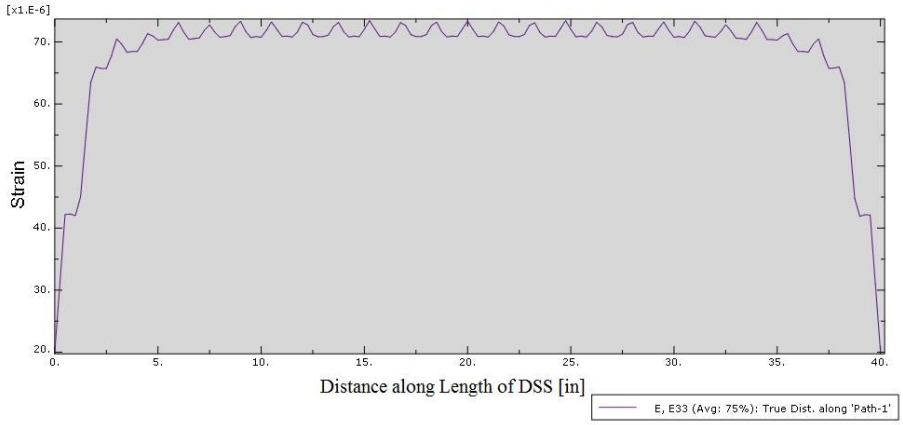

Figure A-6: Figure A 4: Strain along Length of DSS, 40"x1/8"x1" Steel DSS

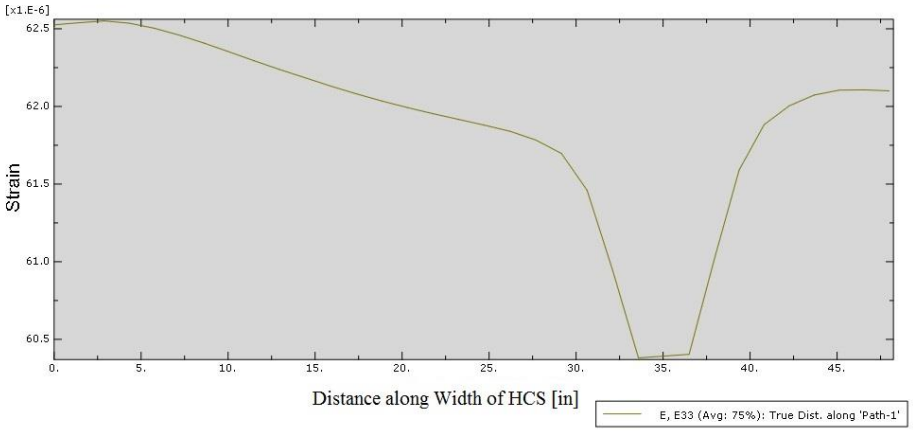

Figure A-7: Strain along Width of HCS, 24"x1/8"x2" Steel DSS

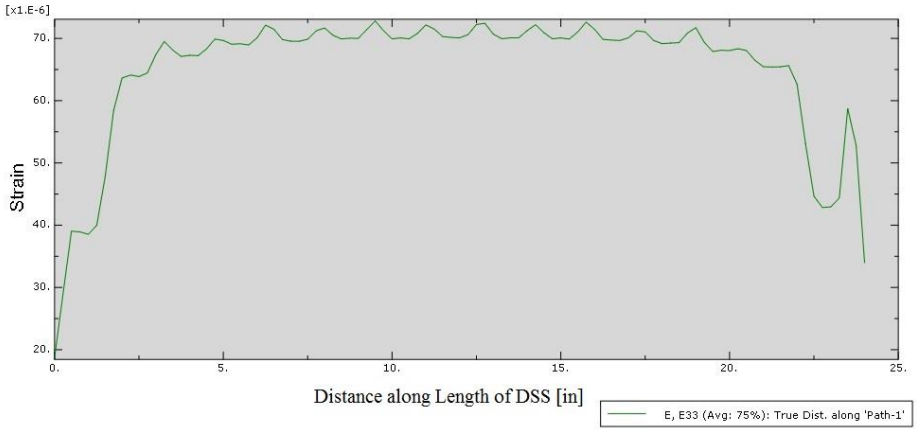

Figure A-8: Strain along Length of DSS, 24"x1/8"x2" Steel DSS

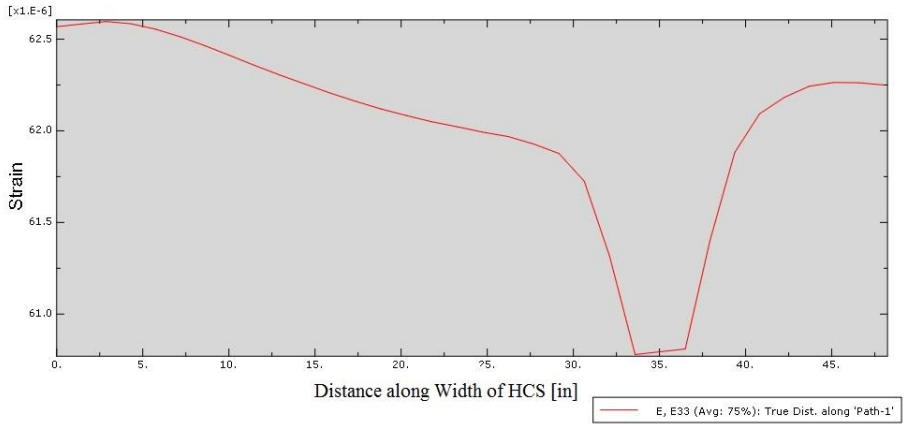

Figure A-9: Strain along Width of HCS, 24"x3/16"x1" Steel DSS

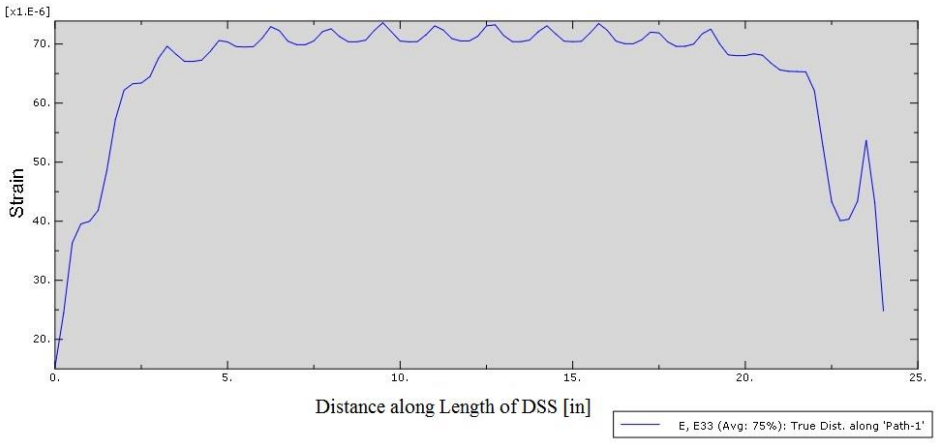

Figure A-10: Strain along Length of DSS, 24"x3/16"x1" Steel DSS

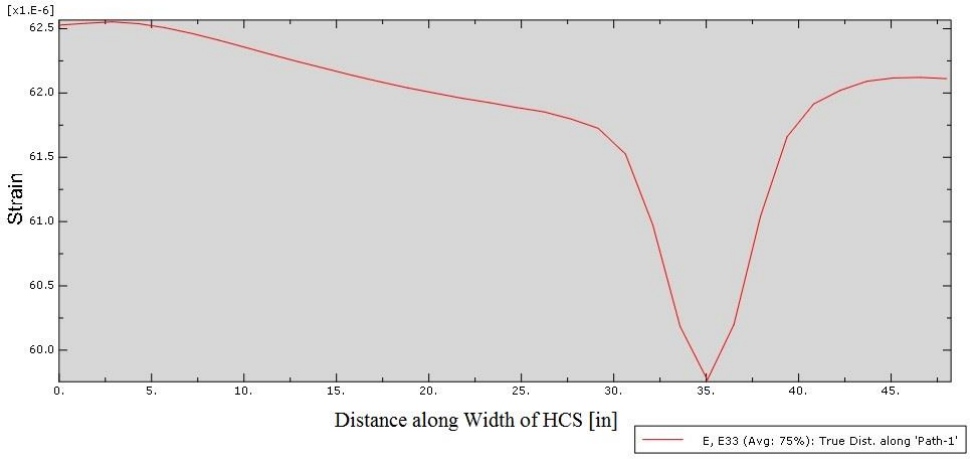

Figure A-11: Strain along Width of HCS, 24"x1/4"x1" Steel DSS

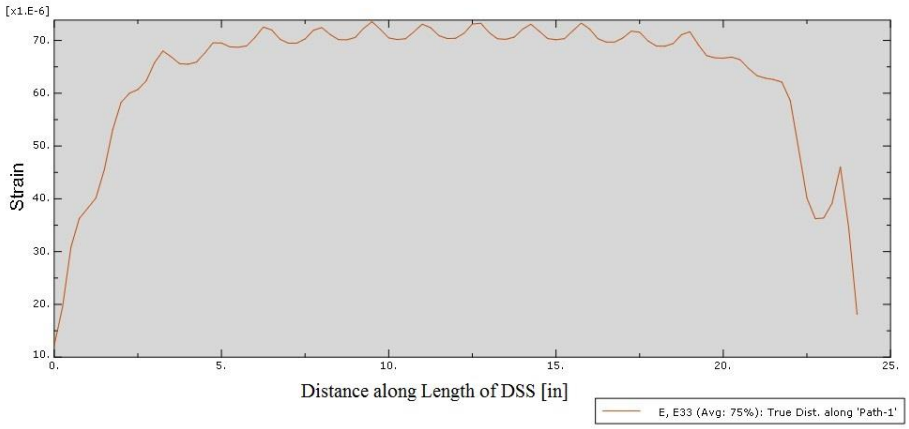

Figure A-12: Strain along Length of DSS, 24"x1/4"x1" Steel DSS

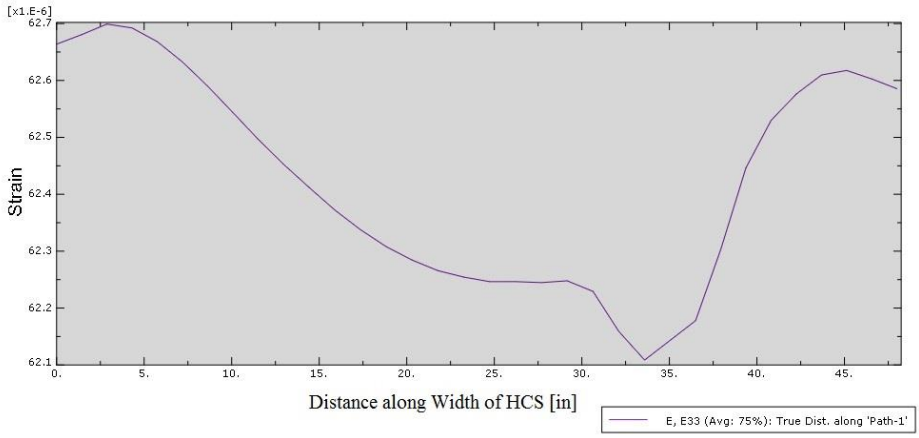

Figure A-13: Strain along Width of HCS, 24"x1/8"x1" Aluminum DSS

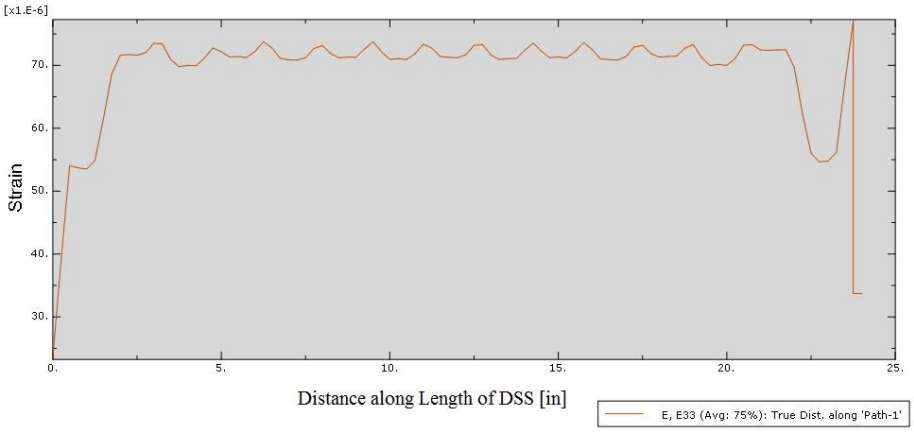

Figure A-14: Strain along Length of DSS, 24"x1/8"x1" Aluminum DSS

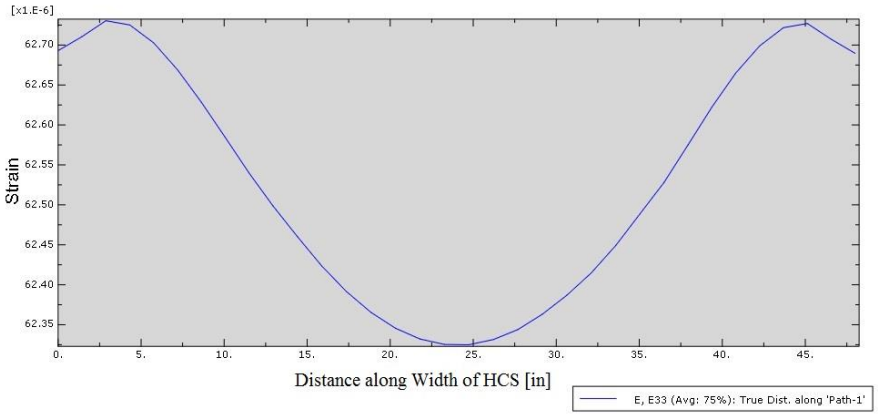

Figure A-15: Strain along Width of HCS, 24"x1/8"x1" Plexiglass DSS

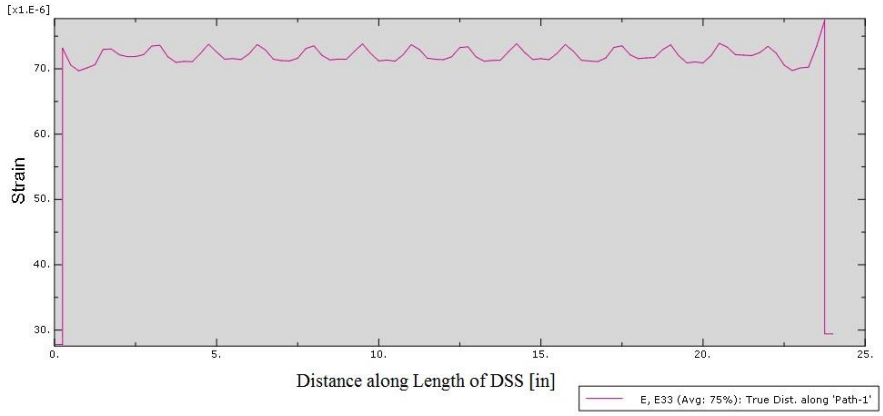

Figure A-16: Strain along Length of DSS, 24"x1/8"x1" Plexiglass DSS

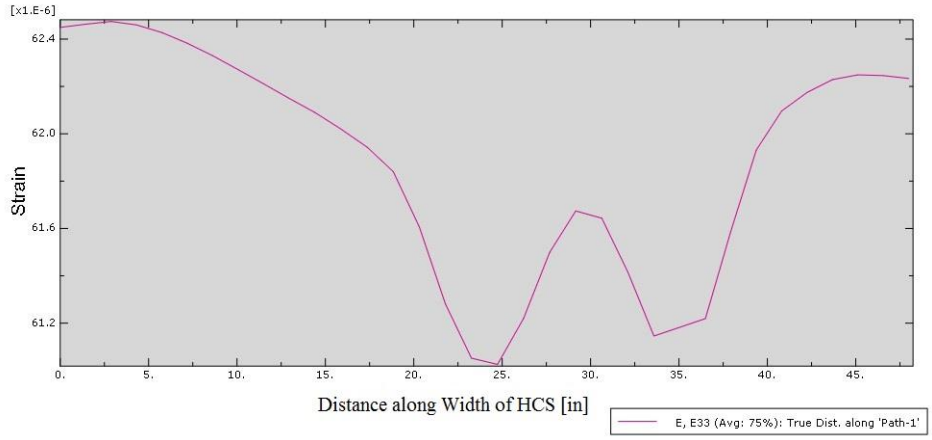

Figure A-17: Strain along Width of HCS, Two 24"x1/8"x1" Steel DSS Side by Side

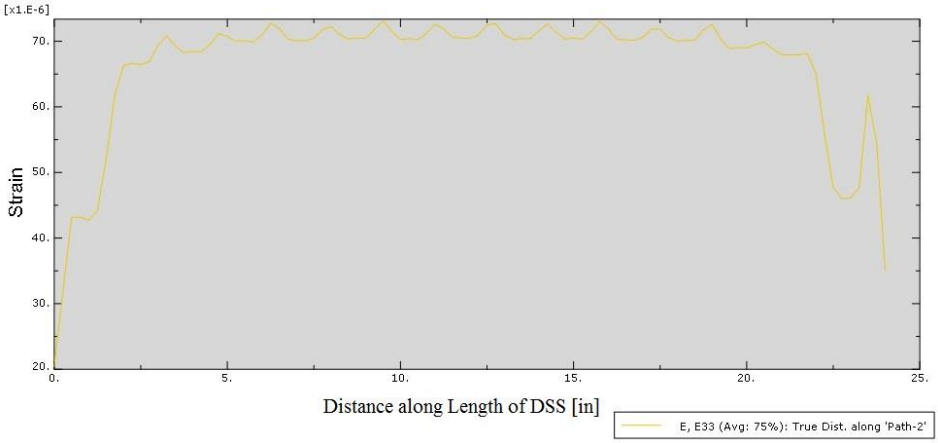

Figure A-18: Strain along Length of DSS, Two 24"x1/8"x1" Steel DSS Side by Side

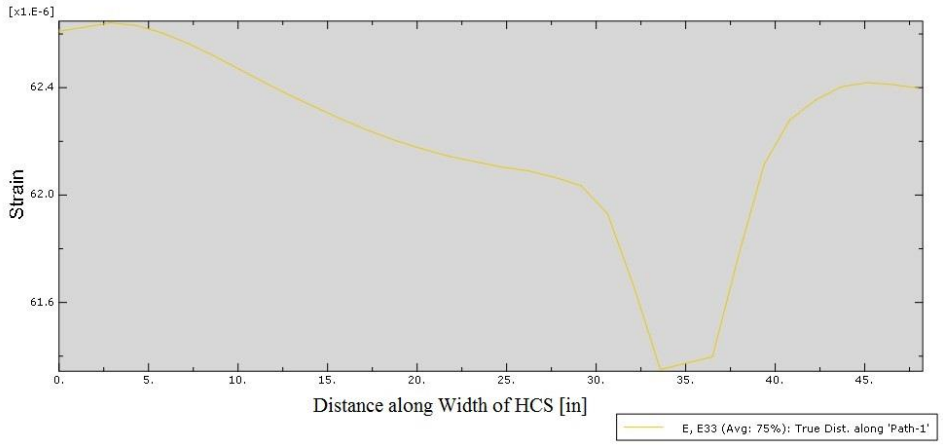

Figure A-19: Strain along Width of HCS, Two 12"x1/8"x1" Steel DSS End to End

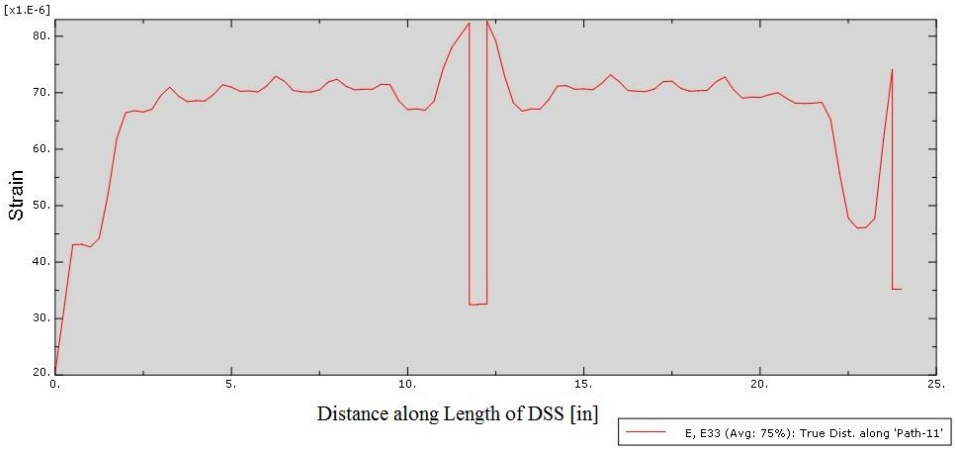

Figure A-20: Strain along Length of DSS, Two 12"x1/8"x1" Steel DSS End to End

Phase II - Adhesive Modeled

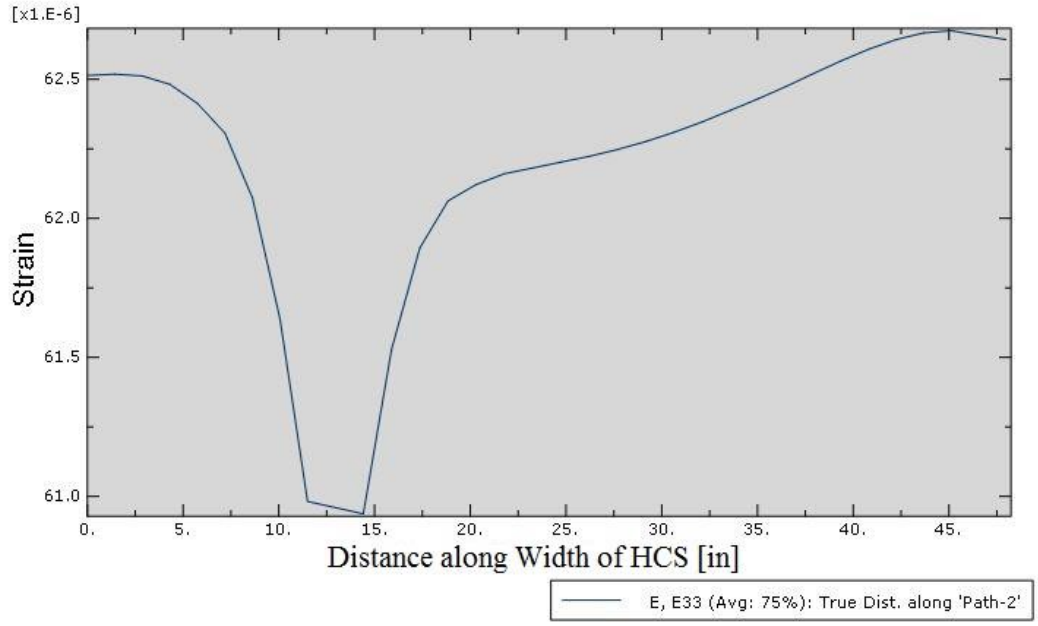

Figure A-21: Strain along Width of HCS, 12"x1/8"x1" Steel DSS with Adhesive

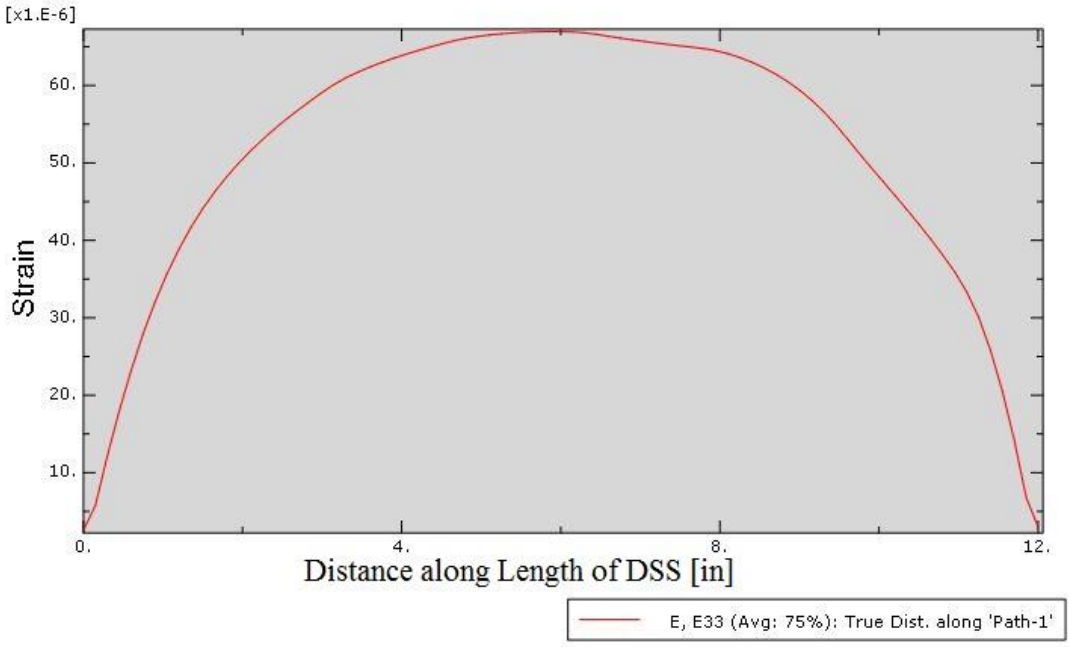

Figure A-22: Strain along Length of DSS, 12"x1/8"x1" Steel DSS with Adhesive

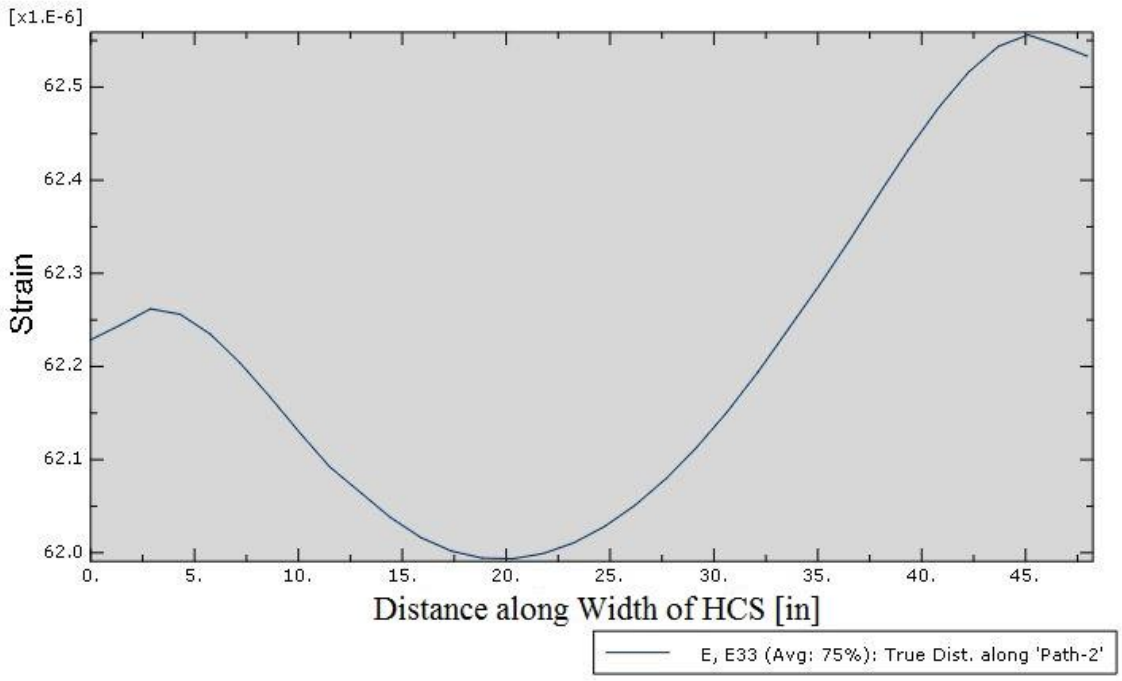

Figure A-23: Strain along Width of HCS, 40"x1/8"x1" Steel DSS with Adhesive

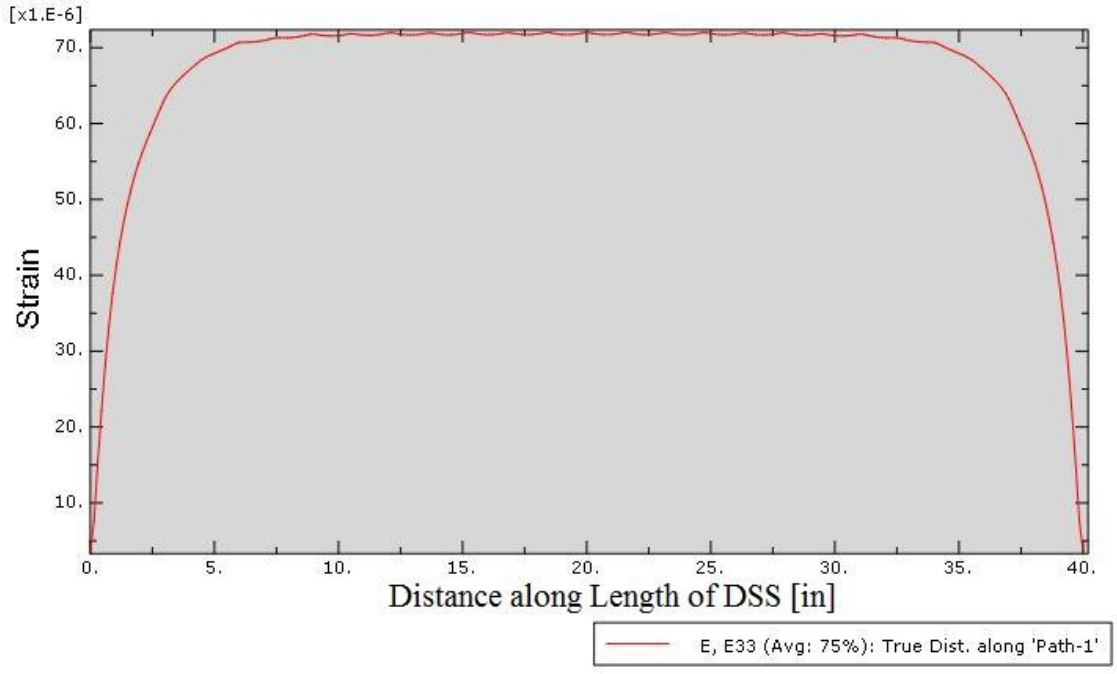

Figure A-24: Strain along Length of DSS, 40"x1/8"x1" Steel DSS with Adhesive

Appendix B Adhesive Tests

This section provides information pertaining to the adhesive tests (AT1, AT2, and AT3) that were conducted and the adhesives that were used in those tests. Section B.1 includes the Material Safety Data Sheets (MSDS) for the glue that was chosen to attach the DSS to the HCS in all of the remaining test, EZ-Bond I-161500. B.2 shows notes that were taken by the authors when attaching and removing each glue in the adhesive test.

B.1 MSDS for EZ-Bond I-161500

This section gives the MSDS for EZ-Bond I-161500 provided by the manufacturer.

K & R International

1533 Summitridge Dr. Diamond Bar, CA 91765
TEL: 909-860-7880 FAX : 909-861-7093
www.e-zbond.com E-mail: sales@e-zbond.com

MATERIAL SAFETY DATA SHEET

Item No. I-161500

1 CHEMICAL PRODUCT AND COMPANY IDENTIFICATION

Product Type: Cyanoacrylate Ester

2 COMPOSITION, INFORMATION ON INGREDIENTS

Ingredients	CAS No.	%
Poly(methyl methacrylate)	9011-14-7	20-30
Ethyl Cyanoacrylate	7085-85-0	70-80
HYDROQUINONE	123-31-9	0-0.5

Ingredients, which have exposure limits

Exposure Limits Ingredients	(TWA) (TLV)	ACGIH (PEL)	OSHA	OTHER
Ethyl Cyanoacrylate	0.2ppmTWA	None	None	
HYDROQUINONE	2mg/m3TWA	2mg/m3TWA	2mg/m3TWA	4mg/m3 STEL
Exposure Limits Ingredients	(STEL) (TLV)	AGGIH (PEL)	OSHA	

3 HAZARDS IDENTIFICATION

Toxicity: Bonds skin rapidly and strongly
Skin and eye irritant
Estimated oral LD50 more than 5000mg/kg
Estimated dermal LD50 more than 2000mg/kg

Signs and Symptoms of Exposure: Vapor is irritating on eyes and mucous membranes above TLV.
Prolonged and repeated overexposure to vapors may produce
Symptoms of non-allergic asthma in sensitive individuals

4 FIRST AID MEASURES

Ingestion: Ingestion is not likely. See supplemental page for emergency procedures.
Inhalation: Remove to fresh air. If symptoms persist, obtain medical attention
Skin Contact : Soak in Warm water. See supplemental pager for emergency procedures.
Eye Contact: Flush with water. See supplemental page for emergency procedure

5 FIRE FIGHTING MEASURES

Flash Point: 180 F
Method: Tag Closed Cup
Recommended Extinguishing Agents: Carbon dioxide, foam, dry chemical
Special Firefighting Procedures: Not available
Hazardous Products formed by fire or thermal decamp: Irritating organic fragments.
Unusual Fire or Explosion Hazards: None
Explosive Limits (% by volume in air) Lower : Not available
Explosive Limits (% by volume in air) Upper : Not available

6 ACCIDENTAL RELEASE MEASURES

Step to be taken in case of spill or leak: Flood with water to polymerize. Soak up with an inert Absorbent.

7 HANDLING AND STORAGE

Safe Storage; Store below 70F
Handling: Avoid contact with skin and eyes. Avoid breathing vapor.

8 EXPOSURE CONTROLS, PERSONAL PROTECTION

Eyes: Safety glasses or goggles
Skin: PE gloves and aprons. Do not use cotton. See section 12 for additional information
Ventilation: Positive down-draft exhaust ventilation should be provided to maintain vapor concentration below TLV
Respiratory: Not available. See Section 2 for Exposure Limits

9 PHYSICAL AND CHEMICAL PROPERTIES

Appearance: Clear liquid.
Odor: Sharp, irritation
Boiling Point: 140-160 F @ 3-5 mmHg
PH: Does not apply
Solubility in Water: Polymerized by water
Specific Gravity: 1.05 @ -10 F
Vapor Pressure: Less than 0.2mm
Evaporation Density: Approximately 3
Evaporation Rate(Ether=1) : Not Available

10 STABILITY AND REACTIVITY

Stability: Stable
Hazardous Polymerization: Will not occur
Incompatibility: Polymerized by contact with amines, alkalies, water and alcohols
Conditions to Avoid: Not available
Hazardous Decomposition product (non-thermal): None

11 OTHER INFORMATION

Estimated NFPA Code:
Health Hazard: 2
Fire Hazard: 2
Reactivity Hazard; 1
Specific Hazard: Does not apply

Estimated HMIS Code:
Health Hazard: 2
Flammability Hazard: 2
Reactivity Hazard: 1
Personal Protection: See Section 8

12 OTHER INFORMATION

Cyanoacrylate adhesive is a very fast setting and strong adhesive. It bonds human tissue including Skin in seconds. Experience had shown that accidents due to Cyanoacrylste are handled best by Passive, non-surgical first aid. Treatment of specific types of accidents is given below.

SKIN CONTACT

Remove excess monomer. Soak in warm, soapy water. The monomer will come loose from the skin Several hours. cured monomer does not present a health hazard even when bonded to the skin. Avoid Contact with clothes, fabrics, rags, or tissue. Contact with these materials may cause polymerization. The polymerization of large amounts of monomer will generate heat causing smoke, skin burns, and Strong, irritating vapors, Wear PE gloves and apron when handling large amounts of adhesive.

SKIN ADHESION

First, immerse the bonded surfaces in warm, soapy water. Peel or roll the surfaces apart with the Aid of a blunt edge, e.g.a spatula or a teaspoon handle: then remove adhesive form the skin with Soap and water. Do not try to pull surfaces apart with a direct opposing action.

EYELID TO EYELID OR EYEBALL ADHESION

In the event that eyelids are stuck together or bonded to the eyeball, wash thoroughly with warm Water and apply a gauze patch. The eye will open without further action, typically in 1-4days. There will be no residual damage. Do not try to open the eyes by manipulation.

B.2 Visual Observations of Adhesive Application and Removal

Notes that were taken by the authors on applying and removing each glue during the adhesive test that were conducted.

Table B-1: Adhesive Application and Removal Notes

Adhesive Name	Application Notes	Removal Notes
JB Weld Clear Syringe	Very thick, hard to apply only a thin layer.	Very rubbery when hardened.
Gorilla Glue Super Glue	The glue is runny and thin. Process must be rushed to apply it because of how short the set time is.	Whole piece pops off with one hit from the hammer and chisel.
Gorilla Glue Epoxy	Thick and difficult to apply a thin layer, also difficult to only discharge the amount desired.	Somewhat difficult to remove. Stiffer than the JB Weld.
VHB Tape	Very easy to apply. No set or cure time.	Very difficult to clean off the back of the steel strip.
Liquid Nails	Very easy application.	Rubbery and easy to remove.
Hilti	Long cure time. Application requires a special gun and mixing nozzle. Nozzle has to be disposed of after each use.	Most difficult to remove. Took several hits of the hammer and chisel to break it free. Very stiff.
Loctite Superglue Gel	Similar to EZ Bond. Sold in a much smaller container.	Similar to EZ Bond.
EZ Bond I-161500	Easy to apply. Slow enough set time that there is plenty of time to apply it, yet it sets fast enough that it would	Easy to remove like GG super glue. Entire steel strip is covered so it seems like it did a

	still be easy to apply to the bottom side of the HCS.	better job of bonding to all of the steel.

Appendix C Experimental Instrumentation Details

Appendix C describes all of the information for the data collection system. Section C.1 describes all of the gauges that were used throughout the experimental program (adhesive tests, full-scale tests, and field tests). Section C.2 provides information on the devices used for the portable data acquisition system as well as the electrical wiring scheme. The process for attaching a linear foil strain gauge is given in C.3 and C.4 gives a sample program that was used in the data logger to record and collect the strain measurements.

C.1 Strain Gauge Information

Strain gauges that were used throughout the experimental investigation are listed below. Table C-1 includes the manufacturer, model number, and the type of experiment in which the gauges were used.

Table C-1: Linear Foil Strain Gauge Information

Instrument Description	Manufacturer	Model No.	Resistance	Length	Experiment Type	DAQ
Linear Foil Strain Gauge	Tokyo Sokki Kenkyujo (Texas Measurments)	FLA-6-11-5LT	120 Ohms	6 mm	Attached to steel strips in adhesive tests (AT1 – AT3)	Campbell Scientific CR1000
Linear Foil Strain Gauge	Tokyo Sokki Kenkyujo (Texas Measurments)	PL-60-11-5LT	120 Ohms	60 mm	Attached to concrete specimen in adhesive	Campbell Scientific CR1000

					tests (AT1 – AT3)	
Linear Foil Strain Gauge	Tokyo Sokki Kenkyujo (Texas Measurments)	PFLA-30-11-5LT	120 Ohms	30 mm	Attached directly to HCS for full scale laboratory tests (FT1 – FT3)	CE DAQ
Linear Foil Strain Gauge	Tokyo Sokki Kenkyujo (Texas Measurments)	UFLA-5-350-11-5LT	350 Ohms	5 mm	Attached to DSS for full scale laboratory tests (FT1 – FT3)	Campbell Scientific CR1000
Linear Foil Strain Gauge	Omega Engineering Inc.	KFH-6-350-C1-11L3 M3R	350 Ohms	6 mm	Attached to DSS for Field Testing (LT1, LT2)	Campbell Scientific CR1000

Note:

Strain gauges were purchased from Omega Engineering Inc. instead of Texas Measurements for the field tests due to order processing time.

C.2 Data Collection Information

This section describes the portable data acquisition system that was used to record the data for the adhesive tests (AT1 – AT3), full-scale tests (FT1 – FT3), and field tests (LT1, LT2). Table C.2 shows the 3 key devices that are needed for the data acquisition system and describes what they do. Figures C.1 and C.2 show the wiring diagram for the system. Figure

3.1 shows the wiring diagram for the CR1000 data logger and Figure C.2 shows the wiring diagram for the AM16/32B multiplexer for one linear foil strain gauge. For more gauges to be read the wiring is repeated for each channel.

Table C-2: DAQ Devices

DAQ Device	Manufacturer	Purpose
CR1000 Data logger	Campbell Scientific	Measures, collects, and stores all of the data that is being measured.
AM 16/32B Multiplexer	Campbell Scientific	This is an extension of the data logger. The multiplexer allows for 16 strain gauges to be recorded through one channel on the data logger. The data logger by itself could only read 8 strain gauges.
4WFBS 350 Completion Resistor	Campbell Scientific	Wheatstone bridge completion resistor that allows the small change in resistance of the linear foil strain gauge to be read with high precision. One is needed for each strain gauge that is measured

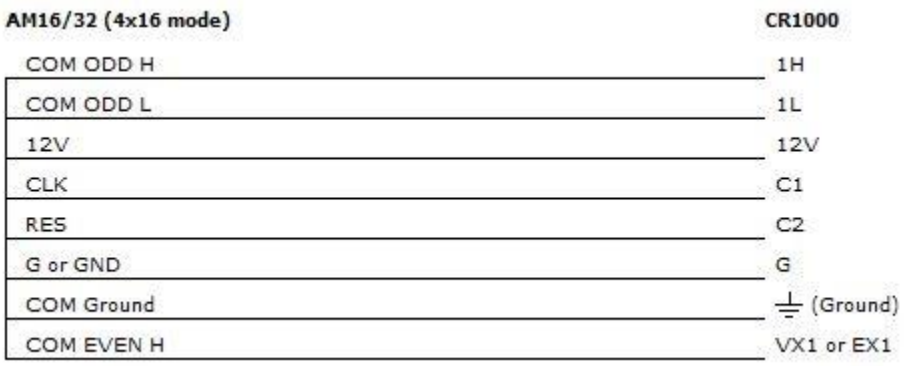

Figure C-1: CR1000 Wiring Diagram

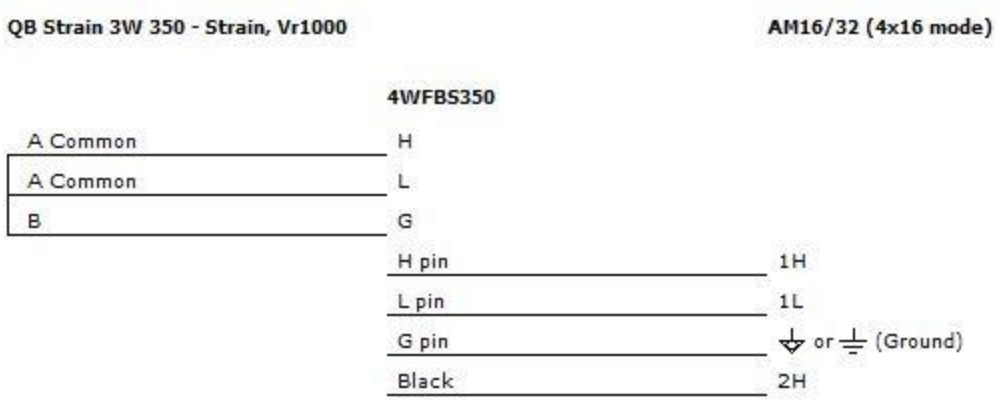

Figure C-2: AM16/32B Multiplexer Wiring Diagram

C.3 Foil strain Gauge Application Techniques

Below are the steps used for installing linear foil strain gauges to both steel and concrete. The surface preparation is different for the two materials but the remainder of the process stays the same. All of the adhesive materials were purchased from Tokyo Sokki Kenkyujo Co., Ltd.

1a. Prepare Steel Surface

a. Sand the steel surface using 100, 220, and 400 grit sandpaper, in that order.
b. Mark the exact strain gauge location using a ballpoint pen.
c. Clean steel surface with acetone until cloth comes away completely clean. A small groove from the ballpoint pen should remain.

1b. Prepare Concrete Surface

a. Apply a thin layer of PS adhesive, which is a two-component room-temperature-curing polyester adhesive, to the concrete face to provide a suitable gauge-bonding surface. This should fill any small voids in the concrete face. Allow the adhesive to dry for 24 hours.
b. Sand the thin adhesive layer with 320 or 400 grit sandpaper until the base concrete material is exposed.
c. Mark the Exact Strain gauge location using a ballpoint pen.

d. Clean the surface with acetone until the cloth comes away completely clean. A small grove from the ballpoint pen should remain.

2. Prepare Strain Gauge for Attachment
   a. Place strain gauge, silver side up, on a clean smooth surface.
   b. Apply clear Scotch™ tape over the gauge making sure to avoid air pockets
   c. Carefully peel tape off of the clean surface with the gauge attached to the tape.
3. Attach the Strain Gauge
   a. Place the gauge in the desired position and secure the gauge with Scotch tape.
   b. Peel the tape back until the bottom of the gauge is entirely visible.
   c. Apply 1-2 drops of CN adhesive (Tokyo Sokki Kenkyujo) to the bottom of the gauge, depending on the size of the gauge
   d. Press the gauge back into position and apply thumb pressure for 60 seconds, rocking thumb carefully to reduce air pockets.
   e. Slowly peel tape off of the strain gauge.
4. Apply Protection for the Gauge
   a. Place a small piece of electrical tape underneath the exposed lead wires to separate them from the bonding surface
   b. Provide strain relief with zip-tie or tape.
   c. Place a small amount of SB tape (Tokyo Sokki Kenkyujo) between the lead wires and electrical tape. Press the lead wires into the SB tape to keep them separated.
   d. Cover the entire gauge and lead wires with SB tape and press down firmly around the edges.
   e. Cover the SB tape with Epoweld 8173 (Tokyo Sokki Kenkyujo) two-part epoxy for waterproofing and mechanical protection. The epoxy requires approximately 24 hours for hardening.

Note:

For applying strain gauges to concrete for laboratory tests part 4e was omitted.

C.4 Sample CR1000 Program Used for Laboratory Tests and Field Tests

Below is a sample program for the Campbell Scientific CR1000 data logger that was used in one of the Adhesive tests. In this test, 11 strain gauges were sampled through an AM16/32 Multiplexer. Two differential voltage readings were recorded as well as outputs of load and displacement from the load frame that was used. Variations of this program were used for most tests conducted but with different numbers of strain gauges read and multiplexers used.

```
-Wiring for CR1000-

  AM16/32 Multiplexer (4x16 mode)
    1H:  COM ODD H
    1L:  COM ODD L
    Ground:  COM Ground
    VX1 or EX1:  COM EVEN H
    G:  GND
    12V:  12V
    C1:  CLK
    C2:  RES

  Differential Voltage (1)
    2H:  High
    2L:  Low
    Ground:  Shield

  Differential Voltage (2)
    Ground:  Shield
    3H:  High
    3L:  Low

-Wiring for AM16/32 Multiplexer (4x16 mode)-

  Quarter Bridge Strain, 3-wire 120 ohm with 4WFBS120 TIM (1)
    1H:  H pin (4WFBS120)
    1L:  L pin (4WFBS120)
    BGround:  G pin (4WFBS120)
    2H:  Black (4WFBS120)

           (4WFBS120) H:  A Common
           (4WFBS120) L:  A Common
```

```
        (4WFBS120) G:  B

Quarter Bridge Strain, 3-wire 120 ohm with 4WFBS120 TIM (2)
  3H:  H pin (4WFBS120)
  3L:  L pin (4WFBS120)
  BGround:  G pin (4WFBS120)
  4H:  Black (4WFBS120)

        (4WFBS120) H:  A Common
        (4WFBS120) L:  A Common
        (4WFBS120) G:  B

Quarter Bridge Strain, 3-wire 120 ohm with 4WFBS120 TIM (3)
  5H:  H pin (4WFBS120)
  5L:  L pin (4WFBS120)
  BGround:  G pin (4WFBS120)
  6H:  Black (4WFBS120)

        (4WFBS120) H:  A Common
        (4WFBS120) L:  A Common
        (4WFBS120) G:  B

Quarter Bridge Strain, 3-wire 120 ohm with 4WFBS120 TIM (4)
  7H:  H pin (4WFBS120)
  7L:  L pin (4WFBS120)
  BGround:  G pin (4WFBS120)
  8H:  Black (4WFBS120)

        (4WFBS120) H:  A Common
        (4WFBS120) L:  A Common
        (4WFBS120) G:  B

Quarter Bridge Strain, 3-wire 120 ohm with 4WFBS120 TIM (5)
  9H:  H pin (4WFBS120)
  9L:  L pin (4WFBS120)
  BGround:  G pin (4WFBS120)
  10H:  Black (4WFBS120)

        (4WFBS120) H:  A Common
        (4WFBS120) L:  A Common
        (4WFBS120) G:  B

Quarter Bridge Strain, 3-wire 120 ohm with 4WFBS120 TIM (6)
  11H:  H pin (4WFBS120)
  11L:  L pin (4WFBS120)
  BGround:  G pin (4WFBS120)
  12H:  Black (4WFBS120)

        (4WFBS120) H:  A Common
        (4WFBS120) L:  A Common
        (4WFBS120) G:  B
```

```
Quarter Bridge Strain, 3-wire 120 ohm with 4WFBS120 TIM (7)
  13H:  H pin (4WFBS120)
  13L:  L pin (4WFBS120)
  BGround:  G pin (4WFBS120)
  14H:  Black (4WFBS120)

         (4WFBS120) H:  A Common
         (4WFBS120) L:  A Common
         (4WFBS120) G:  B

Quarter Bridge Strain, 3-wire 120 ohm with 4WFBS120 TIM (8)
  15H:  H pin (4WFBS120)
  15L:  L pin (4WFBS120)
  BGround:  G pin (4WFBS120)
  16H:  Black (4WFBS120)

         (4WFBS120) H:  A Common
         (4WFBS120) L:  A Common
         (4WFBS120) G:  B

Quarter Bridge Strain, 3-wire 120 ohm with 4WFBS120 TIM (9)
  17H:  H pin (4WFBS120)
  17L:  L pin (4WFBS120)
  BGround:  G pin (4WFBS120)
  18H:  Black (4WFBS120)

         (4WFBS120) H:  A Common
         (4WFBS120) L:  A Common
         (4WFBS120) G:  B

Quarter Bridge Strain, 3-wire 120 ohm with 4WFBS120 TIM (10)
  19H:  H pin (4WFBS120)
  19L:  L pin (4WFBS120)
  BGround:  G pin (4WFBS120)
  20H:  Black (4WFBS120)

         (4WFBS120) H:  A Common
         (4WFBS120) L:  A Common
         (4WFBS120) G:  B

Quarter Bridge Strain, 3-wire 120 ohm with 4WFBS120 TIM (11)
  21H:  H pin (4WFBS120)
  21L:  L pin (4WFBS120)
  BGround:  G pin (4WFBS120)
  22H:  Black (4WFBS120)

         (4WFBS120) H:  A Common
         (4WFBS120) L:  A Common
         (4WFBS120) G:  B
```

```
-Measurement Labels-

  Default Measurements
    BattV
    PTemp_C

  Differential Voltage (1)
    Disp

  Differential Voltage (2)
    Force

  Quarter Bridge Strain, 3-wire 120 ohm with 4WFBS120 TIM (1)
    Strain(1)
    Vr1000(1)

  Quarter Bridge Strain, 3-wire 120 ohm with 4WFBS120 TIM (2)
    Strain(2)
    Vr1000(2)

  Quarter Bridge Strain, 3-wire 120 ohm with 4WFBS120 TIM (3)
    Strain(3)
    Vr1000(3)

  Quarter Bridge Strain, 3-wire 120 ohm with 4WFBS120 TIM (4)
    Strain(4)
    Vr1000(4)

  Quarter Bridge Strain, 3-wire 120 ohm with 4WFBS120 TIM (5)
    Strain(5)
    Vr1000(5)

  Quarter Bridge Strain, 3-wire 120 ohm with 4WFBS120 TIM (6)
    Strain(6)
    Vr1000(6)

  Quarter Bridge Strain, 3-wire 120 ohm with 4WFBS120 TIM (7)
    Strain(7)
    Vr1000(7)

  Quarter Bridge Strain, 3-wire 120 ohm with 4WFBS120 TIM (8)
    Strain(8)
    Vr1000(8)

  Quarter Bridge Strain, 3-wire 120 ohm with 4WFBS120 TIM (9)
    Strain(9)
    Vr1000(9)

  Quarter Bridge Strain, 3-wire 120 ohm with 4WFBS120 TIM (10)
    Strain(10)
    Vr1000(10)
```

```
  Quarter Bridge Strain, 3-wire 120 ohm with 4WFBS120 TIM (11)
    Strain(11)
    Vr1000(11)

--------------------------------------------------
Table: Table1
Interval: 20 SEC
Fields:
 Strain_Max(1)      Units: microstrain
 Strain_Max(2)      Units: microstrain
 Strain_Max(3)      Units: microstrain
 Strain_Max(4)      Units: microstrain
 Strain_Max(5)      Units: microstrain
 Strain_Max(6)      Units: microstrain
 Strain_Max(7)      Units: microstrain
 Strain_Max(8)      Units: microstrain
 Strain_Max(9)      Units: microstrain
 Strain_Max(10)     Units: microstrain
 Strain_Max(11)     Units: microstrain
 Disp_Max    Units: mV
 Force_Max   Units: mV
```

Appendix D Distributed Strain Sensor Information

Appendix D describes the Distributed Strain Sensors that were fabricated and used to measure strains in the HCS. The fabrication, application technique, and cleaning method are listed.

D.1 DSS Fabrication

The following are the steps that were used for the fabrication of the DSS. The steel for the DSS was hot rolled A36 steel that was purchased from a local steel supplier. All of the adhesives that were used were purchased from Tokyo Sokki Kenkyujo Co., Ltd.

1. Cut the steel strip to the desired length.
2. File off any burrs that were created by the saw cut. Square edges on the ends of the strip can also be filed down slightly.
3. Clean both sides of the steel with acetone to remove any grease that may be on the steel as well as any rust.
4. Select the side of the steel strip to which the gauges will be attached. This should be the cleanest side with the small amount of pitting, if any is present.
5. Sand down the side of the steel that the gauges will be attached to with 220 and 400 grit sandpaper in that order
6. Wipe down both sides of the steel with acetone again to remove the sanding dust.
7. Mark the centerline along the length of the steel strip with a ballpoint pen.
8. Mark the location on the centerline where each gauge is to be placed with a ballpoint pen.
9. Wipe the location where the gauge is to be placed with a clean rag and acetone. The ink from the pen will disappear but a small grove will remain. Repeat until the rag comes away clean.
10. Attach the linear foil strain gauge with CN adhesive (Tokyo Sokki Kenkyujo), the center of the gauge should be placed at the mark that was made from the ballpoint pen.

11. Place a small piece of electrical tape beneath the exposed lead wires separating them from the steel. Trim so that the tape does not hang over the edges of the strip.
12. Place a small amount of SB tape (Tokyo Sokki Kenkyujo) beneath the lead wires gently pressing them into the SB tape.
13. Cover the entire gauge and lead wires in SB tape.
14. Provide strain relief for the gauge by using a piece of duct tape to secure the lead wire coming out of the SB tape to the steel. Trim the duct tape.
15. Repeat 9-14 for each gauge that is to be attached.
16. Once all the gauges are attached. Coat each piece of SB tape (Tokyo Sokki Kenkyujo) that is covering the gauge and lead wires with Epoweld 8173 two-part epoxy (Tokyo Sokki Kenkyujo). Allow the adhesive to harden for 24 hours.
17. Use a chisel to carefully scrape off any epoxy that may have dripped over the edge of the steel.

Note:

For added strain relief, imbed the lead wires from a gauge into the epoxy covering the gauge behind it.

D.2 DSS Application Technique

Below are the steps that were used in order to install the DSS to the HCS for the laboratory tests as well as the field tests. The method is the same for every length of DSS, however more assistants will be needed when applying a longer DSS.

1. Mark the spot on the HCS where the DSS is to be placed. It is easiest to place the DSS directly on the HCS where it is to be placed and outlining the ends of the DSS in permanent marker.
2. Make sure that the back of the DSS is clean and free of any glue from any previous tests (See Appendix D.3 for DSS cleaning procedure)

3. Wipe off the back of the DSS using acetone. Using a lint free rag or sturdy paper towel works best. This should be done until the rag comes away almost clean when wiping from one end of the DSS to the other.
4. Apply a bead of EZ-Bond I-161500 cyanoacrylate down the center of the back of the DSS.
5. Spread out the glue evenly one the back of the DSS making sure that the whole surface of back of the DSS is covered. The authors found it easiest to do this with a large nail.
6. Place the DSS on the HCS where it is to be attached applying constant pressure along the length of the DSS for two minutes. This can be done with your hands however more assistants will be needed for longer DSS. Using latex gloves can prevent hands from being stuck to the DSS if too much glue is used.
7. Slowly remove hands making sure that the DSS stays in place.

Note:

Cyanoacrylate glues do not bond well to themselves. If a DSS is attached and removed it cannot be reattached in the same location without cleaning the glue from the concrete surface because the glue will not set.

D.3 Method for Removing and Cleaning DSS after Use

Below are the steps that were used for removing and cleaning the DSS after each use so that it is ready for the next test. In the field tests that were conducted in this study, it took about an hour to remove and clean four five-foot long DSS devices so that they were ready for another test.

Removing:

1. Take a chisel and place the edge it between the DSS and the HCS at one end of the DSS.
2. Gently tap on the chisel with a hammer until the bond between the DSS and the HCS is broken

3. Slide the chisel along the gap between the DSS and the HCS to continue to break the bond, gently peeling off the DSS as the bond is broken. Make sure to not bend or deform the DSS or it will be more difficult to attach in the next test.

Cleaning:

1. Set the DSS on a smooth flat surface
2. Using a chisel, scrape the back of the DSS. This should be done until all of the concrete that is still stuck to the back is removed and most of the glue is as well. A sharp square chisel works best.
3. Use a lint free rag or towel and acetone to wipe off the back of the DSS. This should be repeated until there are no remnants of the glue left. Any hardened glue that is still remaining on the DSS will make reattachment of the DSS more difficult.

Appendix E Transfer Length Data Processing

This section discusses the data processing method that was used to determine the transfer length from the data that was collected in the two transfer length tests at a precast plant. Section E.1 gives a detailed derivation regarding how the data was be processed. E.2 provides the raw data from the tests as well as the corrections that were made to the data from this procedure. Final results are also given.

E.1 Derivation of Data Processing Procedure

Strain data is collected during the transfer length tests that include components requiring correction. These components are associated with bending from gravity loading due to slab self-weight, changes in bending effects upon saw-cutting of the slab (i.e., support conditions change), initial non-zero offset strains, and slab camber due to prestressing.

A. Idealized (Theoretical) Strains

To process the strain data from the transfer length tests, three different idealized (theoretical) load cases are considered.

Load Case 1: The first case represents the instrumented slab over simple supports and span length L after it is placed on the precasting bed and immediately before it is cut. The center support should not be in contact when the strains are measured (i.e., either it has not been placed yet, or it has been placed with a small gap between top of support and the bottom of slab), such that the entire slab is simply-supported.

Load Case 2: The second case represents the idealized case of the instrumented slab after it is cut into two simply-supported spans with length $L/2$, but before the strand is released. Load Cases 2 and 3 occur simultaneously, but the loading effects are considered separately here. This case includes only the effect of the slab self-weight, w_{sw}, over span length $L/2$.

Load Case 3: The third case represents the idealized case of the instrumented slab immediately after the strands are released by saw-cutting, but before slab self-weight is

applied. Load Cases 2 and 3 occur simultaneously, but the loading effects are considered separately here. This case includes only the effect of prestress release.

Strain distributions ε_1, ε_2 and ε_3, respectively, are produced in Load Cases 1, 2 and 3. These are strains on the bottom face of the concrete member, and they vary with distance, x, along the slab beginning at the location of the saw cut. The strains are defined as follows:

$\varepsilon_1 \equiv$ concrete bottom surface strain under slab self-weight, w_{sw}, for a span L

$\varepsilon_2 \equiv$ concrete bottom surface strain under slab self-weight, w_{sw}, for a span $L/2$

$\varepsilon_3 \equiv$ concrete bottom surface strain under strand release for a span $L/2$

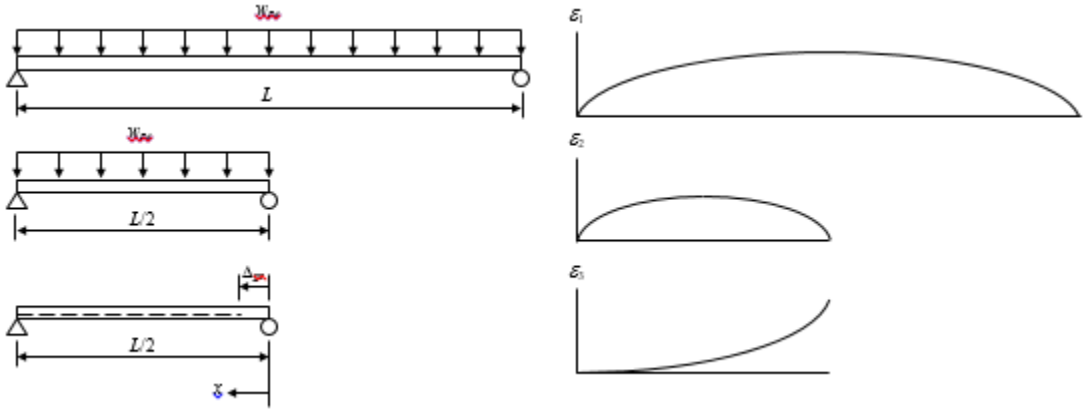

Figure E-1: Loading and Moment Diagrams Due to Changing Support Conditions and Strand Release

B. Measured Strains

The idealized strains, ε_1, ε_2, and ε_3, must be determined from strains measured during the transfer length tests and, if necessary, calculations. The measured strains, ε_A and ε_B, are obtained at two specific Loading Stages.

Loading Stage A: This stage coincides with the slab on the precasting bed and immediately before it is saw-cut. The strain measurement in this stage, ε_A, includes the strain from self-

weight on the full span, ε_1, the initial offset strain, ε_o, and the strain contribution due to camber in Loading Stage A, ε_{cA}. Thus,

$$e_A = e_1 + e_o + e_{cA} \tag{E-1}$$

Loading Stage B: This stage coincides with the slab on the precasting bed immediately after it is saw-cut. The strain measurement in this stage, ε_B, includes the strain from self-weight on the half-span, ε_2, the strain due to prestress release, ε_3, the initial offset strain, ε_o, and the strain contribution due to camber in loading stage B, ε_{cB}. Thus,

$$e_B = e_2 + e_3 + e_o + e_{cB} \tag{E-2}$$

C. Initial Offset Strain

It is assumed that each strain gauge has an initial offset strain reading, ε_o, which corresponds to a state of zero strain in the concrete. It is further assumed that the strain ε_o remains constant for the each gauge during all stages of the transfer length test. These strains vary from one gauge to another, and they cannot be obtained by measurement because they correspond to a condition that is impossible to sample: They correspond to slab conditions before the strands are initially cut and the slabs removed from the precasting bends.

D. Influence of Bending from Self-Weight

During the transfer length tests, the loading is of sufficiently small magnitude that the materials are linear, elastic and that the slab section remains uncracked. For such conditions, the idealized strain, ε_1, in Load Case 1 is

$$e_1 = \frac{s_1}{E_c} = \frac{1}{E_c}\left(\frac{M_1 y_c}{I_n}\right) = \left(\frac{y_c}{E_c I_n}\right) M_1 \tag{E-3}$$

and the moment function, M_1, defining x starting at the location of the saw-cut and increasing to either the right or left, is

$$M_1 = \frac{w_{sw}}{2}\left(\frac{L}{2} - x\right)\left(\frac{L}{2} + x\right) \tag{E-4}$$

Combining Eq. (E-3) and (E-4) gives

$$\varepsilon_1 = \left(\frac{w_{sw} y_c}{2E_c I_n}\right)\left(\frac{L}{2} - x\right)\left(\frac{L}{2} + x\right) \tag{E-5}$$

Similarly, for Load Case 2, the idealized strain, ε_2, is

$$\varepsilon_2 = \frac{\sigma_2}{E_c} = \frac{1}{E_c}\left(\frac{M_2 y_c}{I_n}\right) = \left(\frac{y_c}{E_c I_n}\right) M_2 \tag{E-6}$$

and the moment, M_2, is

$$M_2 = \frac{w_{sw}}{2}\left(\frac{L}{2} - x\right)x \tag{E-7}$$

so that the idealized strain, ε_2, becomes

$$\varepsilon_2 = \left(\frac{w_{sw} y_c}{2E_c I_n}\right)\left(\frac{L}{2} - x\right)x \tag{E-8}$$

E. Camber Strains

It is assumed that all gauges have strain components due to camber, ε_{cA} and ε_{cB}, which remain constant during each of the two loading stages of the transfer length test. The camber strains, ε_{cA} and ε_{cB}, are generated by the moment from eccentric prestressing that

is calculated as the product of $F_{PT,x}$ and e_{PT}, where $F_{PT,x}$ is the prestressing force at a distance x from the saw-cut location, and e_{PT} is the eccentricity of the prestressing tendons. The latter is constant along the slab, and the force $F_{PT,x}$ changes over the transfer length region. The variation in $F_{PT,x}$ over the transfer length region is assumed to be linear.

For Loading Stage A, the distribution of $F_{PT,x}$ is trapezoidal and decreases linearly from the effective value of $F_{PT,e}$ to zero on segments with lengths equal to the transfer length, L_t, on either end of the uncut slab.

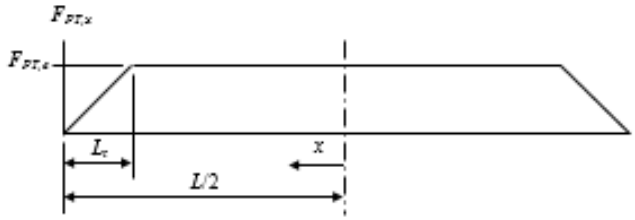

Figure E-2: Diagram of the Force in the Strand before the Saw Cut

For $L/2 - x < L_t$, that is $x > L/2 - L_t$

$$e_{cA} = \frac{e_{cm}}{L_t}\left(\frac{L}{2} - x\right) \tag{E-9}$$

For $L/2 - x \geq L_t$, that is $x \leq L/2 - L_t$

$$e_{cA} = e_{cm} \tag{E-10}$$

The maximum camber strain, ε_{cm}, is computed as the flexural strain arising from the flexural compressive stress, $\sigma_{PT,e}$, in the bottom face of the slab assuming linear elastic behavior and an uncracked section under the moment, $M_{PT,e}$, due to the effective prestressing force, $F_{PT,e}$, that is placed with constant eccentricity, e_{PT}.

$$\varepsilon_{cm} = \frac{\sigma_{PT,e}}{E_c} = \frac{\left(M_{PT,e} y_c / I_n\right)}{E_c} = \left(\frac{F_{PT,e} e_{PT} y_c}{E_c I_n}\right) \tag{E-11}$$

where E_c is the modulus of elasticity of the concrete, and I_n is the net section moment of inertia.

Since the transfer length, L_t is not known, several approaches can be used here. In the more general case, an initial assumption on the transfer length, $L_{t,1}$, can be made in order to process the strain data. The transfer length can then be determined by processing the strain data to evaluate the decay in concrete surface strains, and the computed value, $L_{t,2}$ compared with $L_{t,1}$. If they differ, then $L_{t,1}$ can be set equal to $L_{t,2}$, and the strain data re-processed and the transfer length obtained again. This process can be repeated until $L_{t,1}$ and $L_{t,2}$ converge. A simpler approach is to approximate L_t in Eq. (E-9) according to ACI 318-14 as $50d_b$, where d_b is strand diameter.

In the data analysis that was conducted for field tests that were conducted a third procedure was used. An initial L_t value was chosen based on two criteria. The first criterion was to remove any slope in the inverted strain plateau. The second criterion was to minimize the residuals (root mean squares) of the values in the inverted strain plateau. An initial L_t was chosen that fit these two criteria most suitably.

For Loading Stage B, the distribution of $F_{PT,x}$ is idealized by trapezoids on either side of the saw-cut location. It increases linearly from 0 to the effective value of $F_{PT,e}$ over segments equal to the transfer length, L_t, on either end of the saw-cut location, and then decreases linearly until it vanishes at the slab ends.

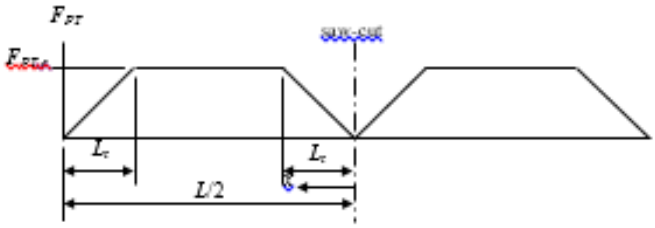

Figure E-3: Diagram of the Force in the Strand after the Saw Cut

For $x < L_t$

$$e_{cA} = e_{cm}\left(\frac{x}{L_t}\right) \tag{E-12}$$

For $L/2 - L_t \le x \le L_t$

$$e_{cA} = e_{cm} \tag{E-13}$$

For $L/2 - x < L_t$, that is $x > L/2 - L_t$

$$e_{cA} = \frac{e_{cm}}{L_t}\left(\frac{L}{2} - x\right) \tag{E-14}$$

and the maximum camber strain, ε_{cm}, is computed according to Eq. (E-11) and L_t obtained as described above.

F. Combining Effects

Obtain the sum of the offset strains, ε_o, and camber strains in Loading Stage A, ε_{cA}, from Eq. (E-1)

$$e_o + e_{cA} = e_A - e_1 \tag{E-15}$$

where it is assumed that w_{sw}, y_c, E_c and I_n are available from the producer. If w_{sw} is not available, then it should be calculated from the net area of the section, A_n, and the unit weight of the concrete, γ_c.

Solve for ε_3 from Eq. (E-2) as follows

$$e_3 = e_B - e_2 - \left(e_o + e_{cB}\right) = e_B - e_2 - \left(e_o + e_{cA}\right) + \left(e_{cA} - e_{cB}\right) \tag{E-16}$$

Combine Eq. (E-15) and (E-16) yields

$$e_3 = \left(e_B - e_A\right) + \left(e_1 - e_2\right) + \left(e_{cA} - e_{cB}\right) \tag{E-17}$$

This calculation is done for every gauge, such that for the jth gauge

$$e_{3,j} = \left(e_{B,j} - e_{A,j}\right) + \left(e_{1,j} - e_{2,j}\right) + \left(e_{cA,j} - e_{cB,j}\right) \tag{E-18}$$

where $\varepsilon_{A,j}$ and $\varepsilon_{B,j}$ are from measured strains from the tests, and $\varepsilon_{1,j}$ and $\varepsilon_{2,j}$ are calculated using Eq. (5) and (8) at $x = x_j$ (which is the distance from the saw-cut to the jth gauge), and $\varepsilon_{cA,j}$ and $\varepsilon_{cB,j}$ are calculated using Eq. (9) – (14) at $x = x_j$.

Substituting Eq. (E-5) and (E-8) and simplifying gives

$$e_{3,j} = \left(e_{B,j} - e_{A,j}\right) + \left(\frac{w_{sw} y_c L}{4 E_c I_n}\left(\frac{L}{2} - x_j\right)\right) + \left(e_{cA,j} - e_{cB,j}\right) \tag{E-19}$$

E.2 Field Transfer Length Test Data and Corrections

This section gives the raw data that was collected during the transfer length tests at the precast plant. Strain corrections for the data are also given for each DSS as well as final results.

LT1 DSS 1

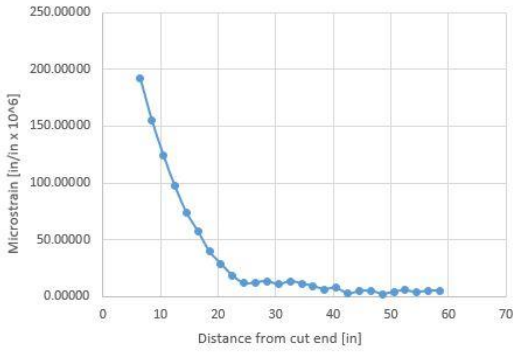

Figure E-4: Corrected Change in Strain LT1 DSS 1

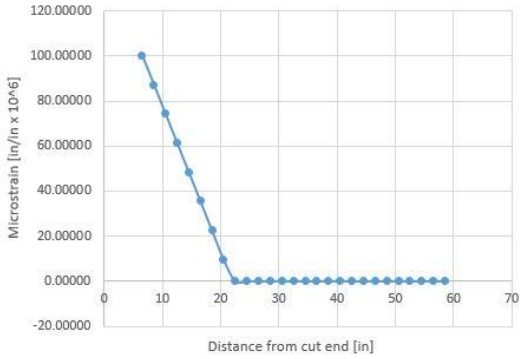

Figure E-5: Change in Eccentric Prestressing Strains LT1 DSS 1

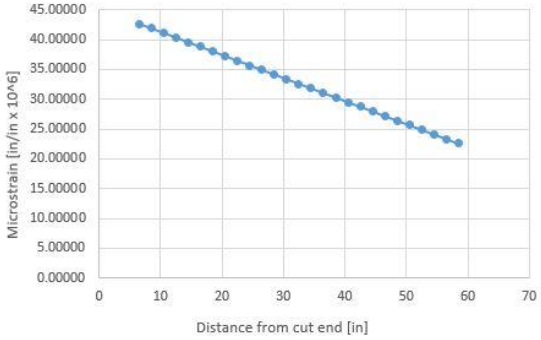

Figure E-6: Change in Strain Due to Changing Support Conditions LT1 DSS 1

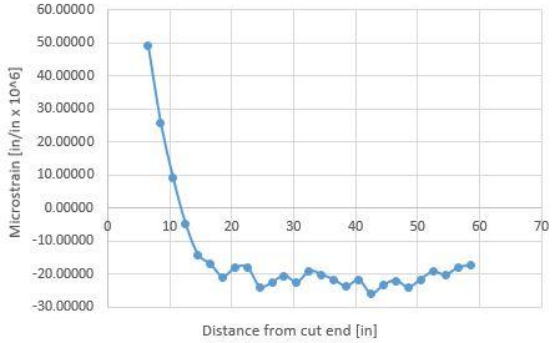

Figure E-7: Measured Change in Strain LT1 DSS 1

LT1 DSS 2

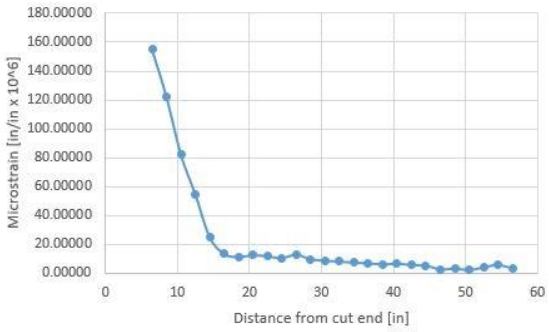

Figure E-8: Corrected Change in Strain LT1 DSS 2

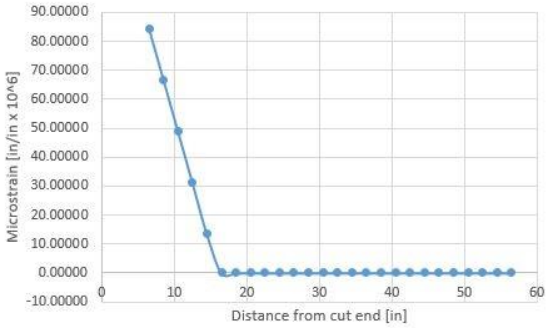

Figure E-9: Change in Eccentric Prestressing Strains LT1 DSS 2

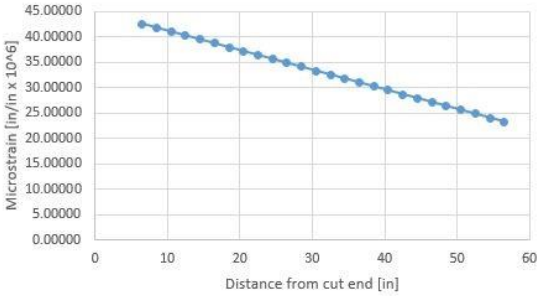

Figure E-10: Change in Strain Due to Changing Support Conditions LT1 DSS 2

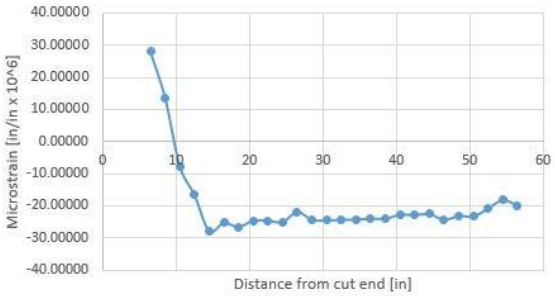

Figure E-11: Measured Change in Strain LT1 DSS 2

LT1 DSS 3

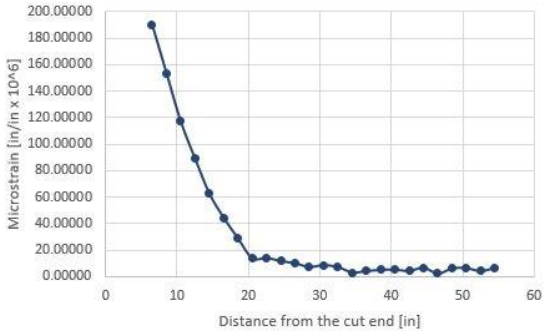

Figure E-12: Corrected Change in Strain LT1 DSS 3

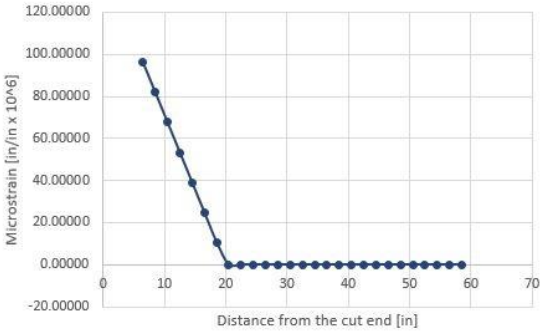

Figure E-13: Change in Eccentric Prestressing Strains LT1 DSS 3

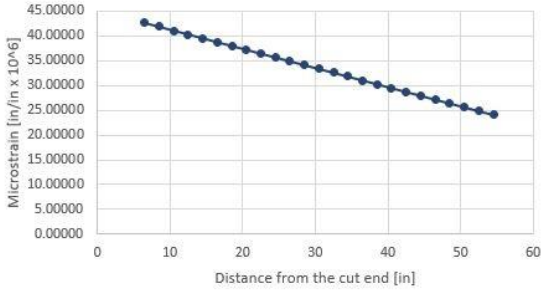

Figure E-14: Change in Strain Due to Changing Support Conditions LT1 DSS 3

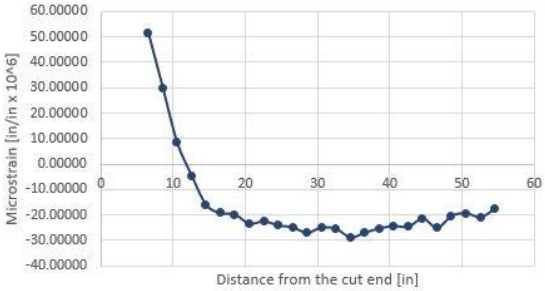

Figure E-15: Measured Change in Strain LT1 DSS 3

LT1 DSS 4

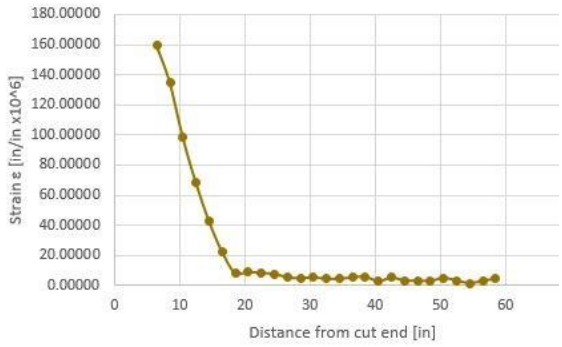

Figure E-16: Corrected Change in Strain LT1 DSS 4

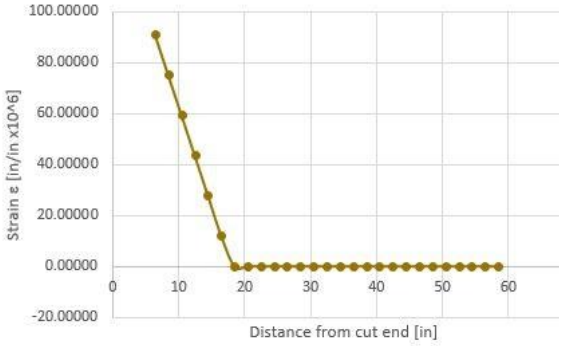

Figure E-17: Change in Eccentric Prestressing Strains LT1 DSS 4

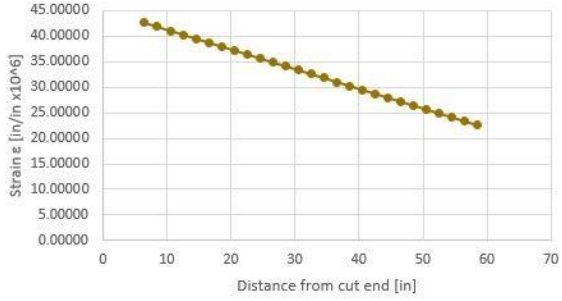

Figure E-18: Change in Strain Due to Changing Support Conditions LT1 DSS 4

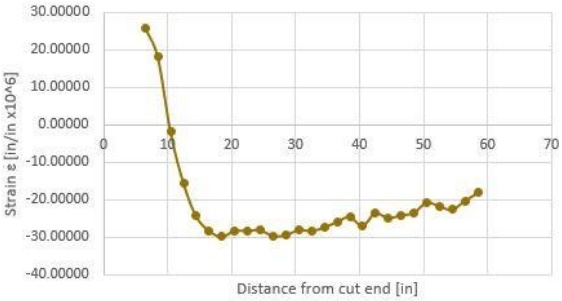

Figure E-19: Measured Change in Strain LT1 DSS 4

LT2 Dss 1

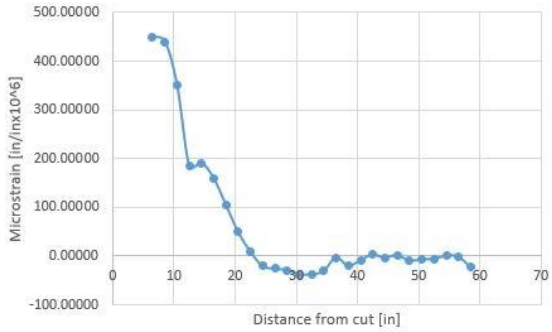

Figure E-20: Corrected Change in Strain LT2 DSS 1

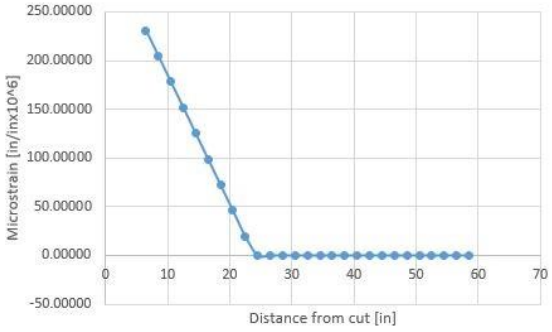

Figure E-21: Change in Eccentric Prestressing Strains LT2 DSS 1

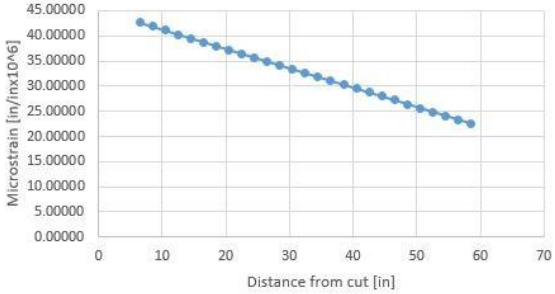

Figure E-22: Change in Strain Due to Changing Support Conditions LT2 DSS 1

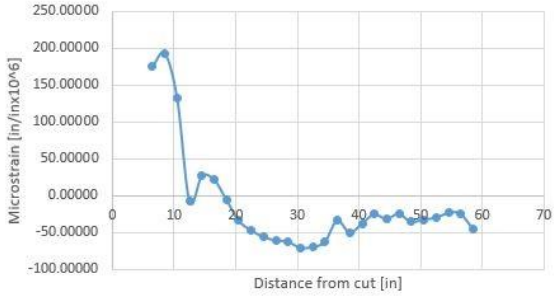

Figure E-23: Measured Change in Strain LT2 DSS 1

LT2 DSS 2

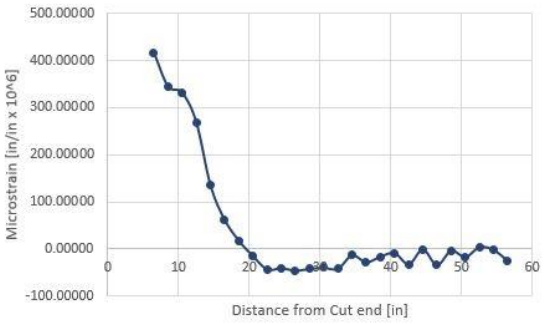

Figure E-24: Corrected Change in Strain LT2 DSS 2

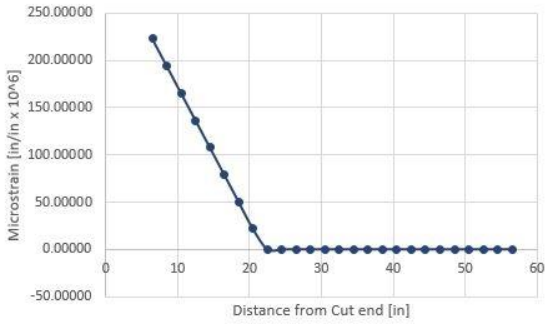

Figure E-25: Change in Eccentric Prestressing Strains LT2 DSS 2

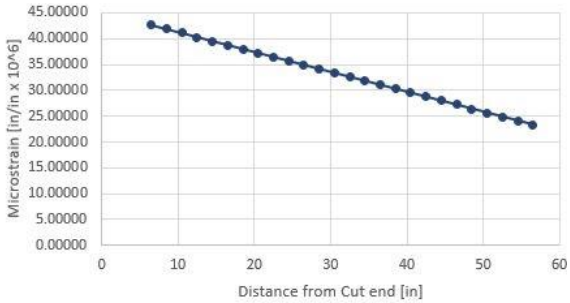

Figure E-26: Change in Strain Due to Changing Support Conditions LT2 DSS 2

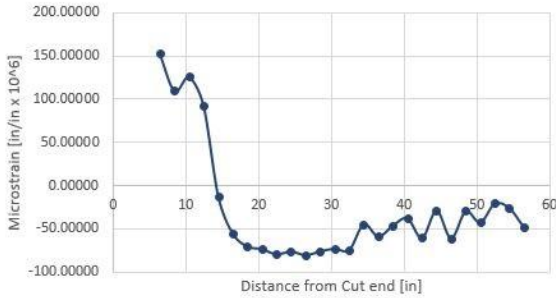

Figure E-27: Measured Change in Strain LT2 DSS 2

LT2 DSS 3

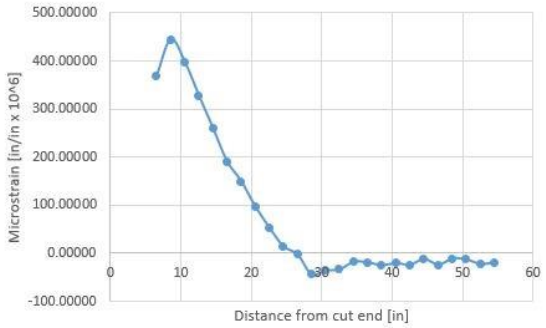

Figure E-28: Corrected Change in Strain LT2 DSS 3

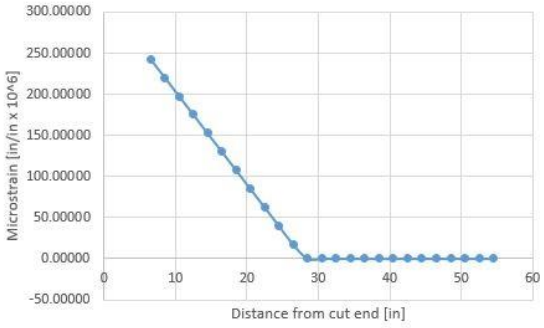

Figure E-29: Change in Eccentric Prestressing Strains LT2 DSS 3

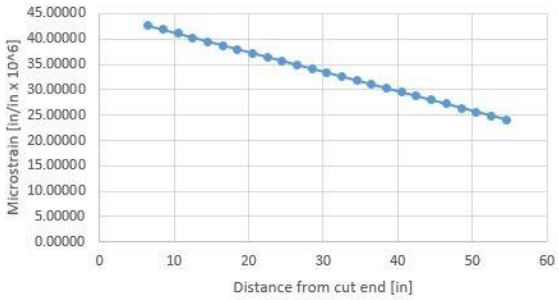

Figure E-30: Change in Strain Due to Changing Support Conditions LT2 DSS 3

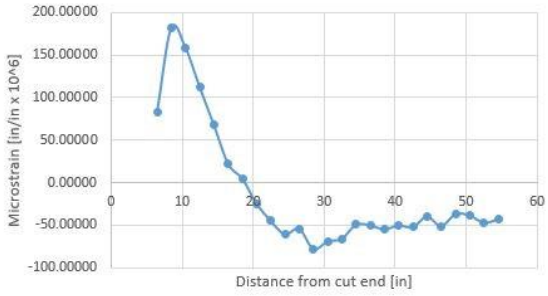

Figure E-31: Measured Change in Strain LT2 DSS 3

LT2 DSS 4

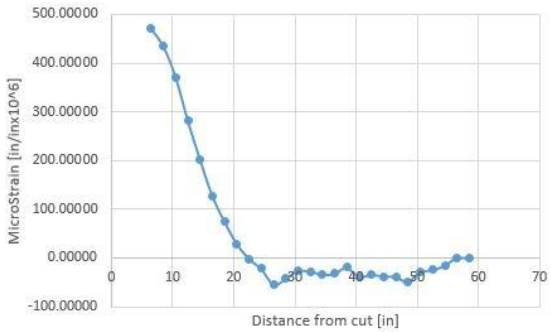

Figure E-32: Corrected Change in Strain LT2 DSS 4

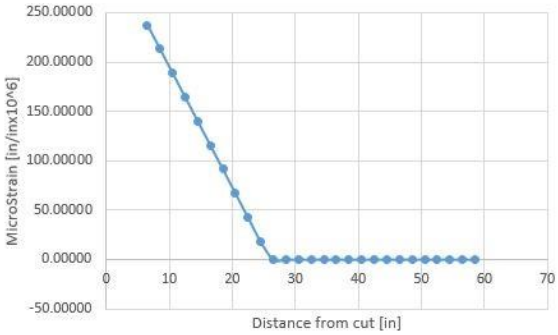

Figure E-33: Change in Eccentric Prestressing Strains LT2 DSS 4

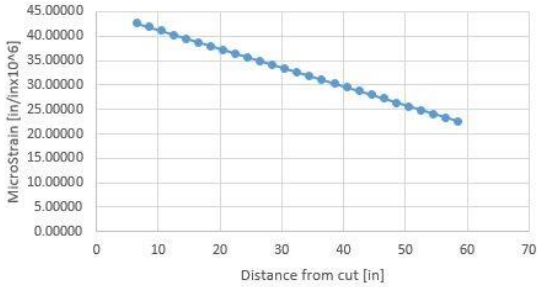

Figure E-34: Change in Strain Due to Changing Support Conditions LT2 DSS 4

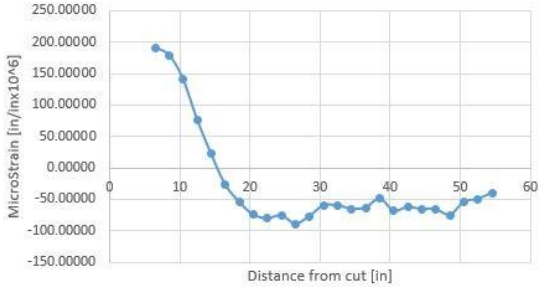

Figure E-35: Measured Change in Strain LT2 DSS 4

Appendix F Field Tests

Appendix F discusses data and observations that pertain to the transfer length tests that were conducted in the field. Section F.1 gives a timeline of the events that occurred on the day of testing. F.2 gives the concrete strength of HCS at the time of the saw cut as well as the 28-day concrete strength. An investigation of the modulus of elasticity of the concrete is presented in F.3. End slips that were measured for the HCS cut are shown in F.4. Section F.5 discusses the saw blade thickness and the saw kerf measurements that were taken after the saw cut.

F.1 Timeline of Events on Day of Testing

Below is a timeline of events that occurred when on the day of testing when both HCS were cut.

5:10am – Data logger turned on
5:15am – HCS 1 lifted off of supports
5:20am – HCS 1 set on bed
5:26am – Saw set on bed
5:45am – Saw lifted off bed
5:50am – HCS 1 reset on bed with Shims
5:55am – Saw set back on bed
5:58am – Saw begins cutting HCS 1
6:01am – Saw done cutting HCS 1
7:04am – Data logger turned off
7:10am – HCS 1 lifted off bed and set to the side. DSS removed and began cleaning.
8:18am – Data logger turned back on
8:41am – All DSS are glued on HCS 2
8:57am – HCS 2 picked up off supports
9:02am – HCS 2 set on bed
9:09am – Saw on bed

9:11am – Saw begins cutting HCS 2

9:15am – Saw done cutting HCS 2

10:08am – HCS 2 lifted from bed

10:12am – HCS 2 Set down on supports

10:22am – Data Collected

F.2 Concrete Strengths

Below are the concrete strengths of the concrete for the HCS that were tested. Concrete cylinders were broken at the time the HCS was saw cut as well as at 28 days. The 28-day strength cylinders were cured in a water bath and then removed and allowed to dry for one day before they were broken. All cylinders were broken according to ASTM C39.

Since HCS are cast with a dry concrete mix, cylinders cannot be made in the typical manner with a tamping rod. Instead the cylinders were cast in three lifts. After each lift the cylinder is put into a vibration machine that vibrates the entire cylinder to consolidate it. This is how the cylinders are made for the plant's quality control process.

Table F-1: HCS 1 Cylinder Breaks at Time of Saw Cut

Cylinder Number	Break Strength [psi]
Cylinder 1	6726
Cylinder 2	6530

Table F-2: HCS 2 Cylinder Breaks at Time of Saw Cut

Cylinder Number	Break Strength [psi]
Cylinder 1	6239
Cylinder 2	5059

Table F-3: HCS 1 28 Day Concrete Strength

Cylinder Number	Break Strength [psi]
Cylinder 1	11,797
Cylinder 2	11,329

Table F-4: HCS 2 28 Day Concrete Strength

Cylinder Number	Break Strength [psi]
Cylinder 1	10,375
Cylinder 2	10,789

F.3 Concrete Modulus Investigation

Concrete modulus tests were conducted on two cylinders from each HCS. This data was needed for the data processing method. The modulus tests were conducted according to ASTM C469.

Table F-5: Modulus Data for HCS 1

Cylinder No.	V_1 [V]	V_2 [V]	P_1 [lbs]	P_2 [lbs]	Strain [in/in]	Stress [psi]	Elastic Modulus [ksi]
Cylinder 1	-9.36	-10.38	990	33,000	5.10x10^6	2547.27	**4994.65**
Cylinder 2	-7.47	-8.44	1560	33,025	4.85x10^6	2503.90	**5162.68**

Table F-6: Modulus Data for HCS 2

Cylinder No.	V_1 [V]	V_2 [V]	P_1 [lbs]	P_2 [lbs]	Strain [in/in]	Stress [psi]	Elastic Modulus [ksi]
Cylinder 1	-1.44	-2.22	1800	25,000	3.94x10^6	1846.193	**4685.77**
Cylinder 2	-7.66	-8.35	1800	25,000	3.45x10^6	1846.193	**5351.28**

F.4 HCS End Slips

End slips were measured on each strand in the HCS after it was saw cut. Readings were also taken several days after the slabs were saw cut. The two pieces of the cut HCS are labeled North and South. The strand in the HCS is labeled West to East with one being the furthest West. Three end slip measurements were taken for each strand. One measurement was in what was assumed to be the center of the strand and the other two were to the left

and right of that measurement. The location of each DSS device on each HCS are given in Table F.7 and Table F.8.

Table F-7: DSS Locations HCS 1

DSS Number	DSS Location
DSS 1	North, Strand 2
DSS 2	North, Strand 4
DSS 3	South, Strand 2
DSS 4	South, Strand 4

Table F-8: DSS Locations HCS 2

DSS Number	DSS Location
DSS 1	North, Strands 2 and 3
DSS 2	North, Strands 6 and 7
DSS 3	South, Strands 2 and 3
DSS 4	South, Strands 6 and 7

Table F-9: HCS 1 North End Slips Day of Test

Strand Number	Center [in]	Left [in]	Right [in]	Average [in]
1	0.0229	0.0266	0.0254	0.0250
2	0.0132	0.0127	0.0180	0.0146
3	0.0043	0.0036	0.0031	0.0037
4	0.0165	0.0121	0.0034	0.0107
5	0.0169	0.0117	0.0120	0.0135
6	0.0316	0.0227	0.0047	0.0197

Table F-10: HCS 1 South End Slips Day of Test

Strand Number	Center [in]	Left [in]	Right [in]	Average [in]
1	0.0152	0.0092	0.0113	0.0119
2	0.0054	0.0083	0.0048	0.0062
3	0.0126	0.0202	0.0222	0.0183

4	0.0061	0.0062	0.0039	0.0054
5	0.0083	0.0075	0.0024	0.0061
6	0.0152	0.0143	0.0097	0.0131

Table F-11: HCS 1 North End Slips 2/21/17 – 5 Days after Saw Cut

Strand Number	Center [in]	Left [in]	Right [in]	Average [in]
1	0.0199	0.0187	0.0186	0.0191
2	0.0129	0.0128	0.0129	0.0129
3	0.0224	0.0206	0.0146	0.0192
4	0.0152	0.0132	0.0165	0.0150
5	0.0151	0.0155	0.0152	0.0153
6	0.0254	0.0279	0.0312	0.0282

Table F-12: HCS 1 South End Slips 2/21/17 – 5 Days after Saw Cut

Strand Number	Center [in]	Left [in]	Right [in]	Average [in]
1	0.0331	0.0356	0.0340	0.0342
2	0.0256	0.0202	0.0226	0.0228
3	0.0126	0.0108	0.0125	0.0120
4	0.0211	0.0197	0.0216	0.0208
5	0.0217	0.0198	0.0206	0.0207
6	0.0336	0.0282	0.0330	0.0316

Table F-13: HCS 2 North End Slips Day of Test

Strand Number	Center [in]	Left [in]	Right [in]	Average [in]
1	N/A	N/A	N/A	N/A
2	0.0372	0.0359	0.0263	0.0331
3	0.0430	0.0391	0.0408	0.0410
4	0.0487	0.0357	0.0466	0.0437
5	0.0266	0.0164	0.0228	0.0219
6	0.0280	0.0305	0.0250	0.0278
7	0.0429	0.0356	0.0365	0.0383
8	0.0467	0.0422	0.0346	0.0412

9	0.0447	0.0343	0.0375	0.0388
10	0.0019	0.0010	0.0015	0.0015

Table F-14: HCS 2 South End Slips Day of Test

Strand Number	Center [in]	Left [in]	Right [in]	Average [in]
1	N/A	N/A	N/A	N/A
2	0.0221	0.0182	0.0201	0.0201
3	0.0419	0.0275	0.0263	0.0319
4	0.0112	0.0102	0.0104	0.0106
5	0.0520	0.0516	0.0518	0.0518
6	0.0153	0.0256	0.0210	0.0206
7	0.0340	0.0309	0.0274	0.0308
8	0.0471	0.0406	0.0249	0.0375
9	0.0429	0.0315	0.0299	0.0348
10	0.0317	0.0314	0.0443	0.0358

Table F-15: HCS 2 North End Slips 2/21/17 – 5 Days after Saw Cut

Strand Number	Center [in]	Left [in]	Right [in]	Average [in]
1	0.0237	0.0298	0.0286	0.0274
2	0.0349	0.0319	0.0322	0.0330
3	0.0507	0.0386	0.0449	0.0447
4	0.0425	0.0396	0.0405	0.0409
5	0.0266	0.0328	0.0332	0.0309
6	0.0406	0.0316	0.0319	0.0347
7	0.0476	0.0452	0.0447	0.0458
8	0.0375	0.0535	0.0562	0.0491
9	0.0450	0.0472	0.0444	0.0455
10	0.0149	0.0190	0.0170	0.0170

Table F-16: HCS 2 South End Slips 2/21/17 – 5 Days after Saw Cut

Strand Number	Center [in]	Left [in]	Right [in]	Average [in]

1	0.0307	0.0206	0.0325	0.0279
2	0.0228	0.0234	0.0213	0.0225
3	0.0269	0.0241	0.0306	0.0272
4	0.0137	0.0141	0.0139	0.0139
5	0.0447	0.0448	0.0426	0.0440
6	0.0258	0.0233	0.0144	0.0212
7	0.0353	0.0358	0.0326	0.0346
8	0.0359	0.0447	0.0539	0.0448
9	0.0436	0.0548	0.0412	0.0465
10	0.0237	0.0200	0.0247	0.0228

Table F-17: HCS 2 North End Slips 2/21/17 – 12 Days after Saw Cut

Strand Number	Center [in]	Left [in]	Right [in]	Average [in]
1	0.0245	0.0325	0.0285	0.0285
2	0.0403	0.0289	0.0285	0.0326
3	0.0482	0.0501	0.0417	0.0467
4	0.0380	0.0382	0.0380	0.0381
5	0.0338	0.0292	0.0226	0.0285
6	0.0317	0.0301	0.0313	0.0310
7	0.0465	0.0436	0.0447	0.0449
8	0.0365	0.0497	0.0542	0.0468
9	0.0460	0.0466	0.0421	0.0449
10	0.0266	0.0208	0.0196	0.0223

Table F-18: HCS 2 South End Slips 2/21/17 – 12 Days after Saw Cut

Strand Number	Center [in]	Left [in]	Right [in]	Average [in]
1	0.0321	0.0347	0.0303	0.0324
2	0.0214	0.0200	0.0171	0.0195
3	0.0270	0.0226	0.0269	0.0255
4	0.0138	0.0166	0.0192	0.0165
5	0.0487	0.0600	0.0461	0.0516

6	0.0267	0.0129	0.0220	0.0205
7	0.0323	0.0368	0.0310	0.0334
8	0.0586	0.0499	0.0416	0.0500
9	0.0542	0.0487	0.0477	0.0502
10	0.0243	0.0185	0.0339	0.0256

F.5 Saw Blade Thickness and Saw Kerf

The saw blade thickness and saw kerf were measured for each test. This was done to see if there was any wobble effect in the saw blade that may affect the end slip readings taken in the HCS. The same saw was used to cut both HCS and had a thickness of **0.3735in.** The HCS settled when it was cut due to the gap between the center support and the HCS, therefore kerf measurements were taken in the mark that was made from the saw in center support. The kerf was not much bigger than the saw blade.

Table F-19: Saw Kerf Measurements

Measurement Number	Test 1 [in]	Test 2 [in]
1	0.3960	0.3995
2	0.3900	0.3765
3	0.3825	0.3785
4	0.3805	0.3745
5	0.3790	0.3750
Average	0.3856	0.3808
Thickness Greater than Saw Blade	0.0121	0.0073

Appendix G End Slip Theory

Appendix G describes the end slip theory that was discussed in Section 3.5. Section G.1 provides a derivation of end slip theory. An explanation of this derivation is given in section G.2.

G.1 End Slip Theory Derivation

1. Assumptions

- The steel strand is a linear, elastic material that is loaded below the yield point, or proportional limit, such that $\sigma_s = E_s \varepsilon_s$.
- The steel bar or strand has a prismatic section with cross-sectional area, A_b, and diameter, d_b, over its length.
- The bond stress, that is, the surface shear stress between the bar or strand and the concrete, u_b, is constant over the transfer (transmission) length, L_t.
- There is not other source of stress on the strand, such as gravity loading, temperature change, concrete creep or concrete shrinkage.

2. Equilibrium over the Transfer Length

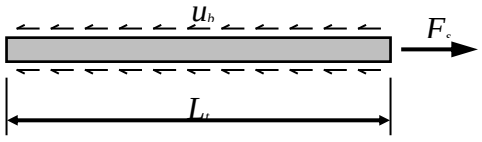

For a segment of strand beginning at the cut (live) end, the bond stresses acting over the surface area of the strand accumulate force that must be resisted by the strand force. Over the transfer length of the strand, the force accumulated from bond, F_b, is

$$F_b = u_b A_o = u_b \left(\Sigma_o L_t\right) = u_b \left(\pi d_b\right) L_t = \pi u_b d_b L_t \qquad \text{(G-1)}$$

where A_o is the surface area of the strand over the transfer length, Σ_o is the circumference of the strand and d_b is the strand diameter.

The strand force, F_s, at the end of the transfer length is

$$F_s = \sigma_{se} A_b = \sigma_{se} \left(\frac{\pi d_b^2}{4} \right) = \frac{1}{4} \pi \sigma_{se} d_b^2 \qquad \text{(G-2)}$$

Equilibrium of the element requires that $F_b = F_s$ from which the transfer length is computed

$$L_t = \frac{\sigma_{se} d_b}{4 u_b} \qquad \text{(G-3)}$$

3. Equilibrium over a Differential Element

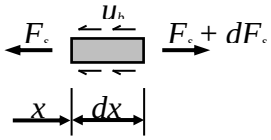

For a differential element of strand of length dx at a distance x from the cut end, force equilibrium would require that

$$\left(F_s + dF_s \right) - dF_s = u_b \left(\Sigma_o dx \right) = u_b \left(\pi d_b \right) dx \qquad \text{(G-4)}$$

Equation (G-4) implies that

$$dF_s = \pi u_b d_b dx \qquad \text{(G-5)}$$

But, from (G-1), at a distance x from the cut end where the strand stress is σ_s, dF_s is also equal to $\frac{1}{4} \pi d_b^2 d\sigma_s$, and the rate of change in strand stress is obtained

$$\frac{d\sigma_s}{dx} = \frac{4}{d_b} u_b \qquad \text{(G-6)}$$

From (G-6), a constant bond stress in the transfer length region means that the strand stress varies linearly, and that beyond the transfer length region, where strand stress is constant, there is no bond stress transfer. Additionally, the strand stress can be obtained from (6) by integration

$$\sigma_s = \int d\sigma_s = \int \left(\frac{4u_b}{d_b}\right) dx = \left(\frac{4u_b}{d_b}\right) x + C_1 \qquad \text{(G-7)}$$

The constant of integration, C_1, vanishes because $\sigma_s = 0$ at the cut end where $x = 0$. Moreover, at the end of the transfer region, when $x = Lt$, σ_s attains a value equal to the effective prestress, σ_{se}

$$\sigma_{se} = \left(\frac{4u_b}{d_b}\right) L_t \qquad \text{(G-8)}$$

from which the constant bond stress is obtained.

$$u_b = \frac{\sigma_{se} d_b}{4L_t} \qquad \text{(G-9)}$$

4. End-Slip

The theoretical end-slip, δ, is obtained from the strand stress distribution given in (G-7).

$$\delta = \int_{L_t} \varepsilon_s \, dx = \int_{L_t} \left(\frac{\sigma_s}{E_s}\right) dx = \int_0^{L_t} \left(\frac{4u_b}{d_b E_s}\right) x \, dx = \frac{4u_b}{d_b E_s} \int_0^{L_t} x \, dx = \frac{2u_b}{d_b E_s} L_t^2 \qquad \text{(G-10)}$$

Incorporating the constant bond stress given in (G-9) gives

$$\delta = \frac{2L_t^2}{d_b E_s}\left(\frac{\sigma_{se} d_b}{4L_t}\right) = \frac{L_t \sigma_{se}}{2E_s} \qquad \text{(G-11)}$$

Solving for transfer length from (G-11) gives the end-slip formula that is commonly used in the precast concrete industry in the USA.

$$L_t = \frac{2E_s}{\sigma_{se}} d \quad \text{(G-12)}$$

G.2 End Slip Theory Explanation

Equation G-12 was first proposed by Guyon in 1953. The derivation of this equation is based on assumptions and approximations that are not necessarily realistic for precast, pre-tensioned concrete beams at the instant of strand release. These include the constant bond stress distribution, the constant coefficient equal to 2.0, and the lack of representation the influence of the method of strand release.

Even though bond stresses between concrete and strand are difficult, if not impossible, to measure, experimental tests suggest that bond stresses do not appear to be distributed uniformly at strand release. For example, Park and Cho (2014) used measured strand strains in pre-tensioned rectangular beam tests to infer bond stress distributions that were not constant. Deng et al. (2016) used strand stresses and end-slips from experimental tests of pre-tensioned beams to calibrate a bond stress vs. end-slip for which the bond stress distribution was far from constant.

Marti-Vargas et al. (2007) evaluated a large number of experimental investigations to determine that the constant in the commonly used "industry" formula for the end-slip vs. transfer length varies from 1.5 to 4.0, and they further recommend a value of 2.44 for this coefficient, instead of the value of 2.0 that is used widely in the USA. Marti-Vargas et al. (2014) later revisited the transfer length vs. end slip relation and used data from a number of tests for 13-mm (0.5-in.) strand to propose a relationship in which end-slip is not linearly proportional to transfer length, but which fits the test data well.

Lastly, Zia and Mostafa (1977) evaluated transfer lengths for beams with strands that were released suddenly or gradually, and they found that the former had transfer lengths that were, on average, 15% longer than the latter. Barnes et al. (2003) later found that for

rusted strands, the use of sudden prestress release methods resulted in transfer lengths that were 30 to 50% larger than those associated with more gradual release.